

Mechanisms that Regulate the Termination of Myosin V Mediated Transport

by

Sara Wong

A dissertation submitted in partial fulfillment
of the requirements for the degree of
Doctor of Philosophy
(Cellular and Molecular Biology)
in the University of Michigan
2020

Doctoral Committee:

Professor Lois S. Weisman, Chair
Assistant Professor Mara C. Duncan
Professor Kristen J. Verhey
Professor Thomas E. Wilson
Professor Yukiko M. Yamashita

Rural Reflections

by Adrienne Rich

This is the grass your feet are planted on.

You paint it orange or you sing it green,
But you have never found
A way to make the grass mean what you mean.

A cloud can be whatever you intend:
Ostrich or leaning tower or staring eye.

But you have never found
A cloud sufficient to express the sky.

Get out there with your splendid expertise;
Raymond who cuts the meadow does not less.

Inhuman nature says:
Inhuman patience is the true success.

Human impatience trips you as you run;
Stand still and you must lie.

It is the grass that cuts the mower down;
It is the cloud that swallows up the sky.

Sara Wong

sawo@umich.edu

ORCID iD: 0000-0001-8606-108X

© Sara Wong 2020

ACKNOWLEDGEMENTS

I would like to thank Dr. Lois Weisman for her mentorship. Through all the ups and downs, she was always an advocate for me.

I would like to thank my thesis committee members, Dr. Mara Duncan, Dr. Tom Wilson, Dr. Kristen Verhey, and Dr. Yukiko Yamashita, for their helpful and insightful discussion. I am grateful for their feedback and encouragement throughout the years.

I would like to thank past and present members of the Weisman Lab: Emily Kauffman, Dr. Beth Strunk, Lily Hahn, Noah Steinfeld, Dr. Ron Benyair, Dr. Sai Srinivas Panapakkam Giridharan, Dr. Yanling Zhang, Dr. Luo Guangming, Dr. Michael Lang, Dr. Junya Hasegawa, and Camille Ackemann. Their knowledge, support, and insights have been essential to my success. I am especially grateful to Dr. Richard Yau who was a close mentor during our overlap in the lab. Many thanks to the undergraduate students I had the pleasure of working with: Petrina Talbot, Nadia Azad, Alim Habib, and Jungwoo Chung. They taught me more than I could ever teach them and brought life and energy to the lab.

I would like to thank our collaborators for their help throughout my research. Dr. Ajit P. Joglekar for discussions of time-lapse microscopy and use of his microscope, which was critical to my studies on Cla4. Dr. Jason M. MacGurn and Dr. Nathaniel L. Hepowit for their hard work and useful discussions related to our manuscript on Yck3 and Vps41. Dr. Sarah A. Port and Dr.

Frederick M. Hughson provided critical reagents for that paper. Dr. Nofar Harpaz, Lihi Gal, and Dr. Maya Schuldiner performed a screen that inspired us to look at Yck3 and Vps41.

I would like to thank the Program in Biomedical Sciences, the Cellular and Molecular Biology Program, the Life Sciences Institute, the Rackham Graduate School, and the American Society of Cell Biology for their support and endless opportunities. Thank you, Nancy Hobbs, Cathy Mitchell, Margherita Bekiaries, Pat Ocelnik, and Lauren Perl for your invaluable administrative support. Thank you, Dr. Laura Schram, Dr. Robert Fuller, Dr. Shoba Subramanian, Dr. Scott Barolo, Dr. Gary McDowell, and Dr. Ashley Lakoduk for their knowledge, guidance, and support. Thank you, Dr. Albert Chen, Dr. Aaron Goldstrom, Seth Wiley, and Charles Lu for taking chances with me as we started various student organizations. I was told that a PhD is a marathon. I assumed that the marathon started on your first day of your first year. I was wrong. The marathon starts the day your mentor and committee tell you that you're ready to write your thesis, apply to jobs, and graduate. Everything before was training, and good training means that you're also cross-training, eating well, and taking care of yourself. My experiences outside of lab have made me a well-rounded scientist; it was my cross training, my self-care, and my community. It has shown me the kind of mentor and leader I aspire to be. I have met and worked with so many amazing students, faculty, and administrators throughout the years and am eternally grateful.

I would also like to thank Dr. Cathie Pflieger's lab and Dr. Nicholas Sibinga's lab for giving me the opportunity to learn and work in their labs. I would like to thank Dr. Alicia Melendez, Dr. Cathy Savage-Dunn, Dr. Kristina Ames, Dr. Nicholas Palmisano, and Dr. Melissa Silvestrini for their continued mentorship and friendship since the beginning of my scientific career. I would

also like to thank the Macaulay Honors College at Queens College, Dr. Ross Wheeler and Dr. Lorna Ronald, for their guidance and support as I transitioned from high school to college to graduate school.

Above all, I would like to thank my family and friends, both from Ann Arbor and New York City. Without their support, advice, and kindness, I am not sure where I would be. Enormous thank you and much love to my Mom, Dad, my brother Andy and his family, my aunts and uncles, Sarah, Iris, Jon, Corey, Danielle, my climbing friends near and far, and many more. Special thanks to Yining, Tejas, Sonya, Alex, Ben, Dana, Rachel, Dimitrijie, Anna, Gillis, Brad, Gus, and everyone else for keeping me sane, fit, and writing during the pandemic.

TABLE OF CONTENTS

ACKNOWLEDGEMENTS	ii
LIST OF FIGURES	viii
LIST OF TABLES	xi
ABSTRACT	xii
CHAPTER I: Introduction	
Intracellular Cargo Transport	1
Regulation of Myosin V Mediated Transport	2
Myosin V Based Organelle Transport in Yeast	6
Myosin V in Mammalian Cells and Disease	14
Unanswered Questions	17
CHAPTER II: Spatial regulation of organelle release from myosin V transport by p21-activated kinases	24
Introduction	25
Results	
PAKs are required for Vac17 degradation and the termination of vacuole transport	26
Cla4 phosphorylates Vac17 <i>in vivo</i> and <i>in vitro</i>	27

Phosphorylation of Vac17-S222 is required for the termination of vacuole transport	29
Vac17-pS222 is required for the ubiquitylation of Vac17	30
Cla4 signaling at the bud cortex initiates the release of the vacuole from Myo2	31
Discussion	33
CHAPTER III: Cargo Release from Myosin V Requires the Convergence of Parallel Pathways that Phosphorylate and Ubiquitylate the Cargo Adaptor	
Introduction	52
Results	
Yck3 and Vps41 have regulate the termination of vacuole transport	54
The roles of Yck3 and Vps41 in the termination of vacuole transport are independent of the HOPS complex, CORVET complex, and AP-3 trafficking	56
The Yck3 and Vps41 pathway is independent of the ubiquitylation of Vac17	58
Yck3 and Vps41 regulate the release of ubiquitylated Vac17 from the Myo2-Vac17-Vac8 complex	60
The AAA-ATPases Cdc48/p97, Vps4, and Sec18/NSF do not extract Vac17 from the complex	62
Yck3 and Vps41 bind and are required for the phosphorylation of Vac17	62
Yck3 and Vps41 phosphorylate Vac17 in the Myo2 binding domain	65

Discussion	69
CHAPTER IV: Future Directions	96
Dbf4 may regulate Dma1 to terminate vacuole transport	97
Yeast Two Hybrid Screen for Vac17-pS222xxF225 Binding Partners	101
Yck3 and Vps41 regulate peroxisome transport	103
Vps41 and Yck3 may regulate the interaction between Myo2 and Vac17	104
Vps41 and Yck3 may regulate the interaction between Vac17 and Vac8	106
Identification of the Vac17 ubiquitylation site	107
Identification of Vac17 binding partners	108
Identification of novel genes required for vacuole transport	109
Open questions without preliminary data	112
CHAPTER V: Methods	123
TABLES	132
REFERENCES	149

LIST OF FIGURES

Figure		
1.1	Myosin V is composed of several unique domains	20
1.2	The use of adaptor proteins is conserved across organelles and organisms	21
1.3	Vacuole transport is coordinated during yeast budding	22
1.4	Insights into vacuole transport may reveal mechanisms of motor-based cargo transport	23
2.1	Deletion of Cla4 or Ste20 causes a partial defect in the termination of vacuole transport	35
2.2	PAKs are required for the degradation of Vac17 and the release of the vacuole from Myo2	37
2.3	Cla4 binds and phosphorylates Vac17	39
2.4	Termination of vacuole transport initiates at the bud cortex	41
2.5	<i>vac17-S222A-GFP</i> and the vacuole travel from the bud tip to the mother-bud neck	43
2.6	Vac17-S222 is required for the ubiquitylation of Vac17	44
2.7	Cla4 localizes to the vacuole after the vacuole contacts the bud cortex	46
2.8	The initiation of Cla4 signaling at the vacuole occurs at the bud cortex	47
2.9	Cla4 co-localizes with Vac17 and the vacuole at the bud cortex	48
2.10	Cla4 spatially regulates the ubiquitylation of Vac17	50

3.1.	Yck3 and Vps41 are required for the termination of vacuole transport	72
3.2.	Yck3 and Vps41 are required for the release of the vacuole from Myo2	74
3.3.	The HOPS complex does not have a role in the termination of vacuole transport	76
3.4.	The core HOPS complex does not have a role in the termination of vacuole transport	78
3.5.	AP-3 and CORVET do not have roles in the termination of vacuole transport	79
3.6.	Yck3 and Vps41 are not required for the ubiquitylation of Vac17	80
3.7.	Yck3 and Vps41 are required to release ubiquitylated Vac17 from the complex	82
3.8.	Vac17 accumulates in aberrant puncta in proteasome mutants	84
3.9.	Myo2 and Vac8 are not affected in the proteasome mutant	85
3.10.	Cdc48, Vps4, and Sec18 are not required for the termination of vacuole transport	86
3.11.	Yck3 and Vps41 are required for the phosphorylation of Vac17	88
3.12.	Yck3 and Vps41 regulate the phosphorylation of Vac17 in its Myo2 binding domain	91
3.13.	Yck3 and Vps41 regulate the phosphorylation of Vac17 in its Myo2 and Vac8 binding regions	93
3.14.	Ubiquitylation and Yck3 and Vps41 - dependent phosphorylation are required to release Vac17 from the vacuole	95
4.1	Vac17-F225 is required for the termination of vacuole transport	114
4.2	Dbf4 may have a role in vacuole transport	115
4.3	Dma1 may be regulated by phosphorylation	116

4.4	Vac17-S222E may function as a phosphomimetic allele	117
4.5	Yeast Two Hybrid screen reveals potential Vac17-pS222 interactors	118
4.6	Upc2 and paralog Ecm22 are not required for Vac17 degradation	119
4.7	Yck3 and Vps41 regulate peroxisome transport	120
4.8	Yck3 and Vps41 may regulate phosphorylation of Vac17 and Vac17 binding partners	121
4.9	Identification of potential regulators of vacuole transport	122

LIST OF TABLES

Table 1.	Yeast Strains used in this study	132
Table 2.	Plasmids used in this study	137
Table 3.	Quantitative analysis of Vac17 phosphorylation in <i>vps41Δ</i> mutant cells	139
Table 4.	Quantitative analysis of Vac17 phosphorylation in <i>yck3Δ</i> mutant cells	140
Table 5.	Alanine mutants tested for defects in the termination	141
Table 6.	Quantitative analysis of Vac17 interactions in <i>vps41Δ</i> mutant cells	142
Table 7.	Quantitative analysis of Vac17 interactions in <i>yck3Δ</i> mutant cells	143
Table 8.	Potential regulators of vacuole transport	144

ABSTRACT

A major question in cell biology is, how are materials, such as organelles, transported within a cell? The mis-localization of organelles underlies diseases in the skin, gut, and brain. Thus, the delivery of organelles to their proper destination is important for cellular function. Molecular motor proteins are one way by which cargoes are transported to their destination within the cell. Yet, little is known about how cargo transport is regulated. Specifically, it is largely unknown how motors release cargo at the correct destination.

In this thesis, I explore mechanisms that regulate how a myosin V motor transports organelles in the budding yeast, *Saccharomyces cerevisiae*. These studies focus on the vacuole, an organelle similar to mammalian lysosomes, which is transported into the daughter bud by myosin V during budding/cell division. Myosin V-based transport requires that cargo-specific adaptor proteins physically link the motor to the cargo. Early in the cell cycle, the vacuole-specific adaptor, Vac17, bridges a myosin V motor, Myo2, to the vacuole. Both the attachment and the detachment of the vacuole to/from Myo2 is highly controlled.

Release of Myo2 from the vacuole is mediated through Vac17. Vac17 is regulated by post-translational modifications. Dma1, an E3 ubiquitin ligase, ubiquitylates Vac17, which targets it for degradation. Interestingly, the bud cortex is a spatial landmark that signals the successful delivery of the vacuole to the bud. Upon arrival at the bud cortex, Vac17 is phosphorylated by a p21-activated kinase (PAK), Cla4. Cla4-dependent phosphorylation is

required for the ubiquitylation and subsequent degradation of Vac17. These studies reveal a critical step in the spatial regulation of myosin V–dependent organelle transport.

In addition to ubiquitylation, a second pathway is required to release the vacuole from Myo2. A vacuole-localized Casein Kinase I, Yck3, along with the homotypic fusion and protein-sorting (HOPS) subunit, Vps41, regulate the phosphorylation of Vac17 in its Myo2 binding region. Yck3 and Vps41-dependent phosphorylation results in the dissociation of ubiquitylated Vac17 from the motor-adaptor complex. Moreover, ubiquitylation of Vac17 can occur independent of Yck3 and Vps41. Conversely, Yck3 and Vps41 -dependent phosphorylation can occur without ubiquitylation. However, both signals must be present for the vacuole to be released from Myo2 and for Vac17 to be degraded. Thus, the termination of cargo transport is tightly regulated and likely critical to cellular health and function.

Overall, these studies reveal some of the mechanisms required to release cargo from their motors at the right place and time. Many of the players are conserved in mammalian cells. Thus, it is tempting to speculate that these mechanisms are conserved for other yeast myosin V cargoes, as well as conserved in mammalian cells. Further work based on these findings has the promise to provide greater insight into motor-based cargo transport, how protein complexes are dissociated, and how proteins are regulated and degraded in coordination with cellular events.

CHAPTER I

INTRODUCTION

Intracellular Cargo Transport

The correct positioning of contents within a cell is crucial to cellular function. The movement and delivery of cellular materials, such as organelles, is essential for response to stimuli and for the establishment and maintenance of homeostasis and cellular identity. Organelles are dynamic and change morphology and location depending on cellular requirements, such as during cell division (Jongsma et al., 2015). For example, lysosomes may change localization in response to stimuli, such as starvation, presumably to help degrade contents that are in other parts of the cell (Oyarzun et al., 2019). Additionally, their position within a cell is linked to their luminal pH, and thus function (Johnson et al., 2016). Cargo transport is mediated in part by molecular motors. Accurate transport by molecular motors requires several regulated steps: 1) correct orientation of cytoskeletal tracks, 2) regulation of motor movement along the cytoskeleton, and 3) loading and unloading of cargoes on the motor. In many eukaryotic cells, including mammalian cells, long range transport occurs via kinesin and dynein on microtubules. At the cell periphery, some cargoes are then transferred from kinesin to myosin V motors for short range transport or tethering on actin networks (Hancock, 2014). In the budding yeast *Saccharomyces cerevisiae*, myosin V moves several cargoes from the mother to the bud during budding, a

version of asymmetric cell division (Weisman, 2006). While myosin V moves towards the positive end of actin filaments, myosin VI may transport and tether cargo at the negative end of actin (Lister et al., 2004). Here, we focus on myosin V-mediated organelle transport.

Regulation of Myosin V Mediated Transport

Regulation of the motor domain and movement along actin

There are three myosin V isoforms in mammalian cells: myosin Va, Vb, and Vc (Hammer and Wagner, 2013). Budding yeast express two myosin V motors: Myo2 and Myo4 (Lu et al., 2014). The myosin V heavy chain consists of the motor domain, neck domain, and globular tail domain (**Figure 1.1**). Regulation of myosin V occurs in each of these regions, such that regulation of the motor and neck domains are largely responsible for movement along the actin cytoskeleton, while the tail domain mediates cargo loading and unloading (Heissler and Sellers, 2016; Lu et al., 2014).

The motor domain is required for movement along actin and is the site of ATP hydrolysis and actin binding (Heissler and Sellers, 2016; Larson, 1996; Lu et al., 2014). ATP hydrolysis regulates the power stroke, a hand over hand movement of the motor domains that allows progress along actin (Trybus, 2008). Upon binding to actin, the motor domain can move processively on actin-tropomyosin (Hodges et al., 2012; Pruyne et al., 1998). Tropomyosin may increase myosin V's processivity, run length, and/or frequency of actin binding (Heissler and Sellers, 2016).

Motor movement is also regulated by the neck domain of myosin V. The neck domain contains IQ motifs that in yeast bind to Mlc1, myosin light chain, for stability (Stevens and

Davis, 1998) as well as to calmodulin (Brockhoff et al., 1994). Calmodulin recruits calcium, which leads to conformational changes in myosin V and activates myosin V movement (Trybus et al., 2007; Wang et al., 2004). Calcium may regulate activity by also relieving the auto-inhibited conformation of mammalian myosin Va *in vitro* (Wang et al., 2004).

Auto-inhibition is when a motor is folded in an inactive state, with the motor domain bound to the tail domain, unless bound to cargo and/or the cytoskeleton (Li et al., 2005; Skolnick et al., 2013). The microtubule based motors, kinesin (Hammond et al., 2010; Kelliher et al., 2018; Siddiqui et al., 2019; Verhey and Hammond, 2009) and dynein (Qiu et al., 2019; Torisawa et al., 2014), exhibit regulation by auto-inhibition and this inhibition is released upon binding to adaptor proteins and cargo. *In vitro* myosin-Va also shows extended and auto-inhibited conformations (Heissler and Sellers, 2016), where the auto-inhibited structure has the motor domains docked to the tail domains (Krementsov et al., 2004; Li et al., 2004; Liu et al., 2006; Sato et al., 2007a; Thirumurugan et al., 2006; Wang et al., 2004). One study in yeast predicted the docking sites and found that genetic mutants may suggest that auto-inhibition has a role in the cellular context (Donovan and Bretscher, 2015). Thus, mechanisms that regulate auto-inhibition may apply to both actin and microtubule based motors.

Globular tail domain and cargo-specific adaptor proteins

Myosin V motors transport cargoes to their correct intracellular locations (Lu et al., 2014). The globular tail domain of myosin V must bind to a variety of cargoes under different conditions. Myosin-V utilizes cargo-specific adaptor proteins, which allows one tail domain to

bind to a variety of cargoes (Cross and Dodding, 2019). A similar strategy also occurs in kinesin and dynein. Adaptor binding regions in both the yeast myosin V, Myo2 (Eves et al., 2012; Tang et al., 2019), and the mammalian myosin-Va globular tail domain overlap with other adaptor binding regions (Wei et al., 2013), which likely causes competition between adaptors and their cargoes. Thus, it is likely that there are mechanisms in place to regulate which cargoes are bound at a given time or location. Although adaptor proteins themselves are not conserved, adaptor proteins are utilized by myosin V motors from yeast to humans and share some common structural and regulatory elements (**Figure 1.2**).

Transport initiates when myosin V binds to an adaptor protein and is thus physically linked to the cargo (Knobloch and Rachubinski, 2016; Weisman, 2006; Westermann, 2014). Binding to the adaptor induces conformational changes in myosin V, as observed in mammalian cells (Pylypenko et al., 2013) and yeast (Tang et al., 2019), and may activate the motor (Donovan and Bretscher, 2012). Studies of myosin Va suggest that regulation of adaptors can influence track selection and actin binding (Oberhofer et al., 2017). The binding of the motor to the adaptor may also be facilitated by additional mechanisms. For example, Cdk1 phosphorylates the yeast vacuole adaptor to regulate its binding to myosin V, and putative Cdk1 sites are present in other cargo specific adaptor proteins (Peng and Weisman, 2008). Rab GTPases also mediate myosin V binding to cargo. For example, Rab11a binds myosin Va and Vb to stimulate membrane tethering (Inoshita and Mima, 2017). Rabs may be part of the motor-adaptor complex, such as Rab27a, which interacts with the adaptor melanophilin and myosin V to mediate melanosome transport (Barral and Seabra, 2004). In yeast, the Rab GTPases Sec4 and Ypt11 are required for secretory vesicle transport (Jin et al., 2011), and Ypt11 also regulates

transport of other organelles (Arai et al., 2008; Chernyakov et al., 2013; Eves et al., 2012; Jin et al., 2009; Lewandowska et al., 2013). Regulation through Rab GTPases may provide additional specificity. For example, Rab3A binds to myosin Va and Vc, but not Vb (Dolce et al., 2020), suggesting that mechanisms regulate specific activity for certain isoforms of myosin V. Rab GTPases may also directly regulate motor-adaptor interactions or otherwise facilitate cargo movement. For example, interaction with Rab11 and Rab8 may stimulate actin nucleation by recruiting Spir (Welz and Kerkhoff, 2019), which is in contrast to the other Rab GTPases described that are related to the cargo-specific adaptor proteins.

Upon arrival at their correct locations, organelles detach from myosin V, thereby terminating transport (Fusheng Tang, 2003). In *Xenopus*, CK2 phosphorylates the myosin tail domain during mitosis (Karcher et al., 2001), to release cargo and reduce the transport of cargo, such as melanosomes (Rogers et al., 1999). During budding in yeast, cargo is released from myosin V late in the cell cycle (Fusheng Tang, 2003), which provides further support to the hypothesis that cargo transport is closely linked with the cell cycle. The degradation of adaptor proteins is also highly regulated and may serve to ensure proper cargo release from the motor. Melanophilin, the mammalian melanosome adaptor (Park et al., 2019b), and Vac17 (Yau et al., 2014; Yau et al., 2017), the yeast vacuole adaptor, are ubiquitinated and degraded by the proteasome. It is likely that additional unknown mechanisms are required to properly position cargoes within cells.

Myosin and kinesin

It is largely unknown how teams of diverse motors are coordinated in a cellular context, whether collaboratively or in opposition. When myosin V is recruited to kinesin-propelled cargo, it reduces their motility near the cell periphery and enhances their localization at the cortex (Kapitein et al., 2013), suggesting that there are mechanisms at the cortex that promote actin-based transport over microtubule-based transport. Such regulation may be due to the cytoskeleton that is available, and myosin V and kinesin may compete with each other for cargo depending on the availability of microtubules (Lu et al., 2020). In some cases, this type of competition may promote function, as one study suggests that myosin V and kinesin enhance each other processivity by acting as tethers (Ali et al., 2008). In yeast, a catalytically inactive kinesin-like protein Smy1 enhances the interaction between Myo2 and the Rab Sec4, which links Myo2 to secretory vesicles (Lwin et al., 2016). Smy1 may also regulate formins and thus influence actin cables (Chesarone-Cataldo et al., 2011; Eskin et al., 2016). Overall, there are many open questions as to how myosin and kinesin motors may cooperate or compete depending on the cellular context.

Myosin V Based Organelle Transport in Yeast

During budding, the cell division that occurs in *Saccharomyces cerevisiae*, Myo4 and Myo2 transport cargoes into the bud to divide cellular components between mother and daughter cells (Bretscher, 2003; Knoblach and Rachubinski, 2015; Weisman, 2006). Myo4 transports messenger ribonucleoprotein (mRNP) (Singer-Kruger and Jansen, 2014), ASH1 mRNA (Dunn et al., 2007) via She2 (Long et al., 2000), and the cortical ER via She3 (Estrada et al., 2003) into the bud during budding. On the other hand, Myo2 transports the vacuole (Kent L. Hill,

1996; Natalie L. Catlett, 1998), mitochondria (Simon et al., 1995), peroxisomes (Hoepfner et al., 2001), secretory vesicles (Pruyne et al., 1998), lipid droplets (Knoblach and Rachubinski, 2014), and late Golgi (Arai et al., 2008) into the bud. Myo2 also has a role in microtubule spindle positioning, which helps position the nucleus for closed mitosis (Hwang et al., 2003; Lee et al., 2000; Liakopoulos et al., 2003; Miller et al., 2000; Yin et al., 2000). Myo2 likely also binds to RNA-containing complexes (Chang et al., 2008). During mating, Myo2 transports Fus2 to the bud tip to break down the cell wall (Sheltzer and Rose, 2009). Thus, Myo2 has diverse cargoes and must coordinate the transport of these cargoes at the right time and to the right destination.

Organelle transport requires organelle-specific events, such as regulation of the cargo-specific adaptor proteins, to allow fine-tuned coordination of movement.

Transport also requires more broad events that control organelle transport in general. For example, the kinase Ptc1 may stabilize the cargo adaptors for mitochondria, vacuole, and peroxisome, and thus promote their transport (Jin et al., 2009; Roeder et al., 1998). Additionally, the Rab Ypt11 has roles in moving mitochondria (Chernyakov et al., 2013; Itoh et al., 2002), ER (Buvelot Frei et al., 2006), and late Golgi (Arai et al., 2008). This suggests conservation of mechanisms across organelles or cooperative mechanisms that links the movement of several organelles.

Even for organelles that can be produced *de novo*, such as the vacuole, inheritance of mature organelles likely provides a competitive advantage (Jin and Weisman, 2015). Another advantage is that asymmetric inheritance allows the cell to rejuvenate the bud and leave potentially toxic materials in the mother, and thus extend

lifespan (Hill et al., 2014; Nystrom and Liu, 2014). It could also act as a protective measure, such as in the case where acute stress inhibits ER inheritance, and thus daughter cells are not viable (Babour et al., 2010). Below we discuss four examples of myosin V cargoes in yeast: two essential cargoes, secretory vesicles and mitochondria, and two other cargoes that have also been extensively studied, peroxisomes and vacuoles.

Secretory vesicles

Secretory vesicles are an essential Myo2 cargo and are required for bud growth and sealing the mother-bud interface during cytokinesis (Johnston et al., 1991; Schott et al., 1999). An early observation found that a myosin V mutant, *myo2-66* (Lillie and Brown, 1994), was impaired in moving secretory vesicles (Johnston et al., 1991). Myo2 motor function is likely activated upon binding to secretory vesicles (Donovan and Bretscher, 2012). GTP-bound Ypt31/32, members of the Rab11 GTPase family, bind to Myo2 to promote secretory vesicle growth and transport (Lipatova et al., 2008). After transport into the bud, secretory vesicles tether at the bud tip before membrane fusion (Donovan and Bretscher, 2015). Tethering and fusion of secretory vesicles requires that Myo2 interacts with the Rab Sec4 and the exocyst subunit Sec15 (Jin et al., 2011). The kinesin-like protein Smy1 may promote Myo2 interaction with Sec4 (Lwin et al., 2016). At a late step, release of secretory vesicles is triggered by GTP hydrolysis during tethering (Donovan and Bretscher, 2012).

Mitochondria

Since mitochondria are essential (McConnell et al., 1990) and cannot be made de novo, multiple pathways, including Myo2-independent pathways, ensure their inheritance. Yeast are able to scale how many mitochondria are inherited to the size of the bud (Rafelski et al., 2012). Ideally, about half of mitochondria are inherited by the bud (Boldogh et al., 2003; Simon et al., 1997). The region of Myo2 that binds to the mitochondria-specific adaptor, Mmr1, has overlap with binding regions to other adaptor proteins (Eves et al., 2012), suggesting that additional mechanisms, such as competition, coordinate cargo transport. The Rab GTPase Ypt11 (Arai et al., 2008; Chernyakov et al., 2013; Itoh et al., 2002; Lewandowska et al., 2013) and Mmr1 (Chernyakov et al., 2013; Eves et al., 2012; Itoh et al., 2004) facilitate Myo2 dependent transport and anchoring in the bud, as well as link mitochondria to cortical ER (Itoh et al., 2002; Swayne et al., 2011). The mitochondrial rho (Miro) GTPase Gem1 also facilitates Myo2 dependent movement, but Ypt11, Mmr1, and Gem1 may function in independent pathways (Frederick et al., 2008). Note that Miro and its function in mitochondrial distribution is conserved in higher eukaryotes (Fransson et al., 2003; Fransson et al., 2006).

In the bud and the mother, mitochondria are anchored to the cell periphery. MECA is a complex of Num1 and Mdm36 that tethers mitochondria and ER to the mother cell cortex (Lackner et al., 2013). Mfb1 also aids in tethering mother cell mitochondria, independent of Num1 (Pernice et al., 2016). In addition to serving as the Myo2 adaptor, Mmr1 may tether mitochondria to the bud cortex (Swayne et al., 2011), though it is difficult to distinguish polarized movement towards the bud tip from tethering at the bud tip, and it is likely that Mmr1 is acting as an adaptor as opposed to a tether (Eves et al., 2012). Mmr1 and Num1 likely oppose each other, as deletion of

Mmr1 results in more mitochondria in the mother (Eves et al., 2012; Itoh et al., 2004; Swayne et al., 2011), while deletion of Num1 results in more mitochondria in the bud (Kleckner et al., 2013; Lackner et al., 2013).

In addition to myosin V mediated movement, the cytoskeleton itself may have roles in mitochondria movement (Kleckner and Westermann, 2020). Puf3 facilitates binding of mitochondria, via the mitochore, to Arp2/3 (Garcia-Rodriguez et al., 2007). Subsequent actin polymerization may propel mitochondria into the bud (Boldogh et al., 2001). Mdm10, Mdm12, and Mmm1, members of the ERMES complex (Kornmann et al., 2009), potentially recruit Arp2/3 (Boldogh et al., 1998; Boldogh et al., 2003). However, it is unknown if this pathway plays a significant role in mitochondrial inheritance. Note that in mammalian cells, actin cycling may regulate mitochondrial fission and fusion dynamics (Moore et al., 2016).

Mitochondrial transport is also linked to mitochondrial morphology, which is maintained through regulated fission and fusion, as well as the health of the mitochondria. Myo2 is required for mitochondrial fusion, which in turn affects mitochondrial inheritance and retention of protein aggregates in the mother (Bockler et al., 2017). Several groups observed that only healthy mitochondria are inherited by the bud (Higuchi et al., 2013; McFaline-Figueroa et al., 2011; Vevea et al., 2013). Anchoring likely enables these healthy mitochondria to be selectively kept in the bud (Knoblach and Rachubinski, 2015). The selection of healthy mitochondria to be moved into the bud may be related to actin cables as well, as healthy mitochondria have to move in the opposite the direction of retrograde actin cable flow (Higuchi et al., 2013). The asymmetrical inheritance of mitochondria likely contributes to rejuvenating the daughter bud

(Hughes and Gottschling, 2012; McFaline-Figueroa et al., 2011; Pernice et al., 2016). Yet, the mechanisms that select which mitochondria are transported, and to where, are still unclear.

Peroxisomes

Peroxisomes are transported by Myo2 via the peroxisome specific adaptors Inp2 (Fagarasanu et al., 2006) and Pex19 (Otzen et al., 2012). Inp2 is phosphorylated in coordination with the cell cycle, with higher levels of phosphorylation at the beginning and end of the cycle, suggesting that post-translational modifications may regulate peroxisome transport (Fagarasanu et al., 2009; Oeljeklaus et al., 2016). Additionally, the Inp2 binding region on Myo2 partially overlaps with the secretory vesicle binding region (Fagarasanu et al., 2009; Tang et al., 2019), suggesting that there may be additional regulatory pathways that determine which cargoes are moved at a given time. Note that peroxisome transport occurs before mitochondrial transport in budding yeast (Knoblach et al., 2013).

After being transported into the bud, Inp2 is degraded and peroxisomes are released from Myo2 (Fagarasanu et al., 2009). Yeast may 'count' how many peroxisomes are in the mother and the bud, and control Myo2-mediated inheritance accordingly, such as by increasing the amount of Inp2 (Fagarasanu et al., 2009; Knoblach and Rachubinski, 2015). Notably, Inp2 also has roles in peroxisome division (Knoblach and Rachubinski, 2015), suggesting that division and transport may be coordinated to achieve the right amount of peroxisomes in the bud. This process may also be regulated by Vps1 (Hoepfner et al., 2001).

In contrast to Inp2, which is only found in the bud (Fagarasanu et al., 2006), Inp1 acts as a peroxisome tether at the cell periphery (Fagarasanu et al., 2005) in the mother cell (Knoblach et al., 2013), and also interacts with the ER-localized Pex3 (Knoblach et al., 2013; Munck et al., 2009). In the filamentous fungus, *Aspergillus nidulans*, peroxisomes hitchhike on early endosomes as a mode of transportation (Salogiannis et al., 2016). In *A. nidulans*, long range organelle transport occurs along microtubules, so it is unknown if these hitchhiking mechanisms are conserved for actin-based transport or in mammalian cells.

Vacuole

Although vacuoles can be made *de novo* in the bud, the presence of a vacuole that is of proper size is required for cell cycle progression and for the initiation of bud emergence (Jin and Weisman, 2015). At the beginning of the cell cycle in *S. cerevisiae*, the myosin V motor, Myo2, binds the vacuole adaptor, Vac17, and transports a portion of the mother vacuole into the bud (Fusheng Tang, 2003; Ishikawa et al., 2003) (**Figure 1.3A**). The attachment between Myo2 and Vac17 is regulated by the cyclin dependent kinase, Cdk1, which phosphorylates Vac17 (Peng and Weisman, 2008). The peroxisome adaptor, Inp2, and the mitochondria adaptor, Mmr1, also contain potential Cdk1 sites (Peng and Weisman, 2008). Vac17 also binds to Vac8, which is associated with the vacuole via myristoylation and palmitoylation (Tang et al., 2006; Yong-Xu Wang, 1998). The formation of the Myo2-Vac17-Vac8 complex physically bridges Myo2 to the vacuole (Fusheng Tang, 2003; Ishikawa et al., 2003). Importantly, translation, phosphorylation, and degradation of Vac17 is coordinated with the cell cycle and Vac17 levels peak at the same time that vacuole transport occurs (Fusheng Tang, 2003; Peng and Weisman, 2008)

Vac8 has other cellular roles, including being part of the nuclear-vacuole junction, an organelle contact site between the ER and vacuole, and the site of piecemeal micro-autophagy of the nucleus (Kvam and Goldfarb, 2007). A recent structure suggests that Vac8 may have different quaternary structures depending on its binding partners, and that these distinct orientations correlate with function (Park et al., 2019a). The structure of Vac8 bound to Vac17 is currently unknown. Note that the structures of Myo2 bound to Smy1, Mmr2, and Inp2 is known (Tang et al., 2019), but the structure of Myo2 bound to Vac17 remains unsolved. One caveat of the Myo2 study is that the adaptors were tethered to the motor, raising the possibility that the structures are artifacts of the tether. Aside from vacuole transport, Vac17 may have a role in the asymmetric inheritance of protein aggregates, as related to aging (Hill et al., 2016). It is unclear if Vac17 has a significant role in the cell aside from vacuole transport.

After it is delivered into the bud, the vacuole is released from Myo2, and Vac17 is degraded (Fusheng Tang, 2003). The E3 ubiquitin ligase, Dma1, ubiquitylates Vac17 and Vac17 is degraded by the proteasome (Yau et al., 2014). Degradation of Vac17 depends on its PEST sequence (Fusheng Tang, 2003). Note that Inp2 also contains PEST sequences and is degraded in the bud (Fagarasanu et al., 2006). Additionally, the astral microtubule adaptor Kar9, is ubiquitylated and degraded (Kammerer et al., 2010). Late in the cell cycle, Myo2 transports secretory vesicles, but not the vacuole, to the mother-bud neck (Govindan et al., 1995; Pruyne et al., 1998; Schott et al., 1999). In mutants defective in the degradation of Vac17, the vacuole remains attached to Myo2 and is inappropriately transported to the mother-bud neck late in the cell cycle (Fusheng Tang,

2003) (**Figure 1.3B**). Dma1 is also essential for the release of peroxisomes from Myo2, suggesting a conserved role for Dma1 in terminating Myo2-mediated cargo transport (Yau et al., 2014).

In yeast, the p21-activated kinases (PAKs) Cla4 and Ste20, localize to the bud cortex and regulate several cell cycle related processes including actin cytoskeleton polarization, septin ring assembly, and cytokinesis (Boyce and Andrianopoulos, 2011; Cvrckova et al., 1995; Kumar et al., 2009; Peter et al., 1996). Moreover, it was proposed that PAKs indirectly regulated vacuole inheritance via Lte1, a Cla4-activated guanine nucleotide exchange factor (Bartholomew and Hardy, 2009). Thus, it is likely that additional mechanisms regulate the transport of the vacuole.

It is largely unknown why such complicated mechanisms are required to detach the vacuole from Myo2, especially since defects in this process are not lethal to the cell. It is possible that the degradation of Vac17 ensures that the Myo2-Vac17-Vac8 complex does not reform, accidentally sequestering Myo2 and Vac8 from their other functions. It is also possible that degradation of Vac17 allows the new synthesis of Vac17 during the next cell cycle to drive vacuole transport. Further studies of vacuole transport may reveal some of the physiological reasons for these mechanisms.

Myosin V in Mammalian Cells and Disease

Myosin V motors are conserved across eukaryotes, and it is tempting to speculate that the mechanisms that regulate myosin V-based transport are also conserved (Hammer and Sellers, 2012; Trybus, 2008). Mammals express three myosin V motors: myosin-Va (MYO5A), -

Vb (MYO5B), and –Vc (MYO5C) (Heissler and Sellers, 2016; van der Velde et al., 2013). Myosin Va is found predominately in the brain, while Myosin Vb and Vc are in non-neuronal tissues, such as epithelial tissues (Rodriguez and Cheney, 2002). Mutations in myosin V motors have been implicated in a variety of diseases (Çağdaş et al., 2012; Chen et al., 2013; Dong et al., 2012; Elodie Pastural, 1997; Hammer and Wagner, 2013; Muller et al., 2008; Takagishi and Murata, 2006; Thoeni et al., 2014; van der Velde et al., 2013). Defects in the attachment of cargoes to motors, as well as the inability to detach cargoes from motors, may cause these diseases since both cases would prevent the proper localization of cargoes. Furthermore, if a motor cannot detach from one cargo, it is likely that it would not be able to attach to and transport other cargoes.

Defects in myosin V based transport become most prominent in polarized tissue types, such as gut epithelial cells. In gut cells, the Rab11/Slp4/Myo5b/Munc18 complex carries vesicles to the apical surface, where they bind to STX3 for membrane fusion (Vogel et al., 2015). Mutations in *MYO5B* cause a loss of cell polarity and identity, resulting in microvillus inclusion disease (MVID), a rare disease where the gut is unable to absorb nutrients (Muller et al., 2008; Thoeni et al., 2014; van der Velde et al., 2013). Both constitutive (Carton-Garcia et al., 2015) and conditional (Schneeberger et al., 2015) knockout of *MYO5B* serve as mouse models for MVID. Loss of function mutants in Rab8 (Sato et al., 2007b) and Rab11 (Sobajima et al., 2014) also mimic MVID. Downregulation of *MYO5B* is also associated with the progression of gastric cancer (Dong et al., 2012), supporting the idea that myosin V mediated transport maintains gut cell identity and function.

Myosin V also has a prominent role in neurons. Myosin Va transports ER into dendritic spines of purkinje neurons (Wagner et al., 2011). Myosin Vb moves recycling endosomes and AMPA receptors (Wang et al., 2008). Myosin Va acts as a tether in synapses to promote neurotransmitter release (Maschi et al., 2018). Myosin Va is recruited to secretory granules that contain Rab27a and granophilin-a/b or rabphilin-3A (Brozzi et al., 2012). Griscelli syndrome, a disease that is characterized by neurologic and pigmentation deficiencies, can be caused by mutations in myosin Va (Çağdaş et al., 2012; Elodie Pastural, 1997; Takagishi and Murata, 2006; Van Gele et al., 2009).

Pigmentation defects can be traced to a role for myosin Va in melanocyte function. Myosin Va positions melanosomes for proper pigmentation (Wu et al., 1998). Melanophilin, Rab27a, and myosin Va form a complex to transport melanosomes to the cell periphery, where they are positioned at the cell cortex for proper delivery to keratinocytes (Fukuda et al., 2002; Strom et al., 2002). Melanophilin/Slac2-a serves as the melanosome specific cargo adaptor (Provance et al., 2002; Wu et al., 2002b) and enhances myosin V processivity (Sckolnick et al., 2013). Rab27a likely interacts with myosin Va indirectly, but is still required for melanosome transport (Wu et al., 2002a). Rab36 may promote RILPL2 interaction with myosin V, which then allows Melanophilin to bind the globular tail domain (Cao et al., 2019). Note that similar to the yeast cargo adaptors Vac17 and Inp2, Melanophilin also contains PEST sequences (Fukuda and Itoh, 2004). Deletion of one of the PEST sequences of Melanophilin results in stabilization of Melanophilin and mis-localization of melanosomes (Fukuda and Itoh, 2004). Thus, studies of how the Vac17-PEST sequence regulates yeast vacuole transport may provide insight into how mammalian cargo adaptors are regulated.

Unanswered Questions

Although recent studies have revealed novel mechanisms in cargo transport, many questions remain unanswered. Even in the case of the yeast vacuole, where several studies have uncovered key mechanisms, there is still more to be learned, and these studies may apply to other cargoes (**Figure 1.4**). It is still unknown how the site of Myo2 attachment to the vacuole is chosen. Although Vac8 is found along the vacuole membrane, only one punctum of Vac17 and Myo2 localize to the vacuole. It is unclear how the leading edge of the vacuole is chosen. It is possible that this signaling depends on cell polarization or bud growth factors, organelle contact sites, signaling phosphoinositide lipids, or trafficking of endosomes. Alternatively, or in addition, the directional movement of Myo2, may bring together a domain of the vacuole that forms the leading edge. In support of this hypothesis, in Myo2 mutants that cannot bind Vac17, Vac17 and Vac8 are distributed throughout the vacuole membrane. During vacuole transport, it is unclear if anything anchors the mother vacuole. Anchor proteins have been identified for other organelles in yeast, but none have been shown to anchor the vacuole.

Additionally, there are likely other factors that contribute to the formation of the Myo2/Vac17/Vac8 complex. While previous studies identified Cdk1 as regulating the interaction between Vac17 and Myo2, it is unclear what facilitates Vac17 and Vac8 binding. It is also unknown if Vac17 binds Myo2 or Vac8 first. It is also possible that

additional binding partners or membrane structures, such as structural and signaling lipids, could stabilize the complex at the leading edge of the vacuole.

After proper delivery of the vacuole, the membrane structure between mother and daughter vacuole, known as the segregation structure, resolves. The segregation structure may either be a long tubule, or several small vacuoles strung together (Weisman, 2003). It is still unknown what regulates the resolution of the segregation structure, both in timing its resolution, as well as physically disconnecting the mother and daughter vacuoles. It is possible that there is a mechanism for fission, or release between two tethered vesicles.

Furthermore, there are still open questions as to how Myo2 releases the vacuole. Although previous work showed that Cla4 phosphorylates Vac17, it is unclear how this phosphorylation event regulates the ubiquitylation of Vac17. This phosphorylation event could be changing Vac17 conformation to reveal a ubiquitylation site, or it may be recruiting a binding partner that activates Dma1 E3 ligase activity. After the ubiquitylation of Vac17, it is unknown how the Myo2/Vac17/Vac8 complex dissociates. Vac17 could be immediately degraded or could be detached from either Myo2 or Vac8 before being delivered to the proteasome. It is also unclear how Yck3 and Vps41 are acting to regulate this step. Further studies into these mechanisms will reveal how cargo transport is regulated in cells.

It is tempting to speculate that the mechanisms we discover in yeast will be applicable to mammalian cells and disease. Very little is known about how cargoes are released from their motors, in any organism. Yet, it is highly likely that the release of cargoes is important for animal physiology. For example, phosphorylation of the kinesin motor KIF17 may be important for the loading and unloading of NMDA receptors, and thus synaptic plasticity (Yin et al., 2012).

Additionally, Melanophilin is ubiquitylated and this ubiquitylation is enhanced in the absence of Rab27a (Park et al., 2019b), suggesting that adaptors are more stable in their motor-adaptor complex. Thus, general themes of how cargoes released from the motor and how motor-adaptor complexes are regulated are likely conserved.

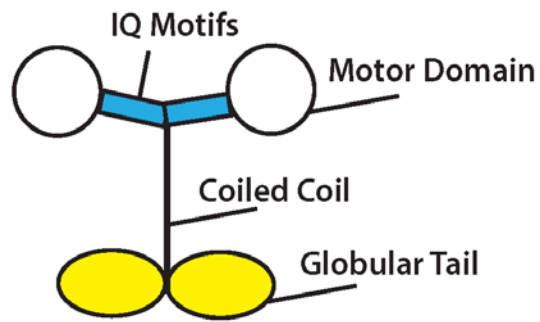


Figure 1.1. Myosin V is composed of several unique domains.

The myosin V monomer dimerizes via the coiled-coil domain. The motor domain is the site of ATP hydrolysis. The IQ motifs bind calmodulin. The globular tail domain binds cargo-specific adaptors.

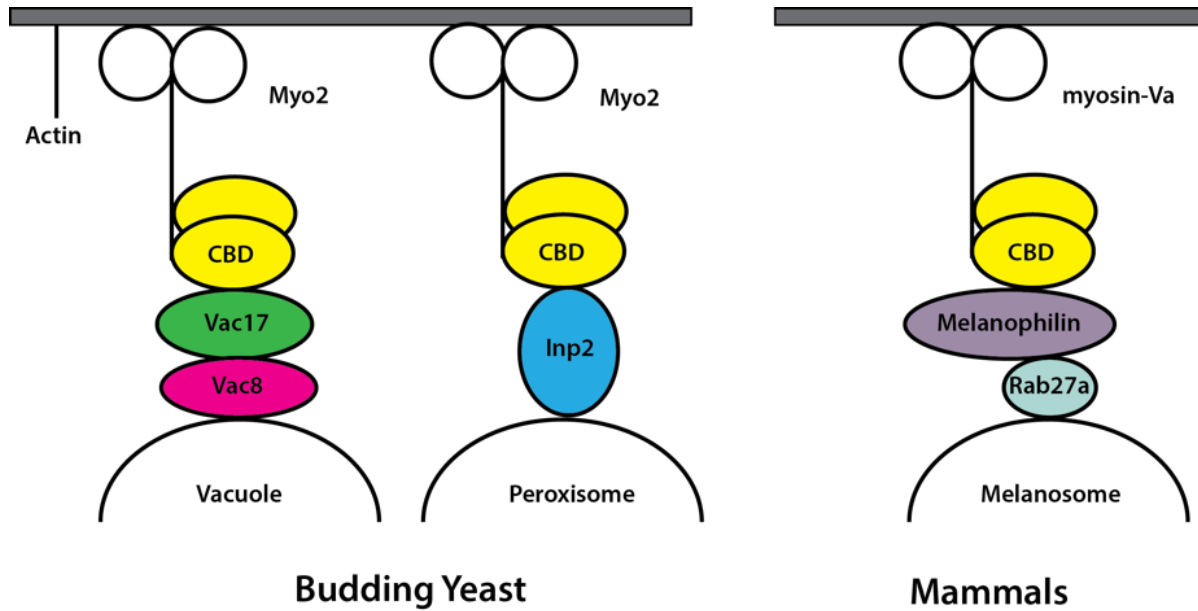


Figure 1.2. The use of adaptor proteins is conserved across organelles and organisms. Myosin V attaches to cargo through cargo-specific adaptor proteins. For example, in yeast, Myo2 can attach to the vacuole via Vac17 and Vac8. If Myo2 is instead bound to Inp2, it will transport peroxisomes. While adaptor proteins are not conserved, mammalian myosin V also attaches to cargoes via adaptors. For example, myosin Va attaches to melanosomes via Melanophilin and Rab27a.

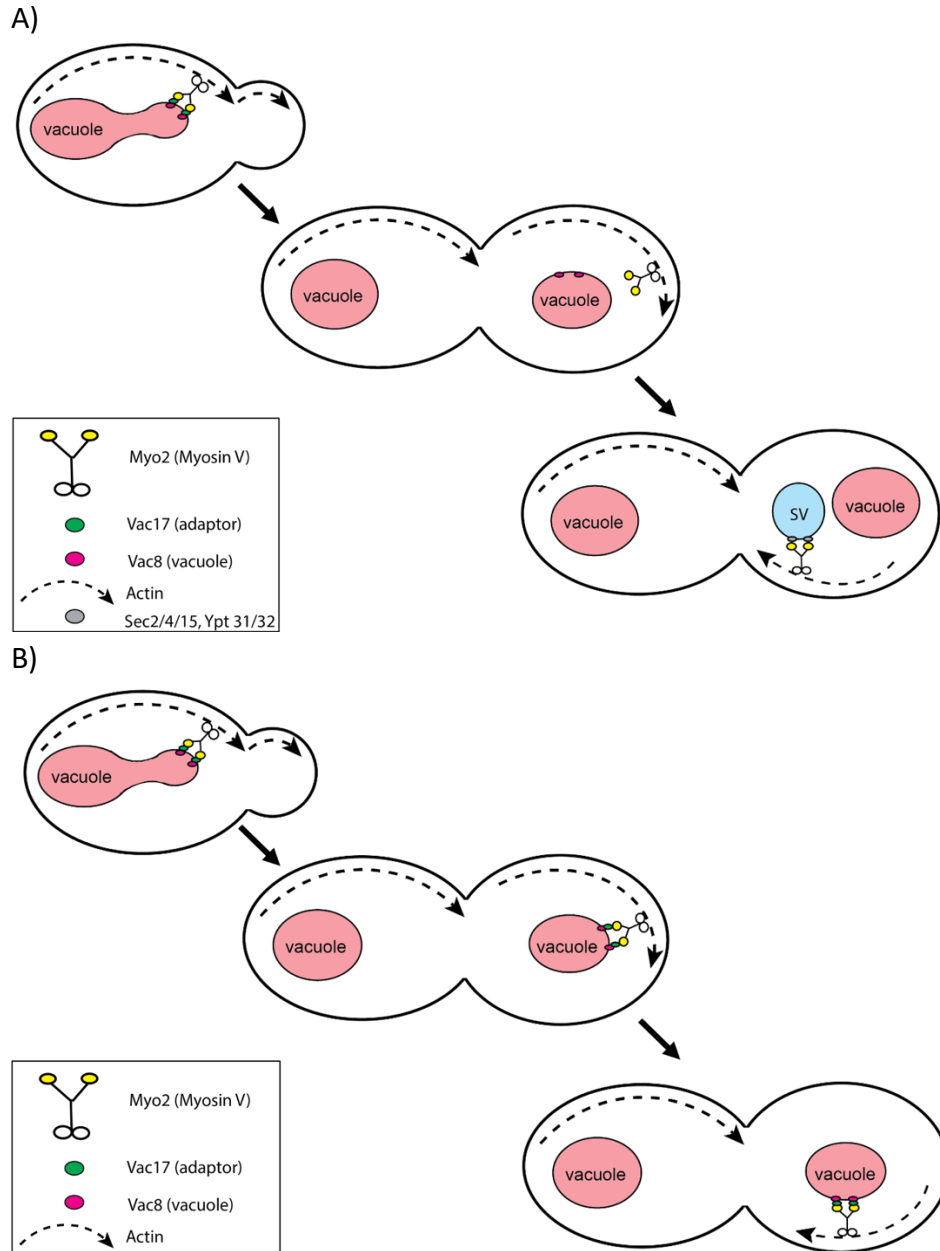


Figure 1.3. Vacuole transport is coordinated during yeast budding.

A) Early in the cell cycle, Vac17 binds to Myo2 and Vac8, allowing Myo2 to bring a portion of the vacuole into the bud. Later in the cell cycle, Vac17 is degraded and the vacuole is released from Myo2. When the actin cytoskeleton reorganizes to the mother-bud neck, Myo2 transports different cargo, such as secretory vesicles (SV).

B) In mutants that are defective in the degradation of Vac17, there are also defects in the termination of vacuole transport. The initiation of transport occurs as normal. However, Vac17 is not degraded and Myo2 does not release the vacuole. Thus, Vac17 and the vacuole accumulate at the bud tip or mother-bud neck.

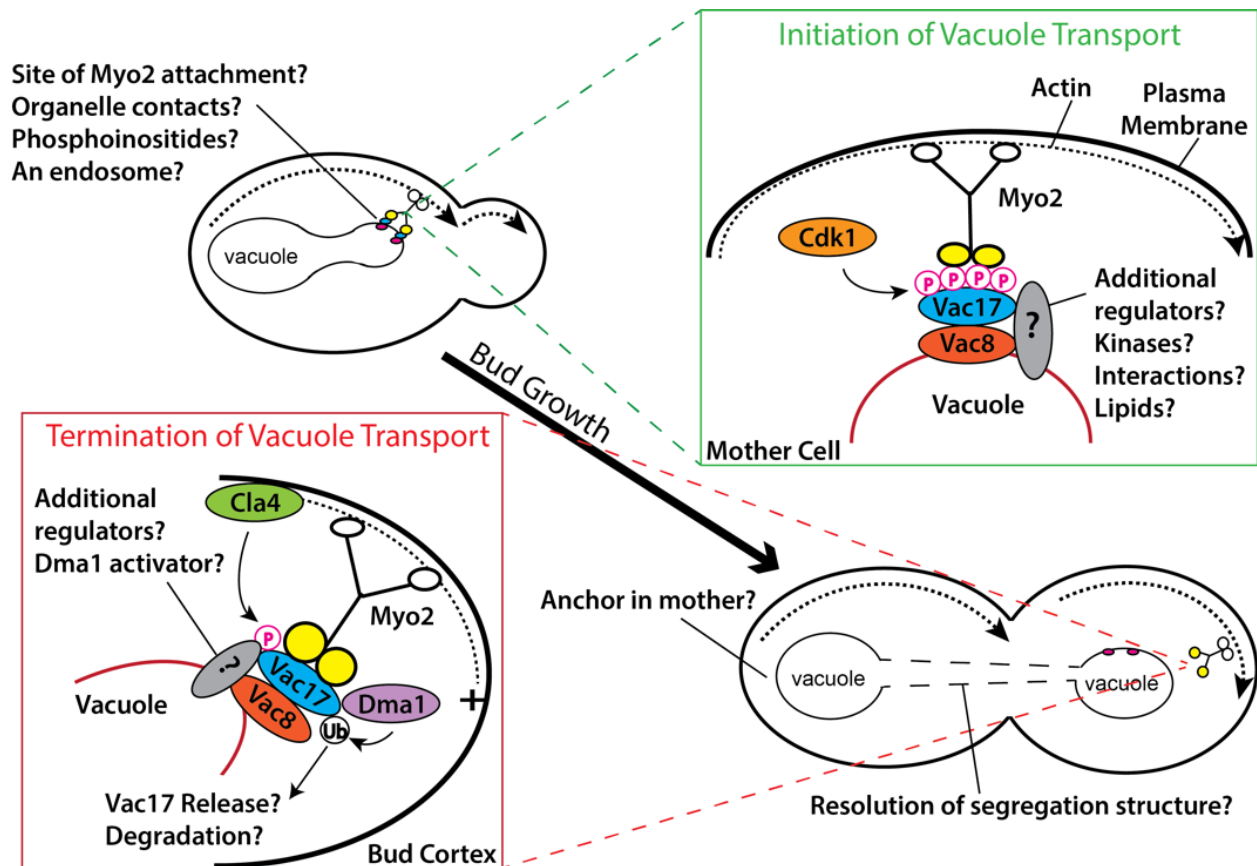


Figure 1.4. Insights into vacuole transport may reveal mechanisms of motor-based cargo transport.

Many open questions about yeast vacuole transport remain. Uncovering mechanistic details about how myosin V moves the vacuole in yeast may reveal key regulatory pathways that are also important for human cells, and thus disease.

CHAPTER II

SPATIAL REGULATION OF ORGANELLE RELEASE FROM MYOSIN V TRANSPORT BY P21- ACTIVATED KINASES

The work in this chapter was previously published as follows: Yau*, R.G., Wong*, S., and Weisman, L.S. (2017) Spatial regulation of organelle release from myosin V transport by p21-activated kinases. *J Cell Biol.* Jun 5;216(6):1557-1566. doi: 10.1083/jcb.201607020. Epub 2017 May 11. * indicates equal contribution.

S. Wong contributed in writing part of the manuscript and revisions, strain generation, and performing experiments represented in Figures 2.1, 2.2, 2.4, 2.5, 2.7, 2.8, and 2.9.

Introduction

Myosin V motors transport organelles to their correct intracellular locations. Transport initiates when myosin V binds cargo specific adaptors and attaches to organelles (Knoblauch and Rachubinski, 2016; Weisman, 2006; Westermann, 2014). Upon arrival at their correct locations, organelles detach from myosin V, thereby terminating transport. The molecular mechanisms that signal the arrival of organelles at their correct locations remain unclear.

At the beginning of the cell cycle in *S. cerevisiae*, the myosin V motor, Myo2, binds the vacuole adaptor, Vac17, and transports a portion of the mother vacuole into the bud (Fusheng Tang, 2003; Ishikawa et al., 2003). In the bud, the vacuole is released from Myo2 and Vac17 is degraded (Fusheng Tang, 2003). Degradation of Vac17 requires phosphorylated Vac17-T240, which recruits the E3 ubiquitin ligase, Dma1. Dma1 then ubiquitylates Vac17, targeting Vac17 for degradation by the proteasome (Yau et al., 2014). Late in the cell cycle, Myo2 transports secretory vesicles, but not the vacuole, to the mother-bud neck (Govindan et al., 1995; Pruyne et al., 1998; Schott et al., 1999). In mutants defective in the degradation of Vac17, the vacuole remains attached to Myo2 and is inappropriately transported to the mother-bud neck late in the cell cycle (Fusheng Tang, 2003; Yau et al., 2014).

In yeast, the p21-activated kinases (PAKs) Cla4 and Ste20, localize to the bud cortex and regulate several cell cycle related processes including actin cytoskeleton polarization, septin ring assembly, and cytokinesis (Boyce and Andrianopoulos, 2011; Cvrckova et al., 1995; Kumar et al., 2009; Peter et al., 1996). Moreover, it was proposed that PAKs indirectly regulated vacuole inheritance via Lte1, a Cla4-activated guanine nucleotide exchange factor (Bartholomew and Hardy, 2009).

Here, we report that PAKs directly phosphorylate Vac17 to signal the arrival of the vacuole at its correct location. We show that before the termination of vacuole inheritance, the vacuole extends to the bud cortex where Vac17 colocalizes with Cla4. In contrast to the previous study, we find that neither degradation of Vac17 nor termination of vacuole transport require Lte1. Instead, Cla4 directly phosphorylates Vac17-S222. This phosphorylation event is required for Dma1-dependent ubiquitylation and degradation of Vac17, and the release of the vacuole from Myo2. Moreover, in a Vac17 mutant that cannot be phosphorylated at S222, the vacuole remains attached to the bud cortex, which suggests that this is the intracellular location where Cla4 phosphorylates Vac17. Together, these studies suggest that at the bud cortex, Cla4 initiates a signaling cascade to regulate the ubiquitylation of Vac17 and complete the termination of vacuole transport, thereby ensuring that the vacuole is deposited at the correct intracellular location.

Results

PAKs are required for Vac17 degradation and the termination of vacuole transport

A previous study suggested that Lte1 regulated Vac17 degradation (Bartholomew and Hardy, 2009). However, it was unknown whether Lte1 directly regulates the termination of vacuole transport. To investigate whether Lte1 acts in this pathway, we tested the *lte1Δ* mutant for the stabilization of Vac17-GFP and the mislocalization of Vac17-GFP and the vacuole to the mother-bud neck in large-budded cells. However, these defects were not observed in the absence of *LTE1* (**Figure 2.1A-C**). We then measured the impact of PAK function on vacuole inheritance. Vac17 levels were not detectably elevated in the *cla4Δ* or *ste20Δ* mutants. Furthermore, only a partial defect in the termination of vacuole was observed, whereby Vac17-

GFP and the vacuole colocalized at the bud tip and mother bud neck in some large-budded cells. These phenotypes were more prominent in the *cla4Δ* mutant (**Figure 2.1D-F**).

Because PAKs are functionally redundant and synthetically lethal, we performed experiments in the *ste20Δ cla4^{ts}* double mutant (Cvrckova et al., 1995; Holly and Blumer, 1999; Martin et al., 1997; Tatebayashi et al., 2006). At 24°C, the levels of Vac17 in the *ste20Δ cla4^{ts}* mutant were similar to wild type levels. In contrast, at 37°C, Vac17 is stabilized and exhibits an increase in electrophoretic mobility, which suggests a loss of post-translational modifications (**Fig 2.2A**). In the *ste20Δ cla4^{ts}* mutant at 24°C, there was partial mislocalization of the vacuole with Vac17-GFP, consistent with the earlier result that the *ste20Δ* mutant has a minor defect in the termination of vacuole transport. In large-budded *ste20Δ cla4^{ts}* cells at 37°C, Vac17-GFP and the vacuole accumulated at the mother-bud neck, similar to the *dma1Δ dma2Δ* mutant (Yau et al., 2014). Intriguingly, we also observed Vac17 and the vacuole at a new aberrant location: the bud tip. This raises the possibility that the bud cortex is the landmark where Myo2 releases the vacuole. In addition, Vac17-GFP and the vacuole mis-localized to the cell cortex at a site adjacent to the mother-bud neck (a location on the cortex between the bud tip and mother-bud neck). This localization had not been previously reported for the vacuole or Myo2 (**Fig 2.2B-C**). The mis-localization of the vacuole to this site may be caused by defects in the organization of the actin cytoskeleton in the *ste20Δ cla4^{ts}* mutant (Holly and Blumer, 1999).

To test if PAK function is required to detach the vacuole from Myo2, we analyzed colocalization between Myo2-Venus and the vacuole in large-budded cells. In wild type cells at 24°C and 37°C the vacuole detached correctly and did not colocalize with Myo2-Venus. In the *ste20Δ cla4^{ts}* mutant at 24°C, there was a modest defect in the termination of vacuole

transport. At 37°C in the *ste20Δ cla4^{ts}* mutant, there is a strong defect in the detachment of the vacuole from Myo2-Venus. The vacuole colocalized with Myo2-Venus at the bud tip, mother-bud neck, and adjacent to the mother-bud neck (**Fig 2.2D-E**). These observations suggest that PAK-dependent signaling regulates Vac17 levels, the release of the vacuole from Myo2 and the termination of vacuole transport.

Cla4 phosphorylates Vac17 in vivo and in vitro

That PAKs regulate Vac17 levels independently of Lte1 suggests that PAKs directly target Vac17. In support of this hypothesis, recombinant GST-Cla4, but not GST alone, binds Vac17-TAP from cell extracts (**Fig 2.3A**). Cla4 phosphorylates serines within the consensus motif RxS (Mok et al., 2010; Versele and Thorner, 2004; Wu et al., 1996). Interestingly, Vac17-S222 matches this motif, Vac17-R₂₂₀LS₂₂₂, and is required for Vac17 degradation and the termination of vacuole transport (Yau et al., 2014). To determine whether Vac17-S222 is a Cla4 phosphorylation site, we generated a phospho-specific antibody for Vac17-pS222 and tested it against Vac17-GFP and *vac17-S222A-GFP* expressed in *vac17Δ* or *dma1Δdma2Δvac17Δ* mutants. Deletion of *DMA1* and *DMA2* stabilizes phosphorylated Vac17, thereby facilitating its detection (Yau et al., 2014). The anti-pS222 antibody recognized Vac17-GFP, but not *vac17-S222A-GFP* (**Fig 2.3B**). Furthermore, this antibody does not recognize de-phosphorylated Vac17-GFP, indicated by an increase in electrophoretic mobility, in λ-phosphatase treated samples (**Fig 2.3C**). These results demonstrate the specificity of this antibody for Vac17-pS222 and that Vac17-S222 is phosphorylated *in vivo*.

To test whether PAK activity is required for the phosphorylation of Vac17-S222 *in vivo*, we analyzed Vac17-S222 phosphorylation in the *ste20Δ cla4^{ts}* mutant. Inactivation of PAK activity reduced phosphorylation of Vac17-S222. This result suggests that PAK activity is required for the phosphorylation of S222 *in vivo*. Phosphorylation of T240 may have been slightly affected by reduced pS222 or by indirect effects of the *ste20Δ cla4^{ts}* mutant (**Fig 2.3D-E**).

Since Vac17-S222 matches the Cla4 consensus site, we tested whether Cla4 directly phosphorylates Vac17. We performed *in vitro* kinase assays using recombinant GST-Cla4 and a 6xHIS-Vac17(96-355) peptide. Phosphorylation was detected via immunoblotting with the anti-pS222 antibody. GST-Cla4, but not kinase-dead *GST-cla4-K594A*, phosphorylated 6xHIS-Vac17(96-355) in an ATP dependent manner. Additionally, the antibody did not recognize products of this reaction if the 6xHIS-*vac17-S222A*(96-355) peptide was used (**Fig 2.3F**). Together, these results demonstrate that Cla4 directly phosphorylates Vac17-S222.

Phosphorylation of Vac17-S222 is required for the termination of vacuole transport

To gain insight into the role of Vac17-pS222, we tested the termination of vacuole transport in cells expressing the non-phosphorylatable *vac17-S222A-GFP* mutant. In large budded cells, *vac17-S222A-GFP* mis-localized with the vacuole at the mother-bud neck similar to *vac17-T240A-GFP*. Upon closer analysis, both *vac17* mutants also accumulated with the vacuole at the bud tip in large budded cells before re-localizing to the mother-bud neck, as seen in the *ste20Δ cla4^{ts}* mutant. In contrast, the vacuole was properly localized in the bud and no GFP signal was detected in cells expressing Vac17-GFP (**Fig 2.4A-B**). These results demonstrate

that phosphorylation of Vac17-S222 is required to terminate vacuole transport and supports the hypothesis that termination of transport initiates at the bud tip. In addition, the localization of Myo2 was not perturbed by the mis-localization of the vacuole (**Fig 2.4C-E**) or Vac17 (**Fig 2.4F-H**) in the *vac17-S222A-GFP* and *vac17-T240A-GFP* mutants. This suggests that the trajectory of Myo2 is not dictated by its bound cargoes.

Vac17-pS222 is required for the ubiquitylation of Vac17

The termination of vacuole transport occurs in regulated steps: (1) Vac17-T240 is phosphorylated, (2) Dma1 is recruited to the vacuole, (3) Dma1 ubiquitylates Vac17, and (4) Vac17 is degraded to release the vacuole from Myo2 (Yau et al., 2014). Since Vac17-S222 is required for the termination of vacuole transport, we tested whether Vac17-S222 functions at any of the above known steps. Immunoblotting with the anti-pT240 antibody demonstrated that Vac17-GFP and *vac17-S222A-GFP*, but not *vac17-T240A-GFP* were phosphorylated at T240. Conversely, Vac17-GFP and *vac17-T240A-GFP*, but not *vac17-S222A-GFP*, were phosphorylated at S222 (**Fig 2.5A-B**). These results demonstrate that phosphorylation of Vac17-S222 and Vac17-T240 occur independently of each other and are consistent with the trend of reduced Vac17-S222 phosphorylation during PAK inactivation (**Fig 2.3D-E**).

To determine whether Vac17-S222 is required for the recruitment of Dma1 we tested the localization of Dma1-GFP during vacuole transport. We observed Dma1-3xGFP at the bud vacuole in the majority of small budded cells expressing *vac17-S222A*, similar to wild type. This contrasts with the *vac17-T240A* mutant, which is defective in Dma1 recruitment (**Fig 2.5C-D**).

That Dma1 is recruited to the vacuole in cells expressing *vac17-S222A* is consistent with the observation that *vac17-S222A* does not impair phosphorylation of Vac17-T240.

Since recruitment of Dma1 to the vacuole is unperturbed in the *vac17-S222A* mutant, we predicted that *vac17-S222A* would be ubiquitylated similar to wild type. To test this hypothesis, *VAC17-GFP* or *vac17-S222A-GFP* were overexpressed in *vac17Δ* cells along with *myo2-D1297N*, a mutant defective in binding Vac17 (Ishikawa et al., 2003). The *myo2-D1297N* mutant was included because overexpression of *vac17-S222A-GFP* likely interferes with the ability of Myo2 to transport essential cargoes (Eves et al., 2012) and did not yield viable cells. Cells were also transformed with a plasmid encoding Myc-ubiquitin driven under an inducible promoter. GFP tagged Vac17 constructs were immunoprecipitated and ubiquitylation was detected via immunoblotting with anti-Myc antibodies. Surprisingly, *vac17-S222A-GFP* was not ubiquitylated *in vivo* (**Fig 2.5E**). These findings indicate that phosphorylation of Vac17-S222 is not required for the recruitment of Dma1 to the vacuole transport complex, but must occur before Dma1 can ubiquitylate Vac17. Thus, phosphorylation of Vac17-S222 may spatially regulate the termination of vacuole transport through regulating Dma1 activity.

Cla4 signaling at the bud cortex initiates the release of the vacuole from Myo2

Cla4 localizes to the bud cortex of small-budded cells and later appears as a punctum on the vacuole in large-budded cells (Bartholomew and Hardy, 2009). To further analyze Cla4 localization in relation to vacuole transport, we performed time-lapse microscopy of cells expressing Cla4-3xGFP and the vacuole marker Vph1-mCherry. In small budded cells, Cla4-3xGFP appears on the bud cortex, as previously described in (Bartholomew and Hardy, 2009). A

portion of the vacuole then enters the bud and extends to the bud cortex, where it colocalizes with Cla4. A punctum of Cla4 then moves onto the vacuole (**Fig 2.6**). These observations suggest that arrival of the vacuole at the bud cortex initiates Cla4 signaling on the vacuole. Additionally, Cla4 activity is required for proper unloading of the vacuole from Myo2. In a wild type cell, Vac17-GFP is barely visible and the vacuole is in the center of the cell (**Fig 2.7A**). In the non-phosphorylatable *vac17-S222A* mutant, the vacuole and *vac17-S222A-GFP* persist at the bud tip and eventually move from the bud tip to the mother-bud neck (**Fig 2.7B**). In further support that Cla4 is acting at the cortex, we find that the Cla4 homologue, Ste20 partially substitutes for Cla4 (**Fig 2.1D-E**), yet Ste20 is solely at the bud cortex (Peter et al., 1996; Takahashi and Pryciak, 2007). Together, these findings suggest that PAKs signal the release of the vacuole from Myo2 at the bud cortex.

To determine if Cla4 and Vac17 colocalize at the bud cortex, we analyzed the localization of Cla4-tdTomato and Vac17-GFP expressed in the *cla4Δvac17Δ* mutant via synchronization with α -factor and imaging at 10 minute intervals. At 50 minutes after release, Cla4-tdTomato and Vac17-GFP co-localized at the bud cortex. At 80 minutes after release, Vac17-GFP was no longer detected, which is consistent with the degradation of Vac17 (Fusheng Tang, 2003; Peng and Weisman, 2008). Additionally, even though Vac17 was degraded, a punctum of Cla4 was observed on the vacuole as previously described (Bartholomew and Hardy, 2009) (**Fig 2.8A** and **Fig 2.9**). We then analyzed the dynamics of Cla4-tdTomato and *vac17-S222A-GFP*. In contrast to wild type, Cla4 and Vac17 colocalized 60 minutes after release. At 80 minutes after release, *vac17-S222A-GFP* accumulated with the vacuole at the bud tip while a punctum of Cla4 localized to a different area of the vacuole. At 120 minutes after release, *vac17-S222A-GFP* mis-

localized with the vacuole at the mother-bud neck (**Fig 2.8B** and **Fig 2.9**). These data suggest that a transient interaction between Cla4 and Vac17 at the leading edge of the vacuole occurs after the vacuole reaches the bud cortex. Moreover, when Cla4 fails to phosphorylate *vac17-S222A*, *vac17-S222A* and the vacuole persist at the bud cortex before mis-localizing to the mother-bud neck (**Fig 2.8B and 2.8B**). These data suggest that Cla4 phosphorylates Vac17-S222 upon arrival of the vacuole at the bud cortex, triggering Vac17 degradation and release of the vacuole from Myo2.

Discussion

These studies reveal that Cla4 provides spatial control for the termination of vacuole transport (**Fig 2.10**). Our studies indicate that the bud cortex is the landmark that signals the successful delivery of a myosin V cargo to its correct intracellular location. We show that contact between Cla4 and Vac17 at the bud cortex (**Fig 2.6**) initiates the termination of vacuole transport. Cla4 directly regulates Vac17 degradation via phosphorylating Vac17-S222 (**Fig 2.3**). Intriguingly, phosphorylation by Cla4 is required for the ubiquitylation and degradation of Vac17 (**Fig 2.4 and 2.5**), but not for the recruitment of Dma1 to the vacuole (**Fig 2.5**). Together, these studies suggest that once the vacuole reaches the bud cortex, Cla4 initiates a signaling cascade that activates Dma1 to ubiquitylate Vac17 and complete the termination of vacuole inheritance. Vac17-S222 phosphorylation may change the conformation of Vac17 so that it is amenable for Dma1-dependent ubiquitylation or recruit a binding partner that activates Dma1. These roles for Cla4 in Myo2 transport suggest a direct molecular link between cell polarity

factors and the positioning of organelles. Our studies reveal that myosin V relies on a spatially regulated signaling cascade to successfully transport of cargoes to their correct destinations.

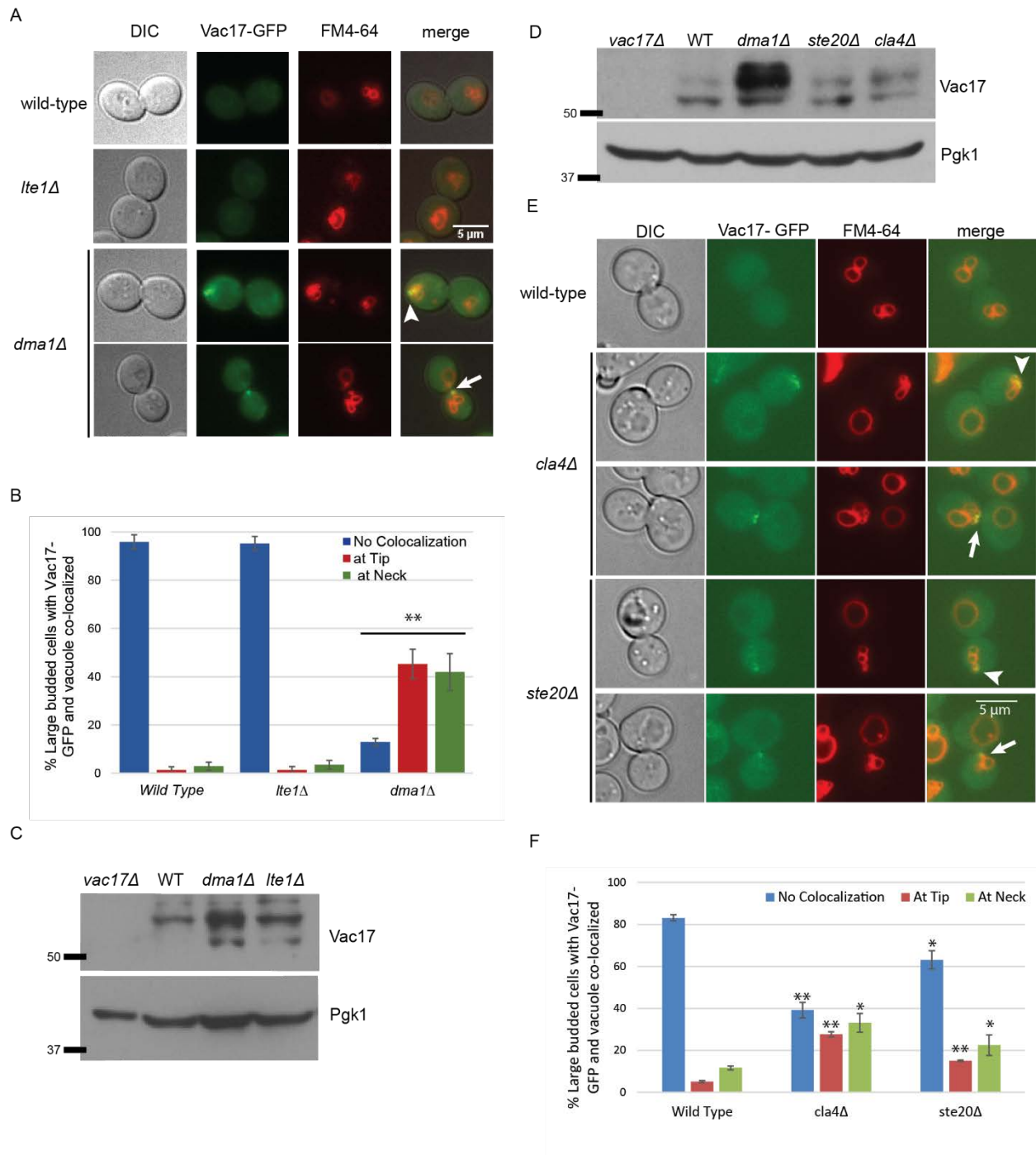


Figure 2.1. Deletion of Cla4 or Ste20 causes a partial defect in the termination of vacuole transport.

A) Large budded *lte1Δ* cells do not exhibit accumulation of the vacuole at the bud tip (arrowhead) and mother-bud neck (arrow) compared to *dma1Δ* cells. Scale bar = 5 μm

B) Quantification of >20 large budded cells per strain per n.

C) The *lte1Δ* mutant does not have elevated levels of Vac17 as indicated by western blot. Pgk1; loading control. Representative of n=3

D) Vac17 levels are similar in wild type, *ste20Δ*, and *cla4Δ* cells. Pgk1; loading control.

E) Large budded *ste20Δ* and *cla4Δ* cells exhibit a partial accumulation of Vac17-GFP and the vacuole at the bud tip (arrowhead) and mother-bud neck (arrow). Scale bar = 5μm

F) Quantification of >50 large budded cells per strain per n. (B, F). Error bars; SEM, n=3. * = p<0.05, ** =p<0.01, two-tailed Student's *t*-test.

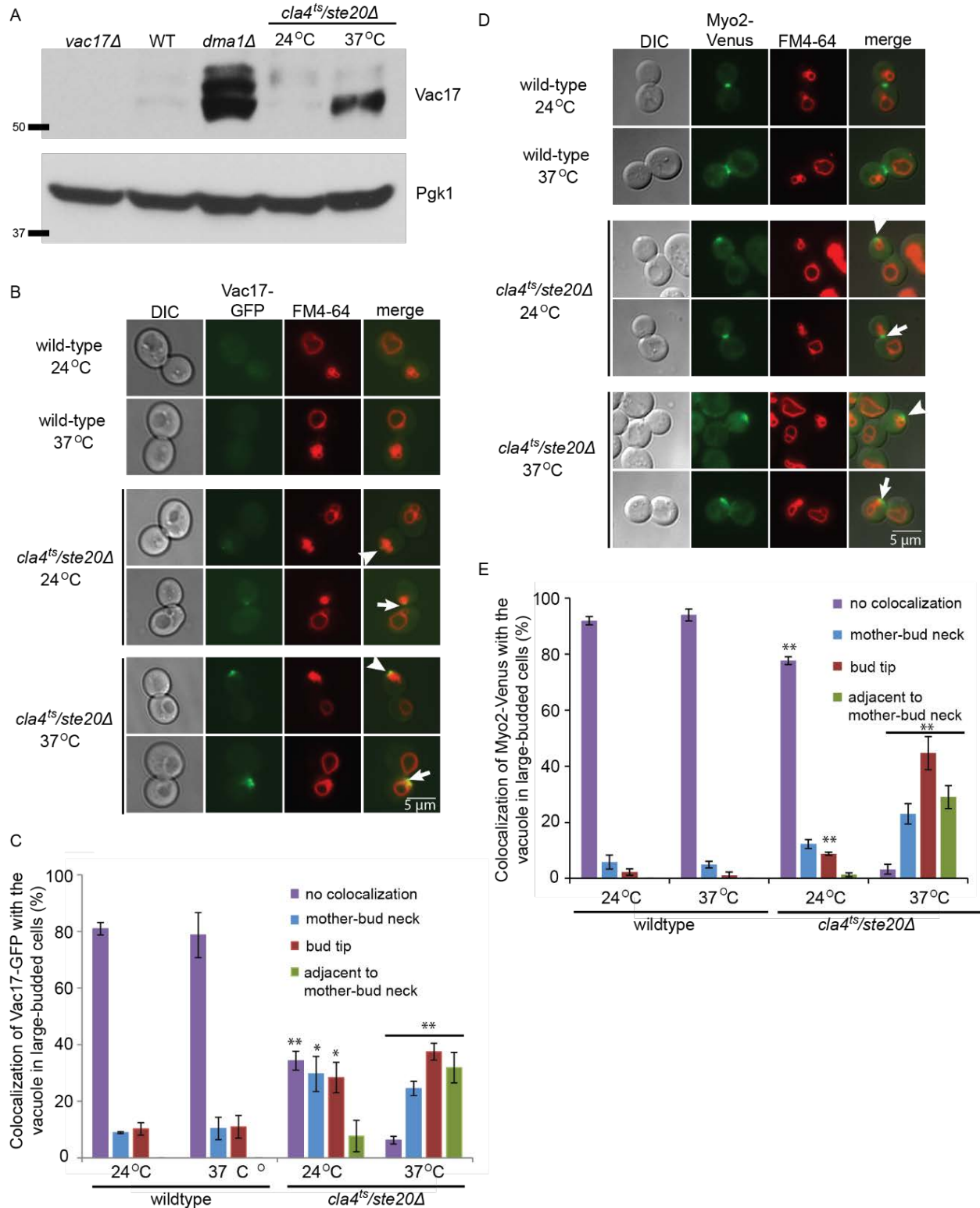


Figure 2.2. PAKs are required for the degradation of Vac17 and the release of the vacuole from Myo2.

A) Vac17 levels are elevated in *dma1Δ* and *ste20Δ cla4^{ts}* mutants. The *ste20Δ cla4^{ts}* mutant was grown at either 24°C or shifted to 37°C for 3 hours prior to lysis. Pgk1; loading control.

B-E) Loss of PAK function results in mis-localization of the vacuole (FM4-64) B, D) and accumulation of Vac17-GFP (B) at the bud tip (arrowheads) or mother-bud neck (arrows). Wild type and *ste20Δ cla4^{ts}* cells transformed with Vac17-GFP (B) or Myo2-Venus (D). After FM4-64 labeling, cells were chased at 24°C for 3 hours or 24°C for 90 minutes and then 37°C for 90 minutes prior to imaging. Scale bar = 5µm.

C, E) Quantification of > 35 large budded cells per condition per n. Error bars; SEM, n=3. * = p<0.05, ** =p<0.01, two-tailed Student's t-test.

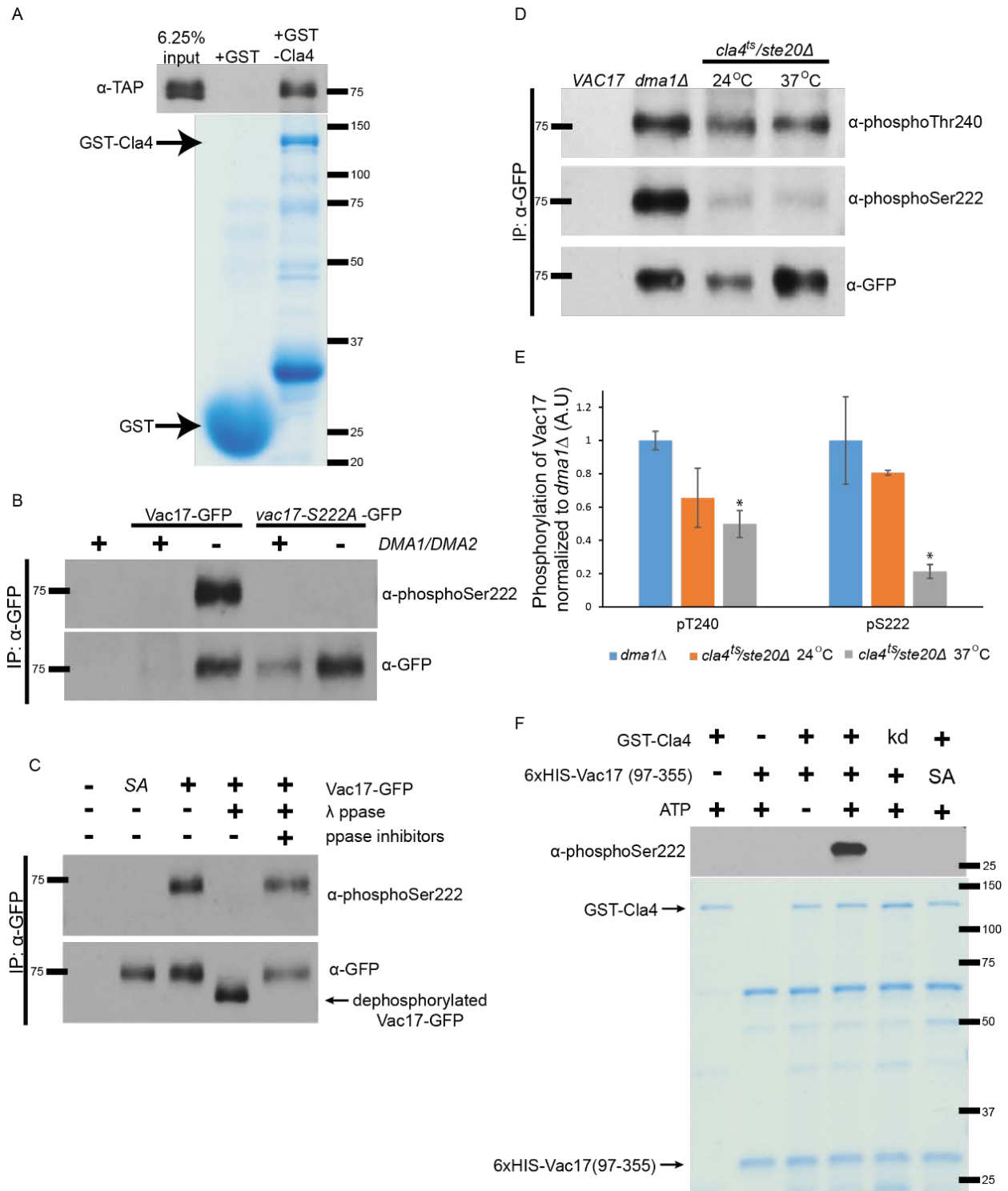


Figure 2.3. Cla4 binds and phosphorylates Vac17.

A) Purified recombinant GST-Cla4, but not GST alone, binds Vac17-TAP from *dma1Δ dma2Δ VAC17-TAP* lysates.

B) The anti-pS222 antibody recognizes wild type Vac17-GFP but not the *vac17-S222A-GFP* mutant.

C) λ -phosphatase treatment causes an increase in the electrophoretic mobility of Vac17-GFP and ablates detection by the anti-pS222 antibody.

D) Inactivation of PAKs decreases the phosphorylation of Vac17-S222 and to a lesser extent, Vac17-T240. Vac17 phosphorylation monitored using anti-pS222 or anti-pT240 antibodies in the *ste20 cla4^{ts}* mutant transformed with Vac17-GFP. Cells were grown at 24°C or shifted to 37°C for 3 hours prior to immunoprecipitation of Vac17-GFP using anti-GFP antibodies. As a positive control, Vac17-GFP immunoprecipitated from a *dma1Δ* mutant is phosphorylated at both sites.

E) Levels of pT240 or pS222 were normalized to GFP and those ratios were normalized to *dma1Δ*. Error bars; SEM, n=2. * = p<0.05, two-tailed Student's t-test.

F) 6xHIS-Vac17 (96-355), but not 6xHIS-*vac17-S222A* (96-355) is phosphorylated by Cla4, but not the kinase dead *cla4-K594A* mutant or in the absence of ATP. Phosphorylation analyzed via immunoblotting with the anti-pS222 antibody.

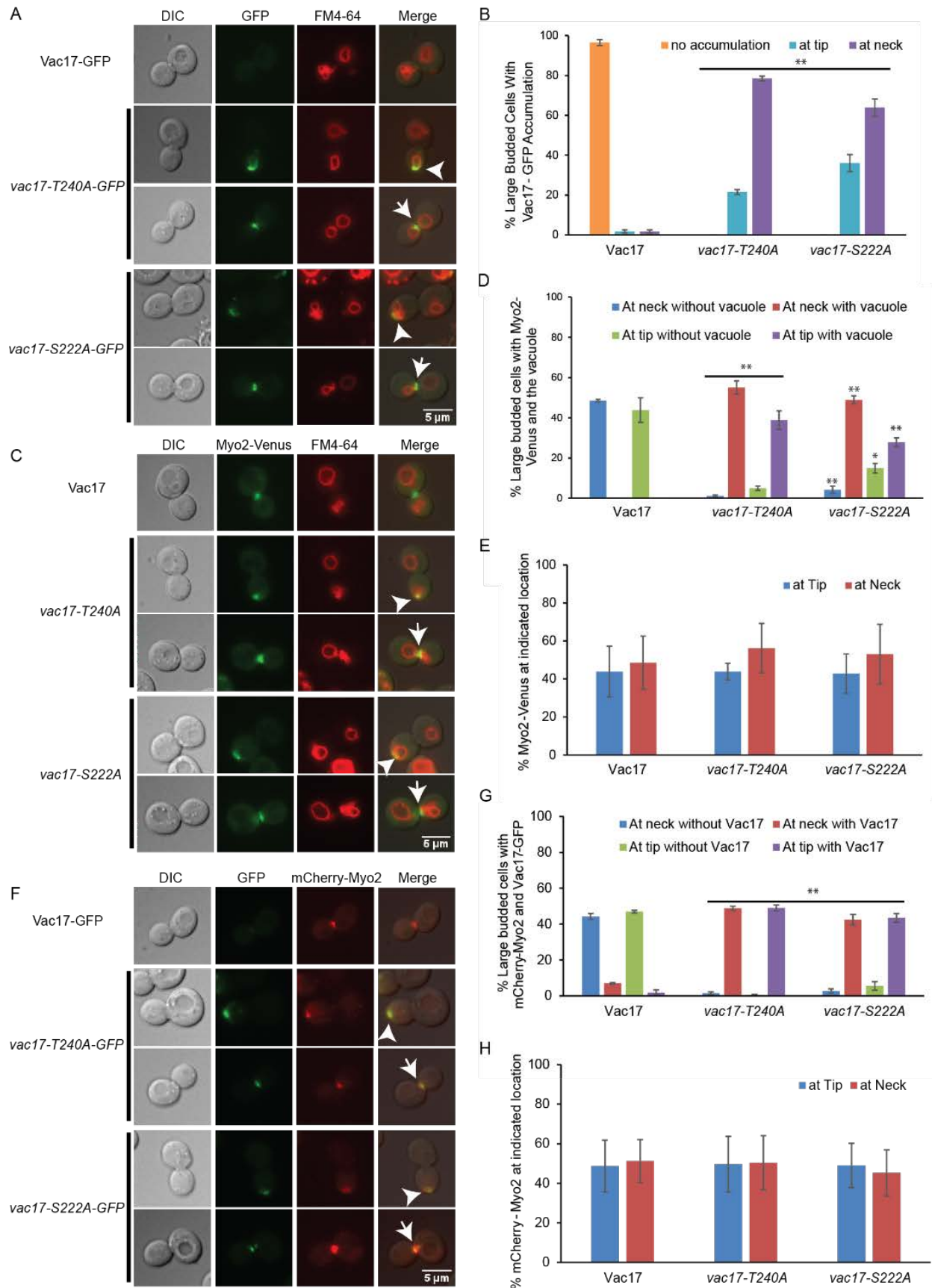


Figure 2.4. Termination of vacuole transport initiates at the bud cortex.

Fluorescence microscopy of a *vac17Δ* strain transformed with plasmids encoding GFP tagged *VAC17* or *vac17* point mutants with or without mCherry or Venus tagged Myo2. Error bars; SEM, n=3. * = p<0.05, ** =p<0.01, two-tailed Student's t-test. Scale bar = 5μm.

A) *vac17-S222A-GFP* and *vac17-T240A-GFP* resulted in mis-localization of the vacuole (FM4-64) to the bud tip (arrowheads) or mother-bud neck (arrows).

B) Quantification of >30 large budded cells per strain per n.

C) Vacuoles colocalize with Myo2-Venus at the bud tip (arrowheads) or mother-bud neck (arrows) in cells expressing *vac17-S222A* or *vac17-T240A*.

D) Quantification of >40 large budded cells per strain per n for the colocalization of Myo2 and the vacuole.

E) Quantification of >40 large budded cells per strain per n for the localization of Myo2.

F) *vac17-S222A-GFP* and *vac17-T240A-GFP* colocalize with mCherry-Myo2 at the bud tip (arrowheads) or mother-bud neck (arrows).

G) Quantification of >58 large budded cells per strain per n for the colocalization of Myo2 and Vac17.

H) Quantification of >58 large budded cells per strain per experiment for the localization of Myo2.

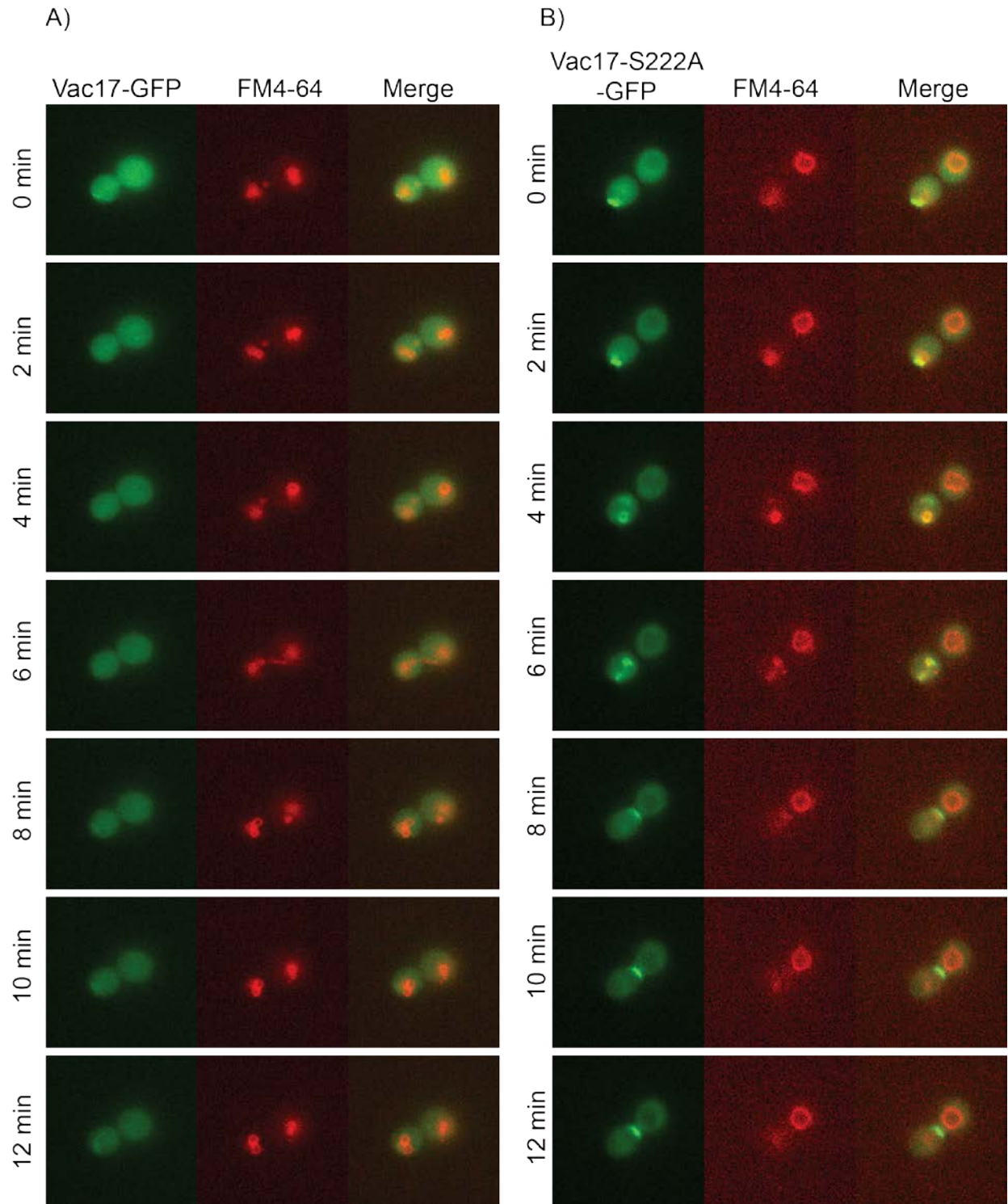


Figure 2.5. *vac17-S222A-GFP* and the vacuole travel from the bud tip to the mother-bud neck. Time lapse microscopy of cells expressing Vac17-GFP (A) or *vac17-S222A-GFP* (B) were labeled with FM4-64 (vacuole,) and imaged every 2 minutes. Representative time lapse from n=3. A) In wild type, Vac17-GFP disappears and the vacuole is in the center of the bud. B) In the *vac17-S222A-GFP* mutant that cannot be phosphorylated, the vacuole and *vac17-S222A-GFP* travel from the bud tip to the mother-bud neck.

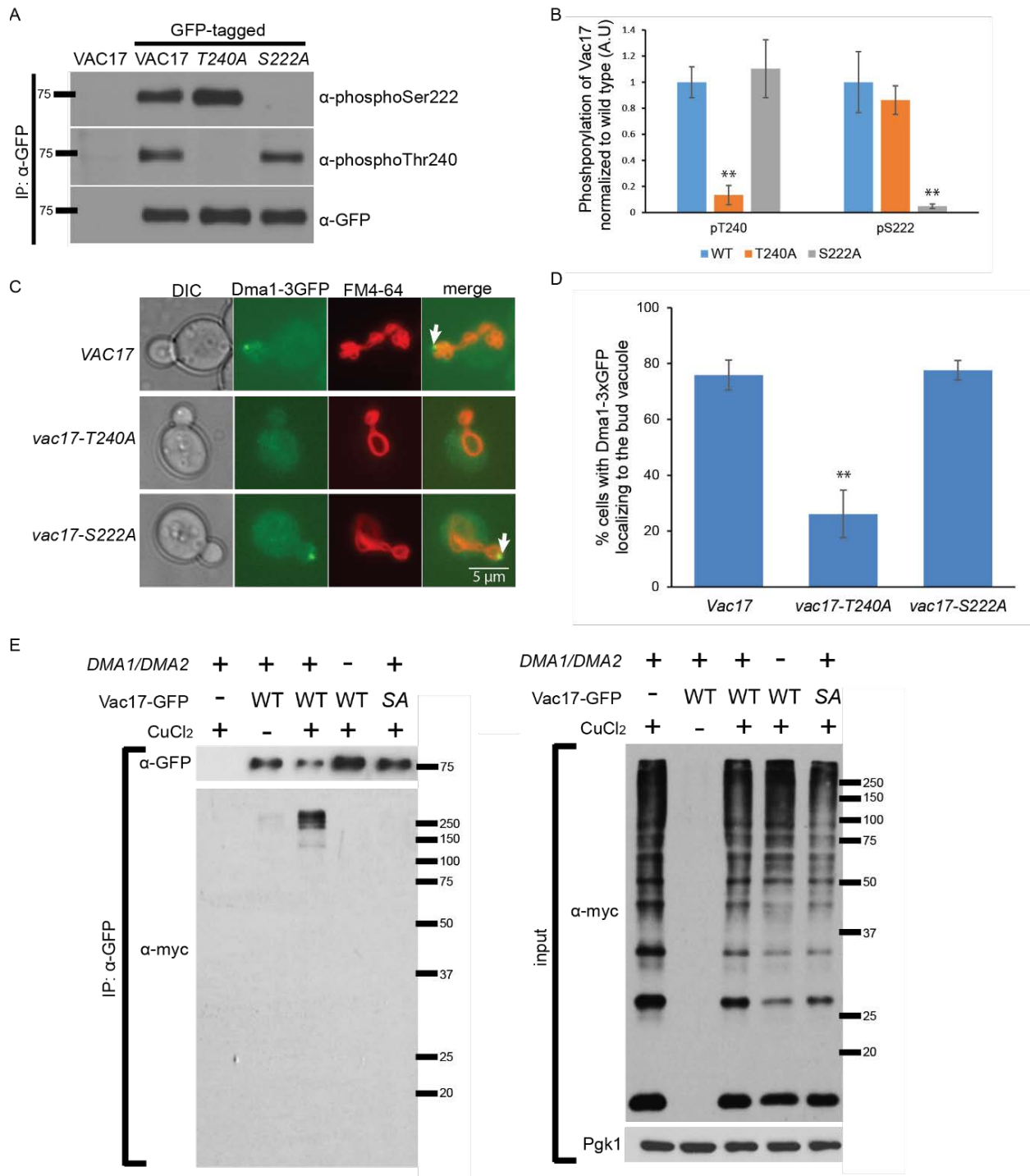


Figure 2.6. Vac17-S222 is required for the ubiquitylation of Vac17.

A) Phosphorylation of Vac17-S222 and Vac17-T240 are independent of each other.

B) Levels of pT240 or pS222 were normalized to GFP and those ratios were normalized to wild type. Error bars; SEM, n=3. ** = p<0.01, two-tailed Student's t-test.

C) Dma1 recruitment to the vacuole (FM4-64) (arrows) does not require Vac17-S222. Wild type *VAC17* or *vac17* point mutants expressed from plasmids in a *DMA-3xGFP vac17Δ* strain. Scale bar = 5μm.

D) Quantification of >21 cells per strain per n. Error bars; SEM, n=3. ** =p<0.01, two-tailed Student's t-test.

E) The *vac17-S222A* mutant is not ubiquitylated *in vivo*. *vac17Δ* and *dma1Δdma2Δvac17Δ* cells were co-transformed with a plasmid encoding myc-ubiquitin under a copper inducible promoter and plasmids encoding GFP tagged *VAC17* or *vac17-S222A*. GFP tagged proteins were immunoprecipitated using anti-GFP antibodies. Ubiquitylation detected via immunoblotting with anti-myc antibody. Pgk1; loading control.

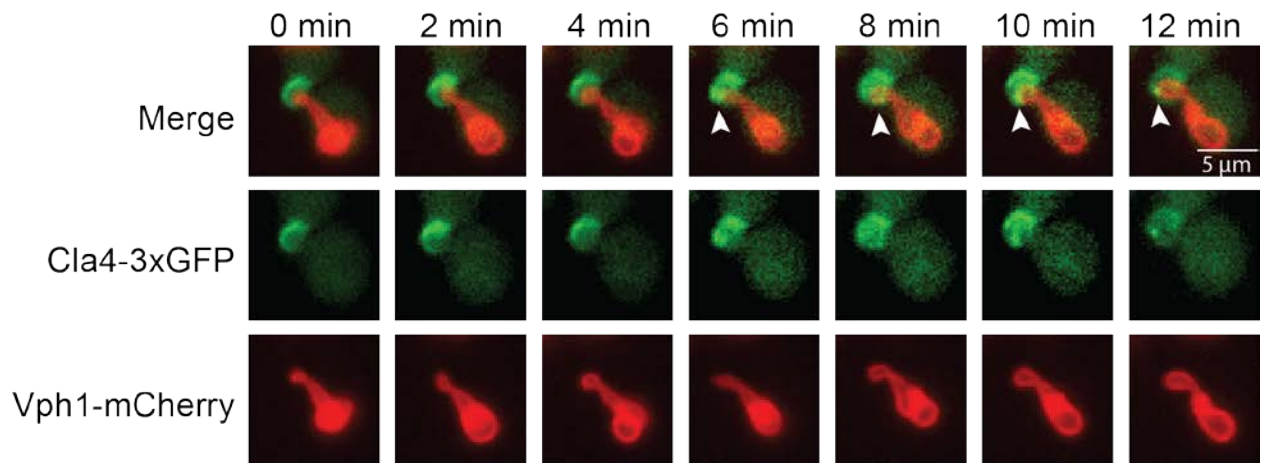


Figure 2.7. Cla4 localizes to the vacuole after the vacuole contacts the bud cortex.

Time lapse microscopy of cells expressing endogenous Cla4-3xGFP and Vph1-mCherry (vacuole) shows that the vacuole extends to the bud cortex and acquires a puncta of Cla4 (arrowheads). Representative time course from n=5. Scale bar = 5 μ m. Note that due to issues with photo bleaching, we chose time courses where the vacuole had crossed the mother-bud neck at time 0.

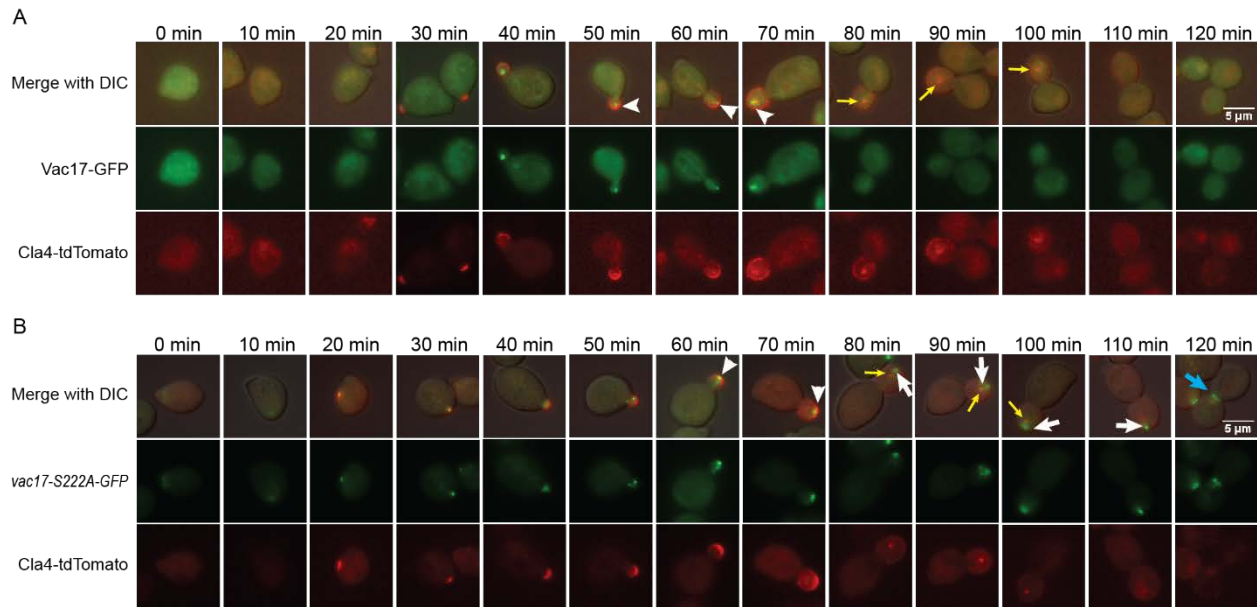


Figure 2.8. The initiation of Cla4 signaling at the vacuole occurs at the bud cortex.

cl4Δvac17Δ mutant transformed with Cla4-tdTomato and either Vac17-GFP or *vac17-S222A-GFP*. Cells synchronized with α -factor were imaged every 10 minutes after release.

Representative images from >25 cells per strain per time point per n. n=3. Scale bar = 5 μ m.

A) Cla4-tdTomato colocalized with Vac17-GFP at the bud cortex (arrowheads). After Vac17-GFP is no longer detected, Cla4-tdTomato is localized away from the cortex (yellow arrow).

B) Cla4-tdTomato and *vac17-S222A-GFP* colocalized at the bud cortex (arrowheads). *vac17-S222A-GFP* persisted at the bud tip (white arrow) and later the mother-bud neck (blue arrow) after Cla4-tdTomato localized to a different location on the vacuole (yellow arrow).

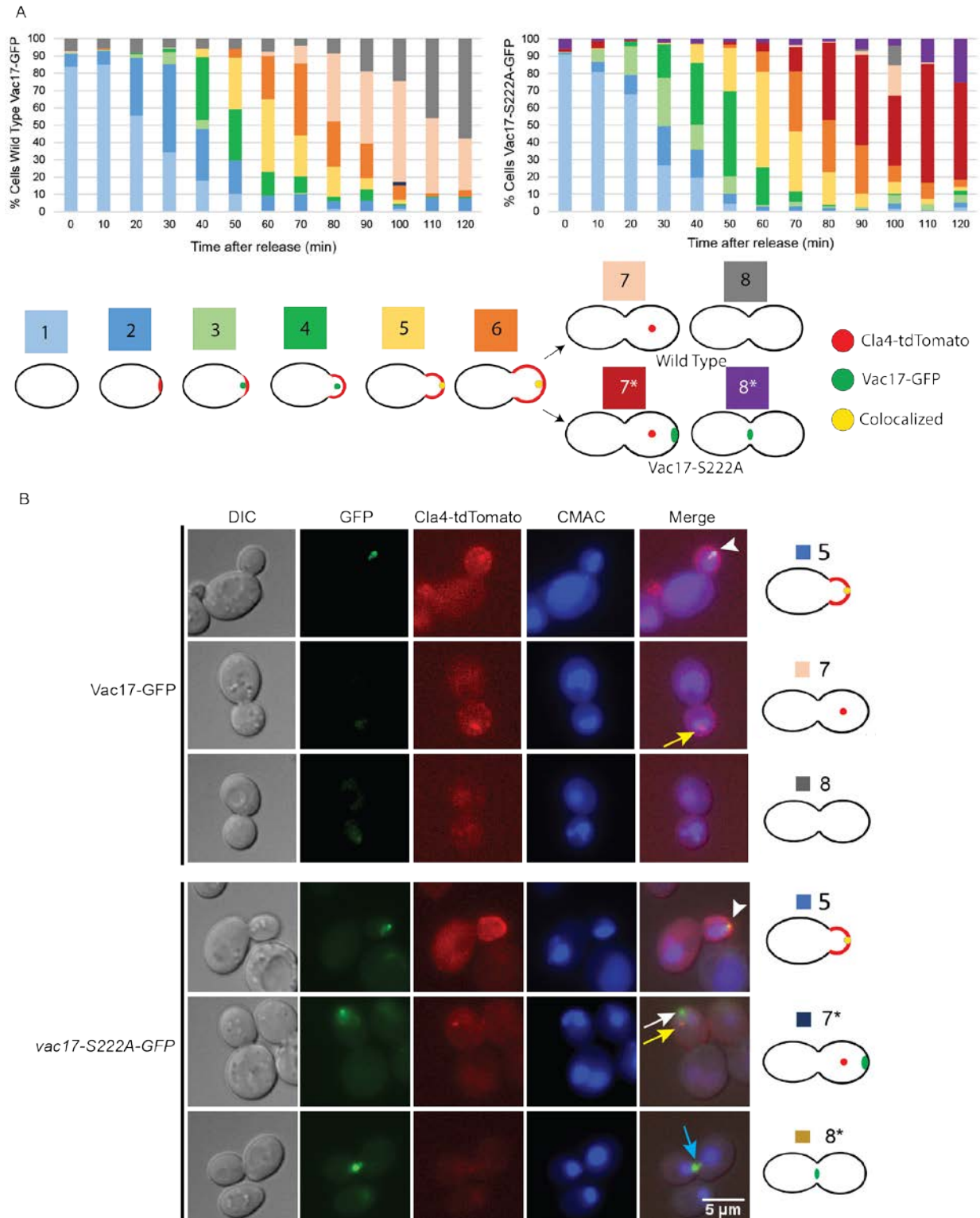


Figure 2.9. Cla4 co-localizes with Vac17 and the vacuole at the bud cortex.

cla4Δvac17Δ mutant transformed with Cla4-tdTomato and either Vac17-GFP or *vac17-S222A-GFP*.

A) Quantification of >25 cells per strain per time point per n, n=3.

B) Cla4-tdTomato colocalized with Vac17-GFP or *vac17-S222A-GFP* and the vacuole (CMAC) in small budded cells (arrowheads). In large budded cells, *vac17-S222A-GFP* colocalized with the vacuole at the bud tip (white arrow) or mother-bud neck (blue arrow), while Cla4-tdTomato localized on the vacuole at a different location (yellow arrow). Representative images of >30 cells per strain per n, n=3. Scale bar = 5 μ m. Schematics in right column refer to time courses in (A).

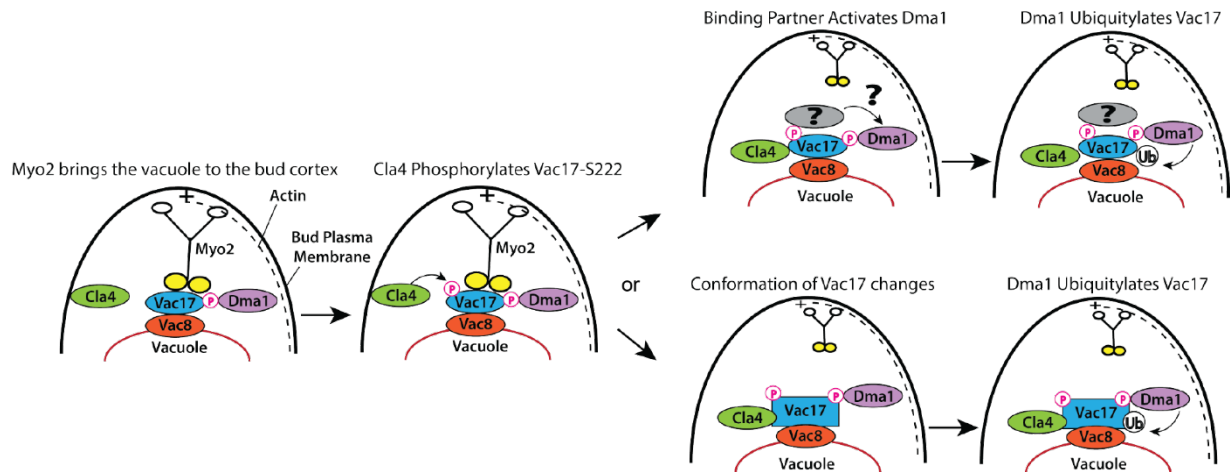


Figure 2.10. Cla4 spatially regulates the ubiquitylation of Vac17

Myo2 brings a portion of the vacuole and Vac17 to the bud cortex where Cla4 phosphorylates Vac17. A punctum of Cla4 then moves onto the vacuole. Cla4-dependent phosphorylation of Vac17 may either recruit a downstream binding partner or change the conformation of Vac17 to facilitate Dma1-dependent ubiquitylation of Vac17 and thus the termination of vacuole transport.

CHAPTER III

CARGO RELEASE FROM MYOSIN V REQUIRES THE CONVERGENCE OF PARALLEL PATHWAYS THAT PHOSPHORYLATE AND UBIQUITYLATE THE CARGO ADAPTOR

The work in this chapter is currently in revision as follows: Wong, S., Hepowit, N.L., Port, S.A., Yau, R.G., Peng, P., Azad, N., Habib, A., Harpaz, N., Schuldiner, M., Hughson, F.M., MacGurn, J.A., and Weisman, L.S. (2020) *Current Biology*, *accepted pending minor revisions*.

S.W. designed the experiments, conducted the experiments, and wrote the paper. N.H. and J.M. conducted the SILAC experiments. S.A.P. and F.M.H. constructed the recombinant Vps41 and designed the purification method. R.G.Y. conducted experiments using the phospho-specific antibodies. Y.P. conducted experiments testing the Yck3 deletion mutant. N.A. conducted experiments testing the Vps39 deletion mutant. A.H. conducted experiments testing Vps41 binding to Vac17. N.H., and M.S. conducted experiments with the Vps41 deletion mutant. L.S.W. designed the experiments and wrote the paper.

Introduction

Myosin V motors transport organelles to their correct intracellular locations. In *Saccharomyces cerevisiae*, a myosin V, Myo2, transports the vacuole (Kent L. Hill, 1996; Natalie L. Catlett, 1998), mitochondria (Simon et al., 1995), peroxisomes (Hoepfner et al., 2001), secretory vesicles (Pruyne et al., 1998), Golgi (Arai et al., 2008), astral microtubules (Hwang et al., 2003; Lee et al., 2000; Liakopoulos et al., 2003; Miller et al., 2000; Yin et al., 2000), and lipid droplets (Knoblach and Rachubinski, 2014) to the bud during cell division. Transport initiates when myosin V binds to cargo-specific adaptors and attaches to organelles (Knoblach and Rachubinski, 2016; Weisman, 2006; Westermann, 2014). Upon arrival at their correct locations, organelles are detached from myosin V, thereby terminating transport.

Vacuole transport in yeast is a highly regulated process. The vacuole-specific cargo adaptor, Vac17, physically links Myo2 to the vacuole (Ishikawa et al., 2003; Tang et al., 2003). Early in the cell cycle, Vac17 is phosphorylated by Cdk1, which facilitates Vac17 association with Myo2 (Peng and Weisman, 2008). Vac17 binds to the vacuole via Vac8, a protein associated with the vacuole membrane, via myristoylation and palmitoylation (Tang et al., 2006; Wang et al., 2001; Yong-Xu Wang, 1998). Formation of the Myo2-Vac17-Vac8 complex bridges the vacuole to Myo2, and allows a portion of the vacuole to be brought into the growing bud. Later in the cell cycle, Myo2 is released from the vacuole via the regulation of Vac17. Upon arrival at the bud cortex, a bud-cortex localized kinase, Cla4, phosphorylates Vac17 (Yau et al., 2017). This spatial cue signals the proper delivery of the vacuole to the bud. Vac17 is then ubiquitinated by the E3 ligase Dma1, which targets Vac17 for degradation by the

proteasome (Yau et al., 2017). In mutants where Vac17 is not degraded, Myo2 is not released from the vacuole (Tang et al., 2003; Yau et al., 2017).

It was previously assumed that ubiquitylation is both necessary and sufficient for the termination of vacuole transport. In that scenario, ubiquitylated Vac17 would be degraded from within the Myo2-Vac17-Vac8 complex and this would be sufficient to release Myo2 from the vacuole. As an alternative, there may be specific mechanisms to dissociate the Myo2-Vac17-Vac8 complex to release Myo2 from the vacuole, and then the released ubiquitylated Vac17 would be degraded by the proteasome.

Here, we report a pathway that functions in parallel with the ubiquitylation of Vac17 to dissociate Vac17 from the Myo2-Vac17-Vac8 complex. We show that the homotypic fusion and protein-sorting (HOPS) subunit, Vps41, regulates an unknown kinase to phosphorylate Vac17. In addition, the vacuole-localized Casein Kinase I, Yck3, is responsible for phosphorylation of a subset of the Vps41-dependent sites and Vps41 may directly regulate Yck3 as well. Importantly, we show that these phosphorylation sites on Vac17 are required for the release of Vac17 and its delivery to the proteasome for its subsequent degradation. However, Myo2 and Vac8 are not degraded and remain in their original locations, sites of polarized growth and the vacuole, respectively. This suggests that Vps41 and Yck3 regulate the dissociation of ubiquitylated Vac17 from the motor-adaptor complex. We find that ubiquitylation of Vac17 can occur independently of phosphorylation of the sites that require Vps41 or Yck3. Conversely, Vps41 and/or Yck3 -dependent phosphorylation can occur without ubiquitylation. However, both the Vps41 and Yck3 -dependent pathways and the ubiquitylation pathway are required together for the vacuole to be released from Myo2 and for Vac17 to be degraded. That parallel pathways

must converge to release Myo2, demonstrates that multiple signals are required to terminate vacuole inheritance. We predict that the association of Myo2 with other cargo adaptors, as well as the association of other myosin V motors with their cargo, undergo similar types of regulation. These studies reveal that the termination of cargo transport is tightly controlled and likely critical to cellular health and function.

Results

Yck3 and Vps41 regulate the termination of vacuole transport

Vac17 is highly phosphorylated (Ishikawa et al., 2003; Peng and Weisman, 2008; Tang et al., 2003; Yau et al., 2014; Yau et al., 2017). Some of the previously identified phosphorylation sites promote the assembly of the Myo2-Vac17-Vac8 complex, while other sites in Vac17 are required for the termination of vacuole transport. We reasoned that currently unknown regulatory sites in Vac17, and/or the discovery of related kinases, have the potential to reveal additional essential steps for the termination of vacuole transport.

We hypothesized that a vacuolar kinase may regulate vacuole transport. Yck3 is one of a few kinases that is constitutively localized on the vacuole (Sun et al., 2004). Moreover, Yck3-dependent phosphorylation of some of its targets releases them from protein complexes on the vacuole membrane (Hickey et al., 2009; Lawrence et al., 2014). These studies raised the possibility that Yck3 may have a role in the regulated disassembly of the Myo2-Vac17-Vac8 complex.

We tested and found that a *yck3Δ* mutant results in the accumulation of Vac17-GFP and the vacuole at the bud tip and mother-bud neck (**Figure 3.1A**). Since these two distinct

phenotypes appear in a similar percentage of cells, we show representative images of both. These phenotypes are similar to a *dma1Δ* mutant which exhibits defects in the disassociation of the Myo2-Vac17-Vac8 complex and the turnover of Vac17. Additionally, deletion of Yck3 results in elevated levels of endogenous Vac17, similar to the *dma1Δ* mutant (**Figure 3.1B**), which further suggests that there is a block in the turnover of Vac17. These studies strongly suggest that Yck3 has a role in the termination of vacuole transport. Although it was previously reported that Yck3 may have a role in the initiation of vacuole transport (LaGrassa and Ungermann, 2005), we only observed a defect in the termination of vacuole transport in the strain backgrounds used in this study.

We then tested if Vps41 also has a role in the termination of vacuole transport. Vps41 is a subunit of the HOPS complex (Nakamura et al., 1997; Radisky et al., 1997; Seals et al., 2000; Ungermann et al., 2000; Wada et al., 1992), and in this capacity is required for fusion of endosomes with the vacuole, and vacuole-vacuole fusion (Seals et al., 2000; Ungermann et al., 2000; van der Beek et al., 2019). Importantly, Vps41 is a downstream target of Yck3 during vacuole fusion (Cabrera et al., 2009; LaGrassa and Ungermann, 2005). Yck3 phosphorylates Vps41 to negatively regulate its role in the HOPS complex (Cabrera et al., 2010; Cabrera et al., 2009; LaGrassa and Ungermann, 2005).

Notably, we found that deletion of Vps41 resulted in the accumulation of the vacuole and Vac17-GFP at the bud tip and mother-bud neck (**Figure 3.1A**), and also resulted in elevated levels of endogenous Vac17 (**Figure 3.1B**). These phenotypes are similar to those observed in the *yck3Δ* and *dma1Δ* mutants. Note that the *vps41Δ* mutant has fragmented vacuoles due to the role of Vps41 in vacuole fusion (Nakamura et al., 1997; Radisky et al., 1997; Seals et al.,

2000; Ungermann et al., 2000; Wada et al., 1992). Moreover, the *yck3Δvps41Δ* double mutant showed similar phenotypes to the *yck3Δ* and *vps41Δ* single mutants (**Figure 3.1A, 3.1B**). These data indicate that both Yck3 and Vps41 have roles in the termination of vacuole transport.

In further support that Vps41 and Yck3 are both required to release the vacuole from Myo2, similar to a *dma1Δ* mutant, the vacuole accumulates at the bud tip and mother-bud neck with Myo2-Venus in the *vps41Δ*, *yck3Δ*, and *yck3Δvps41Δ* mutants (**Figure 3.2A**). Additionally, similar to a *dma1Δ* mutant, Vac17-GFP accumulates at the bud tip and mother-bud neck with mCherry-Myo2 in the *vps41Δ*, *yck3Δ*, or *yck3Δvps41Δ* mutants (**Figure 3.2B**). Together, these data provide additional support for the hypothesis that both Vps41 and Yck3 are required for the release of the *vacuole from Myo2 and the subsequent degradation of Vac17*.

The roles of Yck3 and Vps41 in the termination of vacuole transport are independent of the HOPS complex, CORVET complex, and AP-3 trafficking

Yck3 was previously shown to regulate Vps41 through the phosphorylation of four sites: S367, S368, S371, and S372 (Cabrera et al., 2009; LaGrassa and Ungermann, 2005). In the context of HOPS function in endosome fusion with the vacuole, a non-phosphorylatable mutant phenocopies the *yck3Δ* mutant and results in the localization of Vps41 to the vacuole, while the phosphomimetic mutant displaces Vps41 from the vacuole (Cabrera et al., 2009). We tested if the non-phosphorylatable and/or phosphomimetic Vps41 mutants had defects in the termination of vacuole transport. While these mutants block HOPS function, they support the termination of vacuole transport (**Figure 3.3A**). Although there is a modest increase in accumulation of Vac17 at the bud tip, neither the non-phosphorylatable nor the

phosphomimetic Vps41 mutants recapitulated the *vps41Δ* mutant. This raises the possibility that the roles of Yck3 and Vps41 in vacuole transport are separate from their roles in the HOPS complex. Two previous studies also suggested that Vps41 has functions independent of the HOPS complex (Asensio et al., 2013; Pols et al., 2013).

We tested if other HOPS subunits are also required for the termination of vacuole transport. We found that Vps39, the other HOPS-specific subunit, does not have a role in the termination of vacuole transport. The *vps39Δ* mutant did not result in the accumulation of Vac17-GFP at the bud tip or mother-bud neck (**Figure 3.3B**), and did not have elevated levels of Vac17 by western blot (**Figure 3.3C**).

The other four HOPS subunits, Vps11, Vps16, Vps18, and Vps33, are also found in the class C core vacuole/endosome tethering (CORVET) complex, another vesicle tether complex (van der Beek et al., 2019). It was previously reported that loss of function of these core subunits results in defects in the initiation of vacuole transport (Banta et al., 1990). Thus, we only scored cells that inherited vacuoles. By microscopy, there was neither an accumulation of Vac17-GFP nor mis-localization of the vacuole in temperature sensitive mutants of Vps11, Vps16, Vps18, or Vps33 (**Figure 3.4**). These findings indicate that the other HOPS subunits are not required for release of the vacuole from Myo2, suggesting novel roles of Vps41 and Yck3 that are independent of their known roles in HOPS.

Vps41 also has roles in adaptor protein-3 (AP-3) vesicle trafficking, which is required for the ALP pathway that traffics proteins to the vacuole (Angers and Merz, 2009; Cabrera et al., 2010; Darsow et al., 2001; Rehling et al., 1999). Vps41 may also form intermediate complexes with Vps3 (Peplowska et al., 2007), suggesting a link to CORVET specific subunits. Neither

deletion of AP-3 components Apl5, Ap3, Apl6, and Apm3, nor deletion of CORVET specific subunits, Vps3 and Vps8, resulted in defects in the termination of vacuole transport (**Figure 3.5**). Thus, Vps41 and Yck3 likely act independently of HOPS and CORVET and likely have uncharacterized roles in targeting the Myo2-Vac17-Vac8 complex to terminate vacuole transport.

The roles of Yck3 and Vps41 are independent of the ubiquitylation of Vac17

Ubiquitylation of Vac17 is required for the degradation of Vac17 and the release of the vacuole from Myo2 (Yau et al., 2014; Yau et al., 2017). Thus, we tested whether Yck3 and Vps41 have roles in the ubiquitylation of Vac17. The ubiquitylation of Vac17 requires several steps: 1) the phosphorylation of Vac17-T240, which leads to 2) the recruitment of inactive Dma1 to Vac17, 3) the vacuole is then brought to the bud cortex where Cla4 phosphorylates Vac17-S222, which leads to 4) activation of Dma1 and the ubiquitylation of Vac17. Abolishing any of the above steps prevents the ubiquitylation of Vac17, and thus results in defects in the termination of vacuole transport (Yau et al., 2014; Yau et al., 2017).

We tested and found that Dma1 is recruited to the vacuole in the *vps41Δ* and *yck3Δ* mutants. In small-budded cells, Dma1-GFP localizes to the leading edge of the vacuole in the *vps41Δ* and *yck3Δ* mutants, similar to yeast with wild type VPS41 and YCK3 genes (**Figure 3.6A**). Moreover, the phosphorylation of Vac17-T240, a prerequisite of Dma1 binding, occurs in wild type and the *yck3Δ* mutant, but not the non-phosphorylatable *vac17-T240A* mutant (**Figure 3.6B**). Note that a *dma1Δdma2Δ* mutant was used to elevate Vac17 levels to facilitate detection by the phospho-specific antibody.

We also found that Cla4 is recruited to the vacuole in the *vps41Δ* and *yck3Δ* mutants (**Figure 3.6C**). In small-budded cells, Cla4 is localized on the bud cortex (Bartholomew and Hardy, 2009). After the vacuole contacts the cortex, a punctum of Cla4 localizes to the vacuole (Bartholomew and Hardy, 2009). Our previous studies indicated that Cla4 likely phosphorylates Vac17-S222 when the vacuole reaches the bud cortex (Yau et al., 2017). We tested if Yck3 and Vps41 affect the ability of Cla4 to target Vac17. In small-budded *vps41Δ* and *yck3Δ* mutants, Cla4-GFP co-localizes with the vacuole, similar to wild type (**Figure 3.6C**). Vac17-S222, the target of Cla4, is phosphorylated in wild type and the *yck3Δ* mutant, but not in the non-phosphorylatable *vac17-S222A* mutant (**Figure 3.6B**). Together, these data support the finding that the localization of Dma1 and activity of Cla4 are not affected by loss of Yck3 and Vps41 (**Figure 3.6A-C**).

That Dma1 is recruited to the vacuole and that Cla4 is able to phosphorylate Vac17-S222 strongly suggests that Vac17 is ubiquitylated. To test this hypothesis, Vac17-GFP was overexpressed in *vac17Δ*, *vac17Δdma1Δdma2Δ*, *vac17Δyck3Δ*, and *vac17Δvps41Δ* cells. Cells were also transformed with a plasmid encoding Myc-ubiquitin controlled by a copper-inducible promoter. Vac17-GFP was immunoprecipitated and ubiquitylation was detected via immunoblot with anti-Myc antibodies. Indeed, Vac17 is ubiquitylated in the *vps41Δ* and *yck3Δ* mutants (**Figure 3.6D**). These data show that Yck3 and Vps41 functions are independent of Vac17 ubiquitylation, and that Vac17 ubiquitylation does not require Yck3 and Vps41. Importantly, these data reveal that ubiquitylation of Vac17 is not sufficient to disrupt the complex.

Previous hypotheses assumed that ubiquitylation was the last step prior to the degradation of Vac17. Our studies indicate that at least two independent, non-redundant pathways are required to dissociate the vacuole from Myo2 and degrade Vac17. Yck3 and Vps41 function independently of Cla4 and Dma1, yet ubiquitylation is independent of the pathway(s) governed by Vps41 and/or Yck3 that are required for Vac17 degradation. Since Dma1-dependent ubiquitylation was not impaired, these findings raise the possibility that Yck3 and Vps41 act in another manner on Vac17 to regulate the termination of vacuole transport.

Yck3 and Vps41 regulate the release of ubiquitylated Vac17 from the Myo2-Vac17-Vac8 complex

Since ubiquitylation alone is not sufficient to release Myo2 from the vacuole, we turned to a genetic approach to determine whether Yck3 and Vps41 function with the proteasome to degrade Vac17, or whether they are required upstream of the proteasome. As assessed by western blot, loss of function proteasome mutants result in elevated levels of Vac17 (Yau et al., 2014). However, the localization of accumulated Vac17 in these mutants was not determined. Notably, we found that Vac17 is released from the vacuole in several proteasome mutants, including the *pup1-K58E pup3-E151K* mutant (**Figure 3.7A**), as well as the *pre2-T76A* and *pre1-1* mutants (**Figure 3.8**). Pup1, Pup3, Pre1, and Pre2 comprise Beta subunits of the 20S core particle of the proteasome (Arendt and Hochstrasser, 1997; Chen and Hochstrasser, 1996). In each of the 20S proteasome mutants tested, Vac17-GFP appears in puncta that are not strictly on the vacuole or at the bud tip or mother-bud neck (**Figure 3.7A, Figure 3.8**). These findings

suggest that Vac17 is released from the vacuole, and likely from the Myo2-Vac17-Vac8 complex, before Vac17 is degraded by the proteasome.

The phenotype of Vac17 puncta in proteasome mutants is distinct from mutants where Vac17 is trapped in the Myo2-Vac17-Vac8 complex and Vac17 accumulates solely at the bud tip or mother-bud neck. Thus, we performed epistasis experiments where the phenotype of the double mutant indicates the first step where a pathway is blocked. Strikingly, the double mutants with mutations in the proteasome combined with deletion of either Yck3 or Vps41 phenocopy the single *yck3Δ* or *vps41Δ* mutants where Vac17 accumulates with the vacuole at the bud tip or mother-bud neck (**Figure 3.7A**). These findings show that Yck3 and Vps41 act upstream of the proteasome.

The observation that Vac17 is released from the vacuole in the proteasome mutants raised the question of whether Myo2 and/or Vac8 are also delivered to the proteasome. However, Myo2 and Vac8 levels are not elevated or reduced in the *pup1-K58E pup3-E151K* alone or in combination with the *yck3Δ* or *vps41Δ* mutants by western blot (**Figure 3.7B**). This is in contrast to Vac17-GFP, which is elevated in the *pup1-K58E pup3-E151K* and/or *yck3Δ* or *vps41Δ* mutants to a similar extent when compared to wild type (**Figure 3.7B**). Additionally, neither Myo2 nor Vac8 accumulate in puncta in the proteasome mutant. We found that the localization of Myo2-Venus (**Figure 3.9A**) and Vac8-mCherry (**Figure 3.9B**) are not perturbed in the *pup1-K58E pup3-E151K* mutant. Note that CMAC, a small molecule that stains the lumen of the vacuole (Stefan and Blumer, 1999; Stewart and Deacon, 1995), was used as a vacuole marker when we tested Vac8 localization on the vacuole membrane. Overall, these data indicate that Yck3 and Vps41 act upstream of the proteasome to dissociate ubiquitylated Vac17

from the Myo2-Vac17-Vac8 complex on the vacuole, which releases the vacuole from Myo2 and allows for the degradation of ubiquitylated Vac17.

The AAA-ATPases Cdc48/p97, Vps4, and Sec18/NSF do not extract Vac17 from the complex

Several AAA-ATPases have been shown to extract proteins from membranes or protein complexes to facilitate their degradation. Cdc48/p97 extracts endoplasmic reticulum membrane proteins destined for degradation (Bodnar and Rapoport, 2017). Vps4 aids in the disruption of ESCRT-III complex on endosomes (Migliano and Teis, 2018). Sec18/NSF is AAA-ATPase that disassembles SNARE complexes, and in this capacity also works on SNARE complexes at the vacuole (Lobingier et al., 2014; Song et al., 2017; Steel et al., 1999). However, we tested and found that a Cdc48 temperature sensitive mutant, *cdc48-3*, (**Figure 3.10A**), a *vps4Δ* mutant (**Figure 3.10B**), and a *sec18-DAmP* mutant (**Figure 3.10C**) did not have defects in the termination of vacuole transport. It is possible that a currently unidentified AAA-ATPase is recruited to facilitate the release of Vac17 from the Myo2-Vac17-Vac8 complex, or a different mechanism is required for dissociation of the complex.

Yck3 and Vps41 bind and are required for the phosphorylation of Vac17

Our data suggest that Yck3 and Vps41 target Vac17. Consequently, we tested if Yck3 can bind to full-length Vac17. Since Yck3 function was not required for Cla4 or Dma1 regulation of Vac17, we also tested if Yck3 could bind the vac17-ΔPEST mutant, which is missing the sites of Dma1 binding and Cla4 phosphorylation (**Figure 3.11A**). Recombinant GST-Yck3 (2-516) immobilized on beads was able to bind to Vac17-TAP and Vac17-ΔPEST-TAP from yeast lysates

(Figure 3.11B). This indicates that Yck3 binds to Vac17 and that this interaction does not require the Vac17-PEST sequence. Interestingly, this interaction does not require Vps41, as GST-Yck3 (2-516) immobilized on beads was able to bind to Vac17- Δ PEST-TAP from *vps41* Δ yeast lysates **(Figure 3.11B)**. Note that it is possible that the interaction between Yck3 and Vac17 is indirect and facilitated by an unknown protein present in the yeast lysates. Importantly, Yck3 and Vac17 are in a complex together and Vac17 is thus a candidate substrate for phosphorylation that is either directly or indirectly regulated by Yck3.

We also tested if Vps41 is able to bind to Vac17. We found that recombinant His-Vps41 (124-992) from *C. thermophilum* binds to Vac17-TAP and Vac17- Δ PEST-TAP from yeast lysates **(Figure 3.11C)**. This interaction also occurred in a *yck3* Δ mutant **(Figure 3.11C)**. These data demonstrate that both Yck3 and Vps41 bind, either directly or indirectly, to Vac17 in regions of Vac17 that are outside of the Vac17-PEST sequence. Note that there may also be regions within the PEST sequence with the potential to bind Yck3 and/or Vps41. Importantly, previously known regulators, Cla4 and Dma1, regulate or bind Vac17 via the PEST sequence. That Yck3 and Vps41 bind Vac17- Δ PEST suggests a new mode of regulation in the termination of vacuole transport.

Since Yck3 is a kinase, and the *yck3* Δ and *vps41* Δ mutants have similar phenotypes, we hypothesized that Yck3 and Vps41 regulate the phosphorylation of Vac17. Both Yck3 and Vps41 are able to bind Vac17- Δ PEST. Therefore, we next tested if Yck3 and/or Vps41 are responsible for phosphorylation of Vac17- Δ PEST. Using a gel shift assay, we found that Yck3 and Vps41 - dependent phosphorylation occurred in the *vac17*- Δ PEST mutant. The addition of phosphatase collapses the higher mobility band in Vac17- Δ PEST-GFP, which is rescued by phosphatase

inhibitors (**Figure 3.11D**). In the *yck3Δ* and *vps41Δ* mutants, addition of phosphatase does not result in any change in gel mobility, suggesting that the gel mobility shift in Vac17-ΔPEST-GFP is due to Yck3 and Vps41 -dependent phosphorylation (**Figure 3.11D**).

We also tested if Yck3 and Vps41 –dependent phosphorylation requires an intact Myo2-Vac17-Vac8 complex. We used western blot analysis to test the mobility of Vac17-ΔPEST-GFP in mutants that are blocked in the formation of the motor-adaptor complex. In the *myo2-D1297N* mutant, Myo2 is unable to bind to Vac17, and Vac17 is bound to Vac8 on vacuoles that remain in the mother cell (Eves et al., 2012). We found in a gel shift assay that Yck3 and Vps41 -dependent phosphorylation requires that Vac17 is bound to Myo2 or must be in the bud, as Vac17-ΔPEST-GFP is not phosphorylated in the *myo2-D1297N* mutant (**Figure 3.11E**). Next, we tested a *vac8Δ* mutant in which Vac17 is bound to Myo2 and is brought to the bud, but is not associated with the vacuole (Peng and Weisman, 2008). We found that Vac17-ΔPEST-GFP is not phosphorylated in a *vac8Δ* mutant, (**Figure 3.11F**). This suggests that Vac17 needs to be on the vacuole in the bud and/or in a complex with Myo2 and Vac8 to be phosphorylated by Yck3 and/or the Vps41 pathway. These data suggest that Yck3 and Vps41 regulate the phosphorylation of Vac17 after the Myo2-Vac17-Vac8 complex is formed and vacuole transport is initiated. It remains an open possibility that it is not the complex per se, but rather that phosphorylation occurs if Vac17 is in the bud and on the vacuole.

To determine if Dma1 is required for the Yck3 -dependent phosphorylation of Vac17, we used a gel shift assay to determine the phosphorylation of Vac17 in several mutants. In a *dma1Δdma2Δyck3Δ* mutant, Vac17-ΔPEST-GFP has increased mobility compared to a *dma1Δdma2Δ* mutant (**Figure 3.11G**), indicating that Dma1/Dma2 are not required for Yck3 -

dependent phosphorylation of Vac17. Of note, Vac17- Δ PEST-GFP levels appear to be at lower levels in a *dma1 Δ dma2 Δ* mutant compared to *vac17- Δ PEST-GFP* in wild type or *yck3 Δ* backgrounds (**Figure 3.11G**). This may be due to compensatory mechanisms that lower Vac17- Δ PEST levels in the *dma1 Δ dma2 Δ* mutant. Consistent with previous data, these data overall suggest that Dma1-dependent ubiquitylation vs. Yck3 and/or Vps41-dependent phosphorylation occur through independent pathways.

Yck3 and Vps41 phosphorylate Vac17 in the Myo2 binding domain

To determine Vps41 and Yck3 -dependent phosphosites on Vac17, we performed Stable Isotope Labeling by Amino acids in Cell culture (SILAC) mass spectroscopy. We identified multiple sites in Vac17- Δ PEST whose phosphorylation status is changed in the *vps41 Δ* mutant (**Table 3**). Interestingly, four of the Vac17 phosphosites that are reduced in the *vps41 Δ* mutant reside in the Myo2 binding domain of Vac17: S127, S128, S131, and T149. One of these sites, S131, was also reduced in the *yck3 Δ* mutant (**Table 4**).

We determined whether these sites are required for termination of vacuole transport and the degradation of Vac17 by testing the corresponding non-phosphorylatable alanine mutations. As assessed by microscopy, mutating all four residues to alanine resulted in a defect in the termination of vacuole transport similar to the *yck3 Δ* mutant (**Figure 3.12A**). Alanine mutations in three of these sites, *vac17-S127A-S128A-S131A* (denoted as *vac17-3A*), also had a significant defect, while the *vac17-T149A* mutant on its own showed a trend that was not significant. Note that Vac17-T149 was identified as one of four Cdk1 sites important for the initiation of vacuole transport (Peng and Weisman, 2008). However, the *vac17-T149A* mutant

alone did not have defects in vacuole transport (**Figure 3.12A**). By western blot, mutating all four of these residues to alanine resulted in elevated levels of Vac17, similar to the *yck3Δ* mutant (**Figure 3.12B**). These data suggest that phosphorylation of these residues is required for the release of the vacuole from Myo2 and the degradation of Vac17.

We then tested the putative phosphomimetic mutant, *vac17-4E*. This mutant was not defective in the release of Myo2 from the vacuole and did not elevate levels of Vac17 (**Figure 3.12C-D, Figure 3.13A-D**). Rather, the *vac17-4E* mutant acted like wild type, suggesting that phosphorylation of these residues is required for the termination of vacuole transport.

We further tested the *vac17-4A* mutant and the phosphomimetic *vac17-4E* mutant in combination with the *pup1-K58E pup3-E151K* proteasome mutant to determine whether these sites are required for the release of Vac17 from the Myo2-Vac17-Vac8 complex. Importantly, in the *vac17-4A pup1-K58E pup3-E151K* mutant, Vac17-4A-GFP accumulated at the bud tip or mother-bud neck instead of in puncta in the cytoplasm (**Figure 3.12C**). Moreover, compared to wild type, the *vac17-4A* mutant had elevated levels of Vac17, and the *vac17-4A pup1-K58E pup3-E151K* mutant elevated Vac17 to levels greater than the *pup1-K58E pup3-E151K* mutant alone (**Figure 3.12D**). Since the phenotype of *vac17-4A pup1-K58E pup3-E151K* mutant is the same as the *vac17-4A-GFP* mutant alone, these data further suggest that these phosphosites are important for the release of Vac17 from the Myo2-Vac17-Vac8 complex.

Conversely, when the *vac17-4E* mutant was expressed in a *pup1-K58E pup3-E151K* mutant, Vac17-4E-GFP behaved similarly to a proteasome mutant alone, and accumulated in puncta that were not solely localized to the vacuole (**Figure 3.12C**). Together these findings

suggest that phosphorylation of Vac17- S127, S128, S131, and T149 are required to release Vac17 from the Myo2-Vac17-Vac8 complex.

However, the *vac17-4E* mutant did not suppress the *yck3Δ* mutant (**Figure 3.13A-B**) or *vps41Δ* mutant (**Figure 3.13C-D**). This suggests that phosphorylation of these four sites are necessary but not sufficient for the release of Vac17 from the Myo2-Vac17-Vac8 complex, and that other regulatory steps are also required. Vps41 and Yck3 may have additional roles in the release of Vac17 from the Myo2-Vac17-Vac8 complex. These could be additional essential phosphorylation sites on Vac17 that were not yet identified, and/or other proteins that act in this pathway and require functional Vps41 and/or Yck3 for their activity in removal of Vac17 from the Myo2-Vac17-Vac8 complex.

We also tested whether substitution of S127, S128, S131 and T149 with negatively charged residues impairs the binding of Vac17 to Myo2. While we saw a modest trend of increased association of Myo2 with Vac17-(1-355)-4A, and decreased association with Vac17-(1-355)-4E, these differences were not a statistically significant (**Figure 3.12E**). These findings indicate that beyond phosphorylation of these sites, there are likely additional steps or regulators required for the dissociation of Vac17 from Myo2.

Notably, while Vps41 plays a role in the phosphorylation of Vac17 -S127, -S128, -S131, and -T149, deletion of Yck3 did not result in a loss of phosphorylation of Vac17 -S127, -S128 or T149, but exhibited a decrease in phosphorylation of Vac17-S131 (**Table 4**). This site matches the casein kinase I consensus sites, SxxS, or where the target serine or threonine is 1-3 amino acids downstream of acidic (Flotow et al., 1990; Marin et al., 1994; Pulgar et al., 1999) or primed residues (residues that have already been phosphorylated) (Cesaro and Pinna, 2015;

Flotow et al., 1990; Marchal et al., 2000). Thus, it is likely that Vps41 is regulating additional kinases, such as a potential priming kinase, to phosphorylate these sites. Overall, Vps41 promotes the phosphorylation of the Myo2 binding domain of Vac17 likely via additional kinase(s) and perhaps as an upstream regulator of Yck3.

Additional phosphorylation sites adjacent to the Vac8 binding domain, Vac17 -S269, S272, and S275, were also identified (**Table 3, Table 4**), and importantly, these sites were heavily dependent on Yck3. We tested these residues for a role in vacuole transport. However, the non-phosphorylatable alanine mutant, *vac17-S269A-S272A-S275A*, did not have defects in the termination of vacuole transport or degradation of Vac17 (**Figure 3.12E-F**). Note that the *vac17-S269A-S272A-S275A* mutant exhibited a faster mobility on SDS-PAGE compared with wild type Vac17, suggesting that these are bona fide phosphorylation sites. These data provide further support to the hypothesis that in addition to these phosphorylation sites, there are additional steps required to release Vac17 from the Myo2-Vac17-Vac8 complex. This may be additional unidentified phosphorylation sites in Vac17, unidentified phosphorylation sites on Vac17 binding partners, and/or additional unknown regulators.

Overall, these data suggest that Vps41 and Yck3 are each required to regulate the phosphorylation of Vac17 at the interface between Vac17 and Myo2, and that this phosphorylation is required to dissociate Vac17 from the motor-adaptor complex. Previous studies of Vac17 degradation indicated that the Vac17-PEST sequence is required for the degradation of Vac17 and thus the termination of vacuole transport (Tang et al., 2003; Yau et al., 2014; Yau et al., 2017). Our new studies indicate that Yck3 and Vps41 regulate binding

between Vac17 and Myo2 to release ubiquitylated Vac17 from the Myo2-Vac17-Vac8 complex and terminate vacuole transport.

Discussion

Our data reveal that release of the vacuole from Myo2 requires parallel pathways that act on the adaptor protein, Vac17. In one pathway, the bud-localized kinase, Cla4, phosphorylates Vac17, which facilitates the Dma1-dependent ubiquitylation of Vac17. In the other pathway, Yck3 and Vps41 regulate the phosphorylation of Vac17 in its Myo2 binding domain, and potentially other regions. Both ubiquitylation as well as Yck3 and Vps41-dependent regulation are required to release Vac17 from the Myo2-Vac17-Vac8 complex. Vac17 is then degraded by the proteasome (**Figure 3.14**). In mutants where Yck3 and Vps41 are both present, but ubiquitylation of Vac17 is defective, Vac17 is not released from the complex. Similarly, in mutants where Vac17 is ubiquitylated but Yck3 and/or Vps41 are absent, Vac17 is not released from the complex. However, in loss of function proteasome mutants, where both ubiquitylation and Yck3 and Vps41 -dependent regulation occur, Vac17 is released from the vacuole, but not degraded. Vac17 levels are also elevated in the proteasome mutant where the Myo2-Vac17-Vac8 complex is disassembled. This suggests that elevated Vac17 alone does stabilize the complex. Together, these data support a model where ubiquitylation and a Yck3 and Vps41 -dependent pathway act in parallel to dissociate the Myo2-Vac17-Vac8 complex, which leads to the degradation of Vac17 by the proteasome (**Figure 3.14**). Yck3 and Vps41 may function in different steps of this pathway, but a fully detailed molecular mechanism remains unclear.

Our data strongly suggest that Vps41 acts in the release of Vac17 via regulation of kinase(s) that phosphorylate Vac17 in four residues within the Myo2 binding region: S127, S128, S131, and T149. Yck3 is one candidate kinase, which plays a role in the phosphorylation of Vac17-S131. An unidentified kinase may be responsible for phosphorylation of the other three sites. It is possible that Vps41 is regulating multiple steps in this pathway, or acts upstream of several kinases, and may also regulate Yck3.

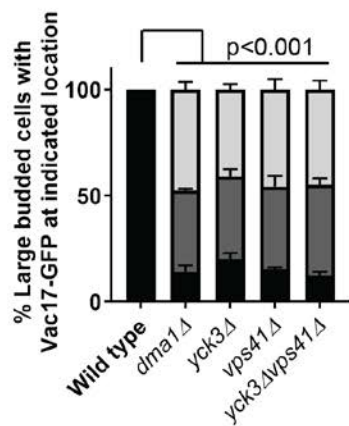
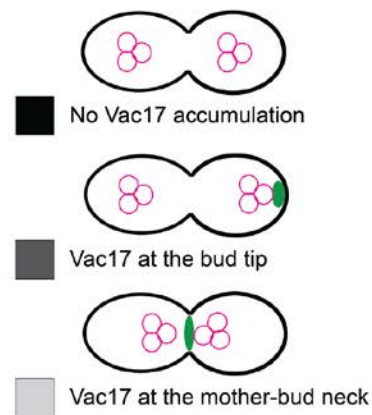
Given the strong phenotype of *yck3^Δ*, it is likely that additional critical Yck3 sites within Vac17, Vac8, and/or Myo2, are not yet identified. While Yck3 and Vps41 are required for the phosphorylation of three sites in the Vac8 binding region of Vac17, the function of these sites are unknown and additional regulatory steps may be required. Moreover, Yck3 and/or Vps41 may regulate the phosphorylation of residues within the Vac17-PEST sequence. The phosphorylation of these potentially unidentified residues may depend on the ubiquitylation status of Vac17 or other sites of posttranslational modifications.

The requirement for parallel pathways of ubiquitylation and phosphorylation leads us to speculate that an additional factor may act as a coincidence detector that establishes that both events have occurred and then allows dissociation of the complex. Such a factor may recruit machinery that physically releases Vac17, such as a currently untested AAA-ATPase. In budding yeast, there are about fifty AAA ATPases (Neuwald et al., 1999), with at least ten confirmed as unfolding ATPases (Vale, 2000). Alternatively, Yck3 and Vps41-dependent phosphorylation may change Vac17 conformation and/or work with the proteasome to dissociate Vac17 from the complex.

The involvement of Yck3 and Vps41 raises interesting possibilities as to why and how Yck3 and Vps41 act independently of their known roles in the HOPS complex. These new roles in vacuole transport may indicate their ability to function separately from HOPS. Alternatively, these separate roles may link the status of vacuole function with vacuole transport.

A question raised by these studies is why release of Myo2 from the vacuole involves multiple mechanisms. Note that Myo2 transports the vacuole, a relatively large organelle, through the viscous, crowded cytoplasm and the narrow mother-bud neck. It is likely that Myo2, Vac17, and Vac8 are tightly associated with each other in the complex to prevent premature release of the vacuole. Thus, it makes sense that an independent pathway is dedicated to opening the complex. The regulated release of Myo2 from the vacuole is likely critical for Myo2 attachment to its essential cargo, secretory vesicles, which seal the membrane at the mother-bud neck during cytokinesis (Govindan et al., 1995). Degradation of free Vac17 may be required to prevent reassembly of the complex and untimely attachment of the vacuole to Myo2. It is also possible that additional cues regulate the Yck3 and Vps41-dependent phosphorylation of Vac17 to coordinate vacuole delivery with other cellular processes, such as vacuole membrane fusion. Overall, these studies reveal a mechanism of how a cargo is released from myosin V. To our knowledge, it remains to be determined how myosin V is released from other cargoes, or how cargoes are detached from other classes of molecular motors.

A



B

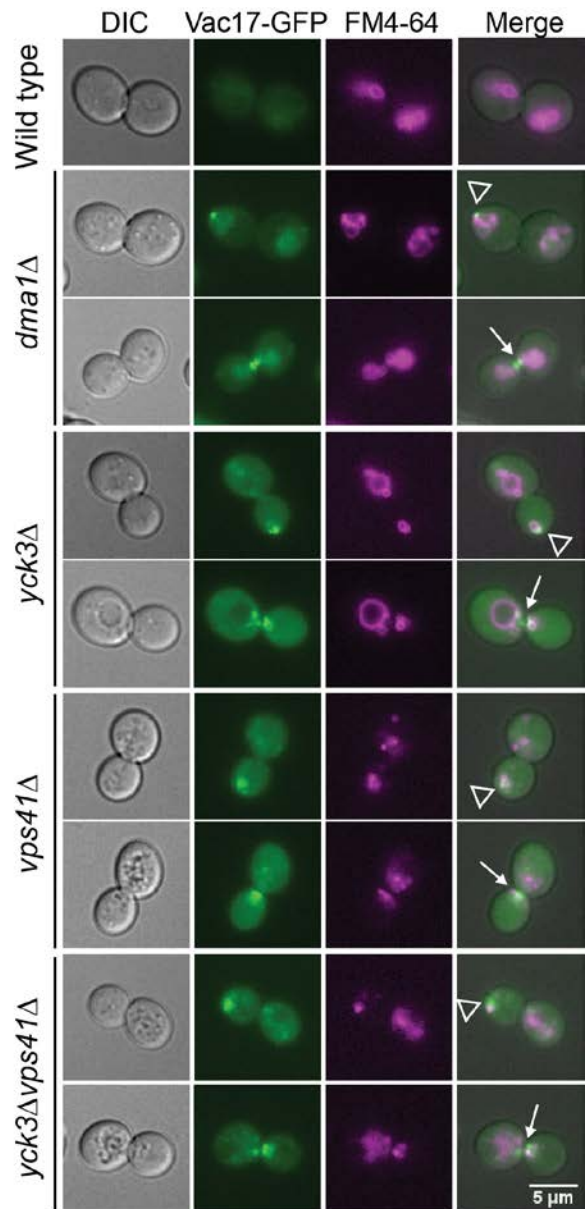
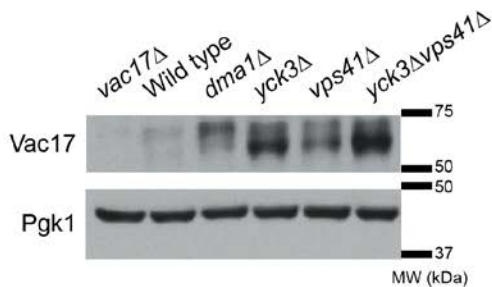


Figure 3.1. Yck3 and Vps41 are required for the termination of vacuole transport.

A) Similar to deletion of *Dma1*, deletion of *Yck3* and/or *Vps41* results in mislocalization of the vacuole (FM4-64) and accumulation of Vac17-GFP at the bud tip (open arrowheads) or mother-bud neck (closed arrows). Representative images of both phenotypes are shown. Wild type, *dma1*Δ, *yck3*Δ, *vps41*Δ, and *yck3*Δ*vps41*Δ mutant cells were transformed with pRS415-Vac17-GFP. After FM4-64 labeling, cells were chased at 24°C for 3 h before imaging. DIC, differential interference contrast. Quantification of 40 large-budded cells per *n*, *n*=3. Error bars indicate SEM. Two-way ANOVA and Dunnett's post-hoc test. Scale bar = 5 μM.

B) Compared to wild type, endogenous levels of Vac17 are elevated in *dma1Δ*, *yck3Δ*, *vps41Δ*, and *yck3Δvps41Δ* mutants. Pgk1 was used as a loading control. Molecular mass is shown in kilodaltons. Representative of n=3.

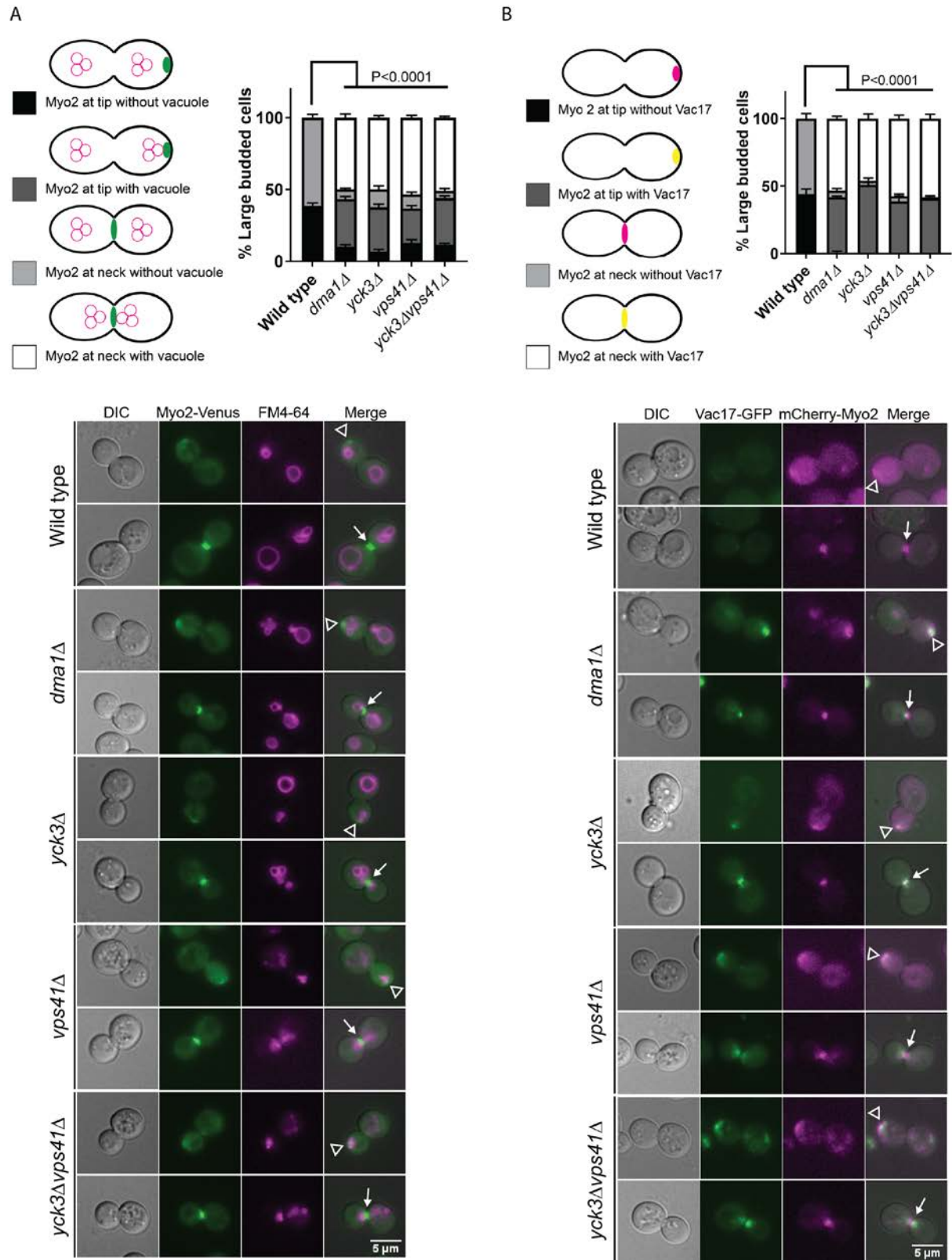


Figure 3.2. Yck3 and Vps41 are required for the release of the vacuole from Myo2.

A) Deletion of Yck3 and/or Vps41 results in mislocalization of the vacuole (FM4-64) at the bud tip (open arrowheads) or mother-bud neck (closed arrows) with Myo2-Venus. Wild type, *dma1Δ*, *yck3Δ*, *vps41Δ*, and *yck3Δvps41Δ* mutant cells were transformed with pRS413-Myo2-Venus. After FM4-64 labeling, cells were chased at 24°C for 3 h before imaging. DIC, differential interference contrast. Quantification of 40 large-budded cells per n, n=3. Error bars indicate SEM. Two-way ANOVA and Dunnett's post-hoc test. Scale bar = 5 μM.

B) Deletion of Yck3 and/or Vps41 results in mislocalization and accumulation of Vac17-GFP at the bud tip (open arrowheads) or mother-bud neck (closed arrows) with mCherry-Myo2. Wild type, *dma1Δ*, *yck3Δ*, *vps41Δ*, and *yck3Δvps41Δ* mutant cells were transformed with pRS413-mCherry-Myo2 and pRS415-Vac17-GFP. DIC, differential interference contrast. Quantification of 40 large-budded cells per n, n=3. Error bars indicate SEM. Two-way ANOVA and Dunnett's post-hoc test. Scale bar = 5 μM.

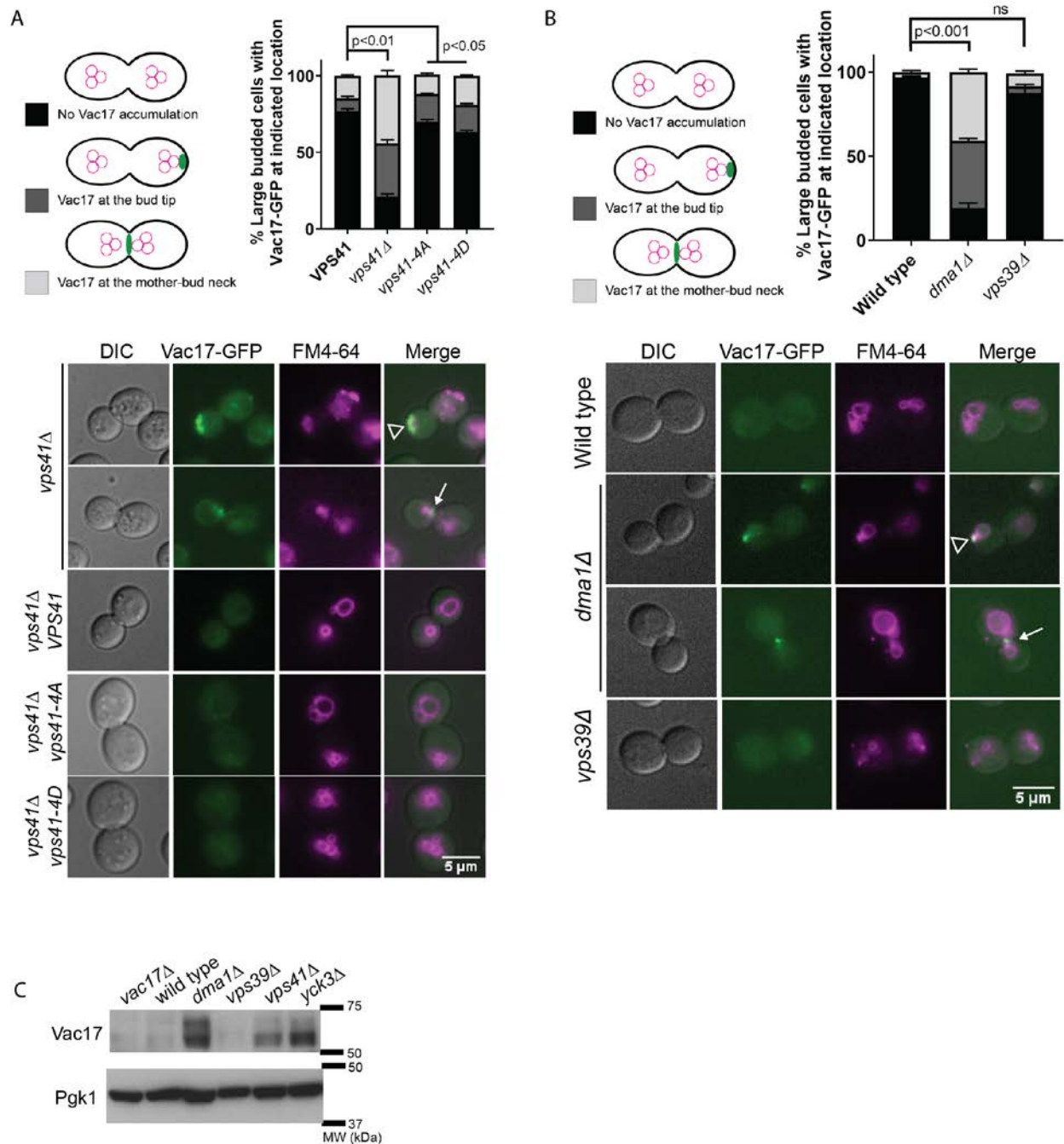


Figure 3.3. The HOPS complex does not have a role in the termination of vacuole transport.

A) The known Yck3-dependent phosphosites on Vps41 are not essential for the release of the vacuole from Vac17 or degradation of Vac17. Mutants in the Yck3-dependent phosphosites on Vps41 were scored for mislocalization of the vacuole (FM4-64) and accumulation of Vac17-GFP at the bud tip (open arrowheads) or mother-bud neck (closed arrows). *vps41Δ* mutant cells were integrated with vector, wild type, *VPS41*, *vps41-4A*, or *vps41-4D*, in the genome using the pRS406 yeast integrative vector. Strains were then transformed with pRS415-Vac17-GFP. After

FM4-64 labeling, cells were chased at 24°C for 3 h before imaging. DIC, differential interference contrast. Quantification of 40 large-budded cells per n, n=3. Error bars indicate SEM. Two-way ANOVA and Dunnett's post-hoc test. Scale bar = 5 μM.

B) Unlike a deletion of *Dma1*, deletion of *Vps39* does not result in mislocalization of the vacuole or accumulation of Vac17-GFP at the bud tip (open arrowheads) or mother-bud neck (closed arrows). Wild type, *dma1Δ*, and *vps39Δ* mutant cells were transformed with pRS415-Vac17-GFP. After FM4-64 labeling, cells were chased at 24°C for 3 h before imaging. DIC, differential interference contrast. Quantification of 40 large-budded cells per n, n=3. Error bars indicate SEM. Two-way ANOVA and Dunnett's post-hoc test. Scale bar = 5 μM.

C) Unlike a deletion of *Dma1*, deletion of *Vps39* does not result in elevated Vac17 levels. Endogenous levels of Vac17 are elevated in a *dma1Δ* mutant, but not in a *vps39Δ* mutant compared to wild type. Pgk1 was used as a loading control. Molecular mass is shown in kilodaltons. Representative of n=3.

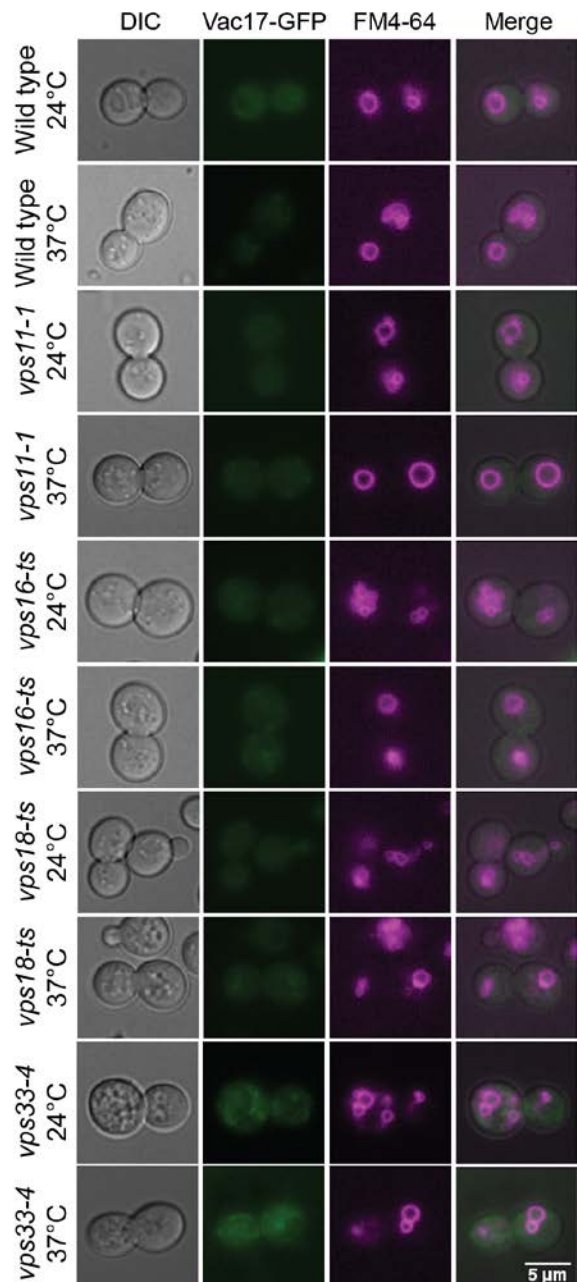
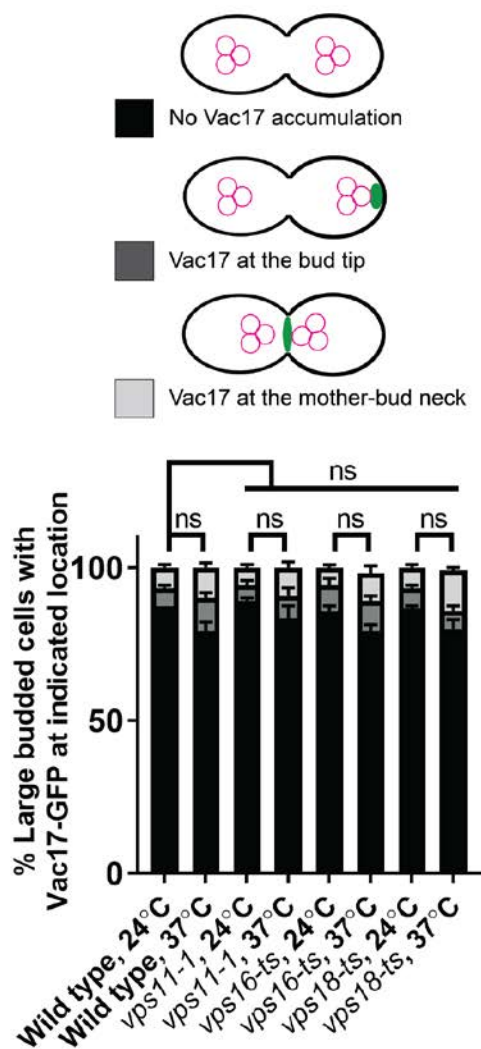


Figure 3.4. The core HOPS complex does not have a role in the termination of vacuole transport.

Temperature sensitive mutations in Vps11, Vps16, Vps18, or Vps33 do not disrupt the termination of vacuole transport. Wild type, *vps11-1*, *vps16-ts*, *vps18-ts*, and *vps33-4* mutant cells were transformed with pRS415-Vac17-GFP. After FM4-64 labeling, cells were chased either at 24°C for 3 hr or 37°C for 3 hr before imaging. DIC, differential interference contrast. Quantification of 40 large-budded cells per n, n=3. Error bars indicate SEM. Two-way ANOVA and Dunnett's post-hoc test. Scale bar = 5 μM.

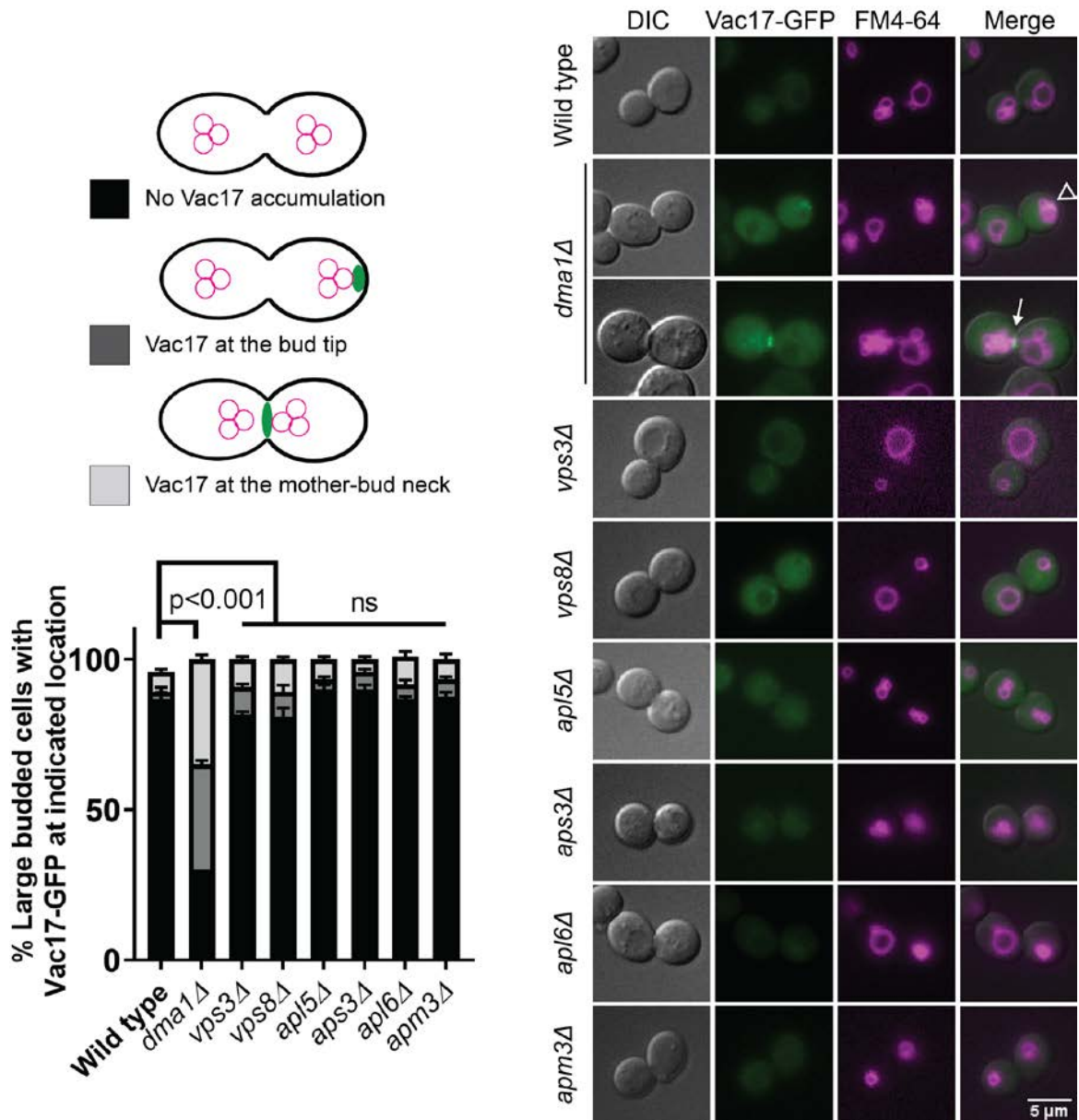
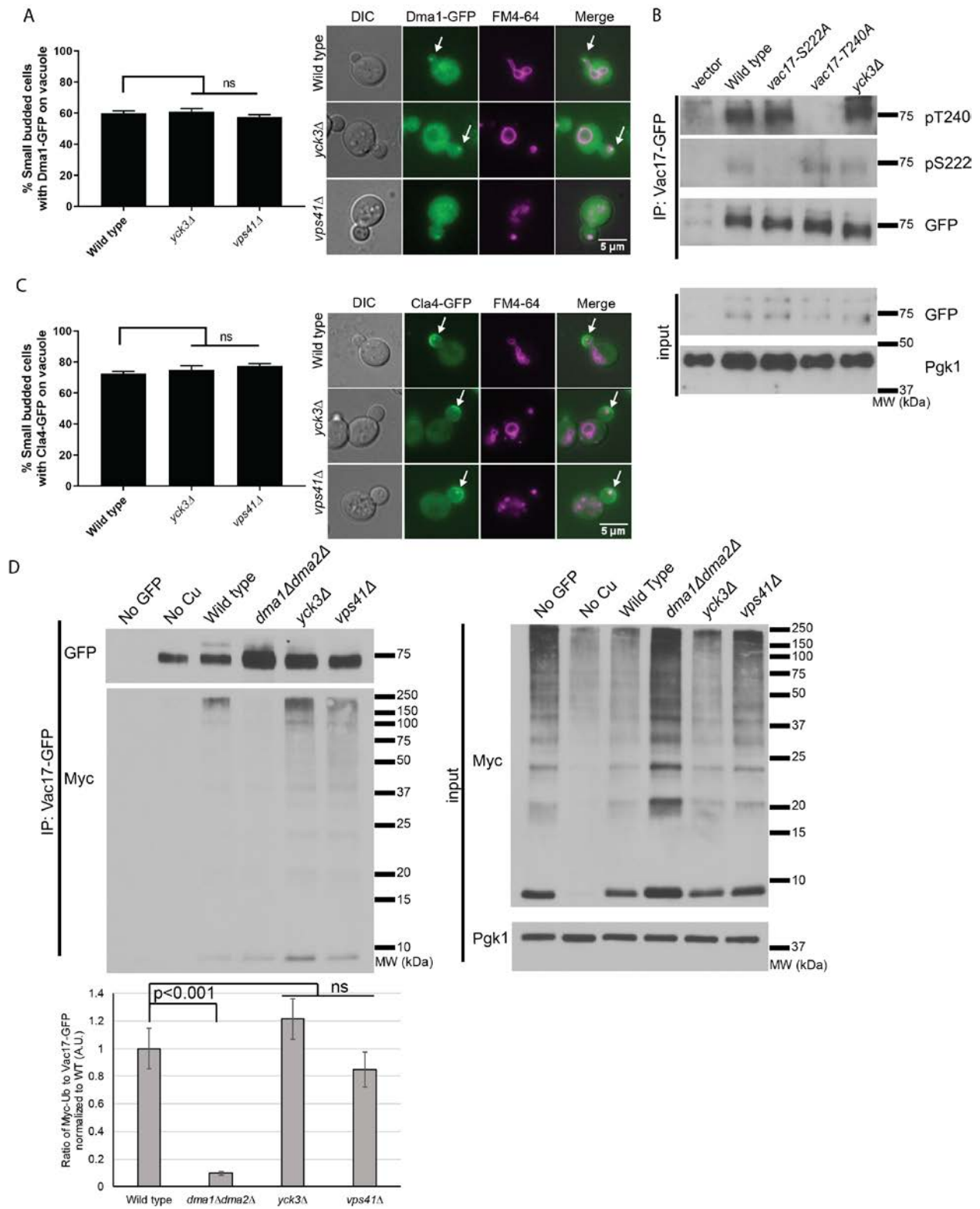


Figure 3.5. AP-3 and CORVET do not have roles in the termination of vacuole transport. AP-3 and CORVET components are not required for the termination of vacuole transport. Wild type, *dma1Δ*, *vps3Δ*, *vps8Δ*, *apl5Δ*, *aps3Δ*, *apl6Δ*, and *apm3Δ* mutant cells were transformed with pRS415-Vac17-GFP. After FM4-64 labeling, cells were chased at 24°C for 3 h before imaging. DIC, differential interference contrast. Quantification of 40 large-budded cells per n, n=3. Error bars indicate SEM. Two-way ANOVA and Dunnett's post-hoc test. Scale bar = 5 μM.



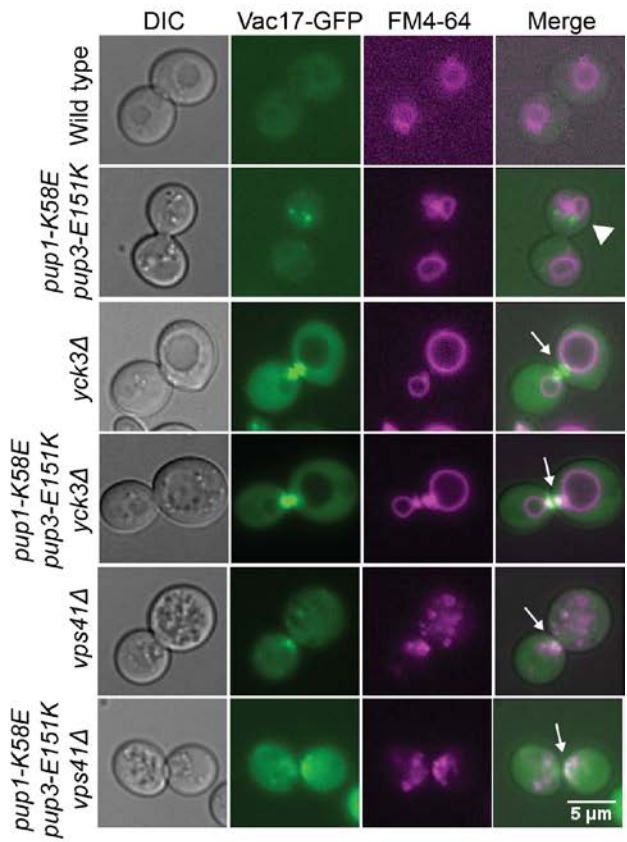
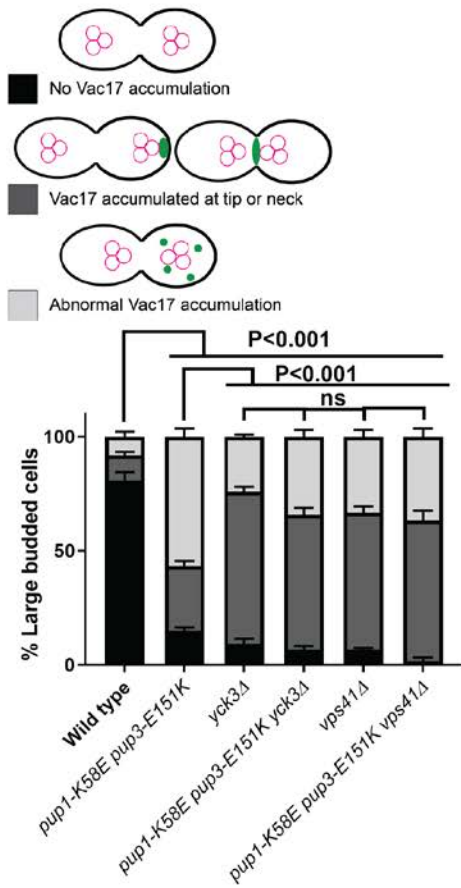
A) Dma1 is recruited to the vacuole in *yck3Δ* and *vps41Δ* mutant cells, similar to wild type (arrows). Wild type, *yck3Δ*, and *vps41Δ* mutant cells were transformed with pRS415-Vac17-GFP. After FM4-64 labeling, cells were chased at 24°C for 3 h before imaging. DIC, differential interference contrast. Quantification of 40 small-budded cells per n, n=3. Error bars indicate SEM. Student's t-test. Scale bar = 5 μM.

B) Yck3 is not required for the phosphorylation of Vac17-S222 or Vac17-T240. *dma1Δdma2Δ* (lanes 1-4) or *dma1Δdma2Δyck3Δ* (lane 5) mutant cells were transformed with pRS415-Vac17-GFP, *pRS415-vac17-S222A-GFP*, or *pRS415-vac17-T240A-GFP*. Vac17-GFP was immunoprecipitated with anti-GFP antibodies and analyzed via western blot. Pgk1 was used as a loading control. Molecular mass is shown in kilodaltons. Representative of n=3.

C) Cla4 is recruited to the vacuole in *yck3Δ* and *vps41Δ* mutant cells, similar to wild type (arrows). Wild type, *yck3Δ*, and *vps41Δ* mutant cells were transformed with pRS415-Vac17-GFP. After FM4-64 labeling, cells were chased at 24°C for 3 h before imaging. DIC, differential interference contrast. Quantification of 40 small-budded cells per n, n=3. Error bars indicate SEM. Student's t-test. Scale bar = 5 μM.

D) Yck3 and Vps41 are not required for the ubiquitylation of Vac17. *vac17Δ* (lanes 1-3), *dma1Δdma2Δvac17Δ* (lane 4), *yck3Δvac17Δ* (lane 5), and *vps41Δvac17Δ* (lane 6) mutant cells were co-transformed with a plasmid encoding Myc-ubiquitin under a copper-inducible promoter and pVT102u-Vac17-GFP. Vac17-GFP was immunoprecipitated using anti-GFP antibodies and analyzed via western blot. Ubiquitylation was detected via immunoblotting with anti-Myc antibody. Pgk1 was used as a loading control. Molecular mass is shown in kilodaltons. Quantification of n=3. Error bars indicate SEM. Student's t-test.

A



B

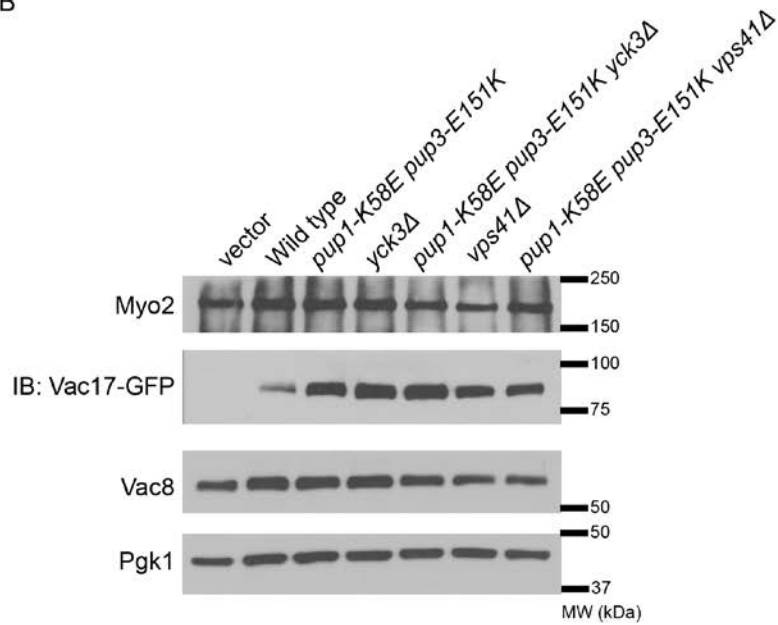


Figure 3.7. Yck3 and Vps41 are required to release ubiquitylated Vac71 from the complex.

A) Yck3 and Vps41 act upstream of the proteasome to release Vac17 from the vacuole. In a proteasome mutant, Vac17-GFP accumulates in aberrant puncta (closed arrowheads). However, Vac17-GFP accumulates at the bud tip or mother-bud neck (closed arrows) in *pup1-K58E pup3-E51K yck3Δ* and *pup1-K58E pup3-E51K vps41Δ* triple mutants, similar to the *yck3Δ* and *vps41Δ* mutants. This indicates that Yck3 and Vps41 act upstream of Pup1 and Pup3. Wild type, *pup1-K58E pup3-E51K*, *yck3Δ*, *pup1-K58E pup3-E51K yck3Δ*, *vps41Δ*, and *pup1-K58E pup3-E51K vps41Δ* mutant cells were transformed with pRS416-Vac17-GFP. After FM4-64 labeling, cells were chased at 24°C for 3 hr before imaging. DIC, differential interference contrast. Quantification of 40 large-budded cells per n, n=3. Error bars indicate SEM. Two-way ANOVA and Tukey's post-hoc test. Scale bar = 5 μM.

B) Myo2 and Vac8 levels are not affected by the *pup1-K58E pup3-E51K*, *yck3Δ*, or *vps41Δ* mutations. Wild type was transformed with pRS416 vector (vector) or pRS416-Vac17-GFP and the other indicated strains were transformed with pRS416-Vac17-GFP. Vac17-GFP levels are low in wild type and elevated in the mutants. However, Myo2 and Vac8 levels are not elevated compared to wild type. Pgk1 was used as a loading control. Molecular mass is shown in kilodaltons. Representative of n=3.

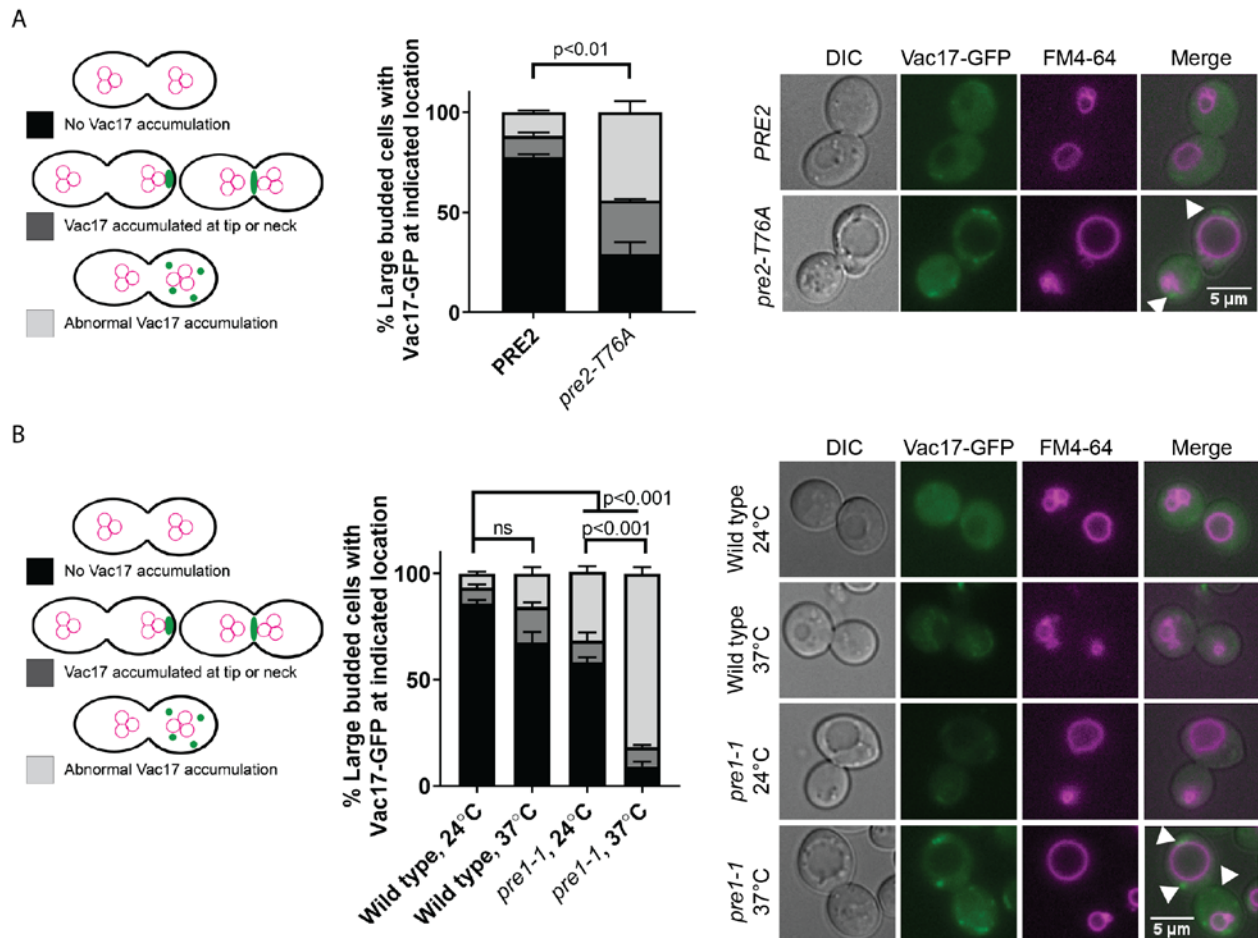
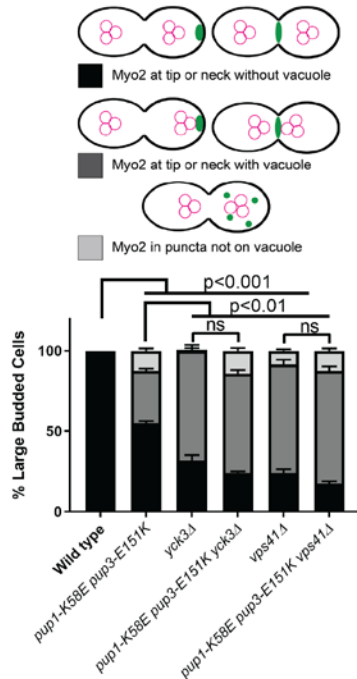


Figure 3.8. Vac17 accumulates in aberrant puncta in proteasome mutants.

A) Vac17 predominately accumulates in proteasome mutants in aberrant puncta (closed arrowheads). Wild type (PRE2) and *pre2-T76A* mutant cells were transformed with pRS415-Vac17-GFP. After FM4-64 labeling, cells were chased at 24°C for 3 hr before imaging. DIC, differential interference contrast. Quantification of 40 large-budded cells per n, n=3. Error bars indicate SEM. Two-way ANOVA and Dunnett’s post-hoc test. Scale bar = 5 μM.

B) Vac17 accumulates in aberrant puncta (closed arrowheads) in a Pre1 temperature sensitive mutant. Wild type and *pre1-1* mutant cells were transformed with pRS416-Vac17-GFP. After FM4-64 labeling, cells were chased at 24°C for 3 hr or 37°C before imaging. DIC, differential interference contrast. Quantification of 40 large-budded cells per n, n=3. Error bars indicate SEM. Two-way ANOVA and Dunnett’s post-hoc test. Scale bar = 5 μM.

A



B

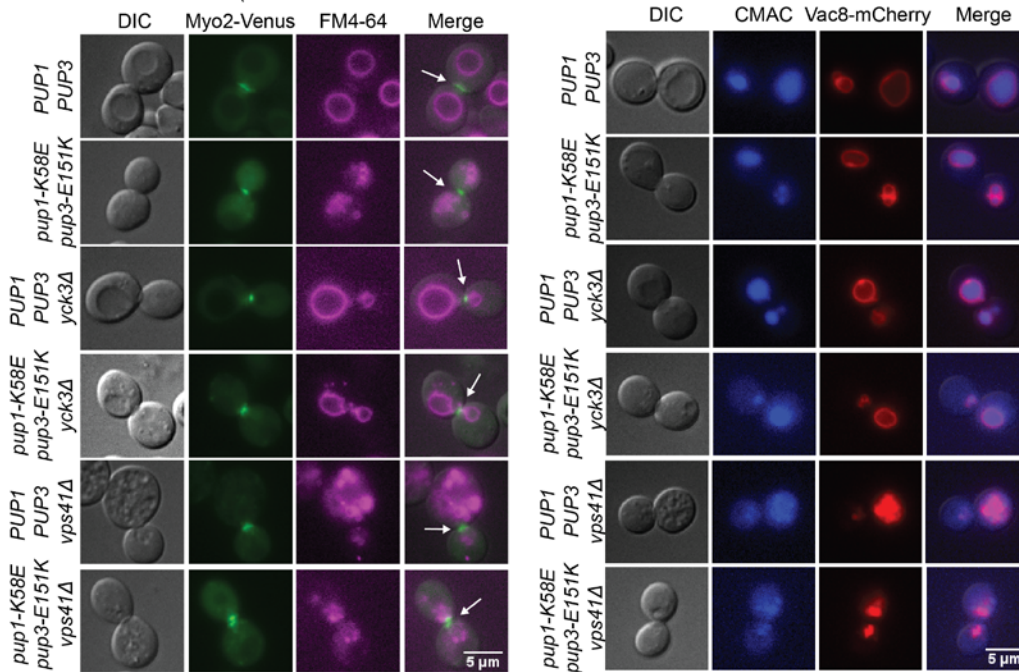
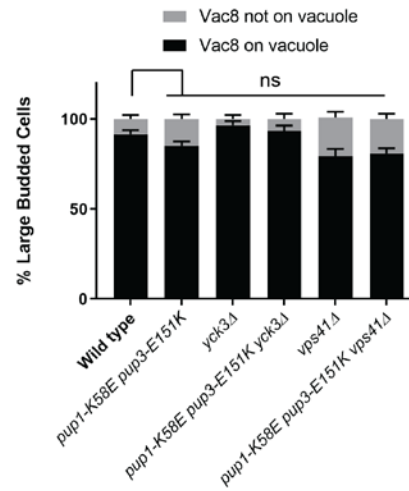


Figure 3.9. Myo2 and Vac8 are not affected in the proteasome mutant.

A) Detachment of Myo2 from the vacuole likely does not require the proteasome. Wild type, *pup1-K58E pup3-E151K*, *yck3Δ*, *pup1-K58E pup3-E151K yck3Δ*, *vps41Δ*, and *pup1-K58E pup3-E151K vps41Δ* mutant cells were transformed with pRS413-Myo2-Venus. Myo2-Venus localized to the bud tip or mother-bud neck (closed arrows) similar to wild type and unlike Vac17-GFP (Fig 5B). After FM4-64 labeling, cells were chased at 24°C for 3 hr before imaging. DIC, differential

interference contrast. Quantification of 40 large-budded cells per n, n=3. Error bars indicate SEM. Two-way ANOVA and Dunnet's post-hoc test. Scale bar = 5 μ M.

B) Yck3 and Vps41 do not regulate Vac8 localization on the vacuole. Wild type, *pup1-K58E pup3-E51K*, *yck3 Δ* , *pup1-K58E pup3-E51K yck3 Δ* , *vps41 Δ* , and *pup1-K58E pup3-E51K vps41 Δ* mutant cells were transformed with pRS413-Vac8-mCherry. After labeling with CMAC, cells were chased at 24°C for 30 min before imaging. DIC, differential interference contrast. Quantification of 40 large-budded cells per n, n=3. Error bars indicate SEM. Two-way ANOVA and Dunnet's post-hoc test. Scale bar = 5 μ M.

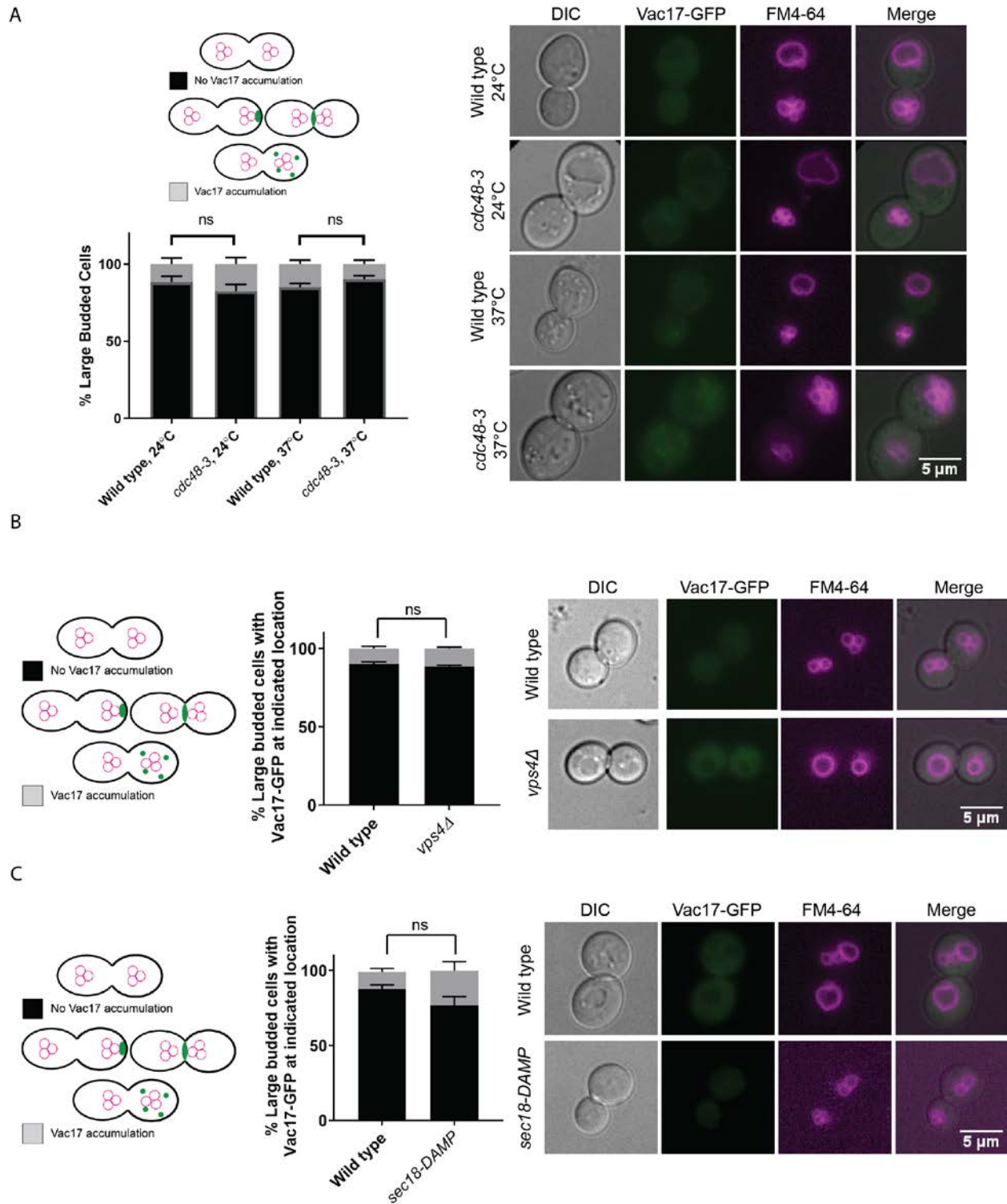


Figure 3.10. Cdc48, Vps4, and Sec18 are not required for the termination of vacuole transport.

A) Cdc48 is not required for the degradation of Vac17. Wild type or *cdc43-3* mutant cells were transformed with pRS415-Vac17-GFP. After FM4-64 labeling, cells were chased either at 24°C

for 3 hr or 37°C for 3 hr before imaging. DIC, differential interference contrast. Quantification of 40 large-budded cells per n, n=3. Error bars indicate SEM. Two-way ANOVA and Tukey's post-hoc test. Scale bar = 5 μ M.

B) Vps4 is not required for the degradation of Vac17. Wild type or *vps4 Δ* mutant cells were transformed with pRS415-Vac17-GFP. After FM4-64 labeling, cells were chased for 3 hr before imaging. DIC, differential interference contrast. Quantification of 40 large-budded cells per n, n=3. Error bars indicate SEM. Two-way ANOVA and Sidak's multiple comparison. Scale bar = 5 μ M.

C) Sec18 is not required for the degradation of Vac17. Wild type or *sec18-DAmP* mutant cells were transformed with pRS416-Vac17-GFP. After FM4-64 labeling, cells were chased for 3 hr before imaging. DIC, differential interference contrast. Quantification of 40 large-budded cells per n, n=3. Error bars indicate SEM. Two-way ANOVA and Sidak's multiple comparison. Scale bar = 5 μ M.

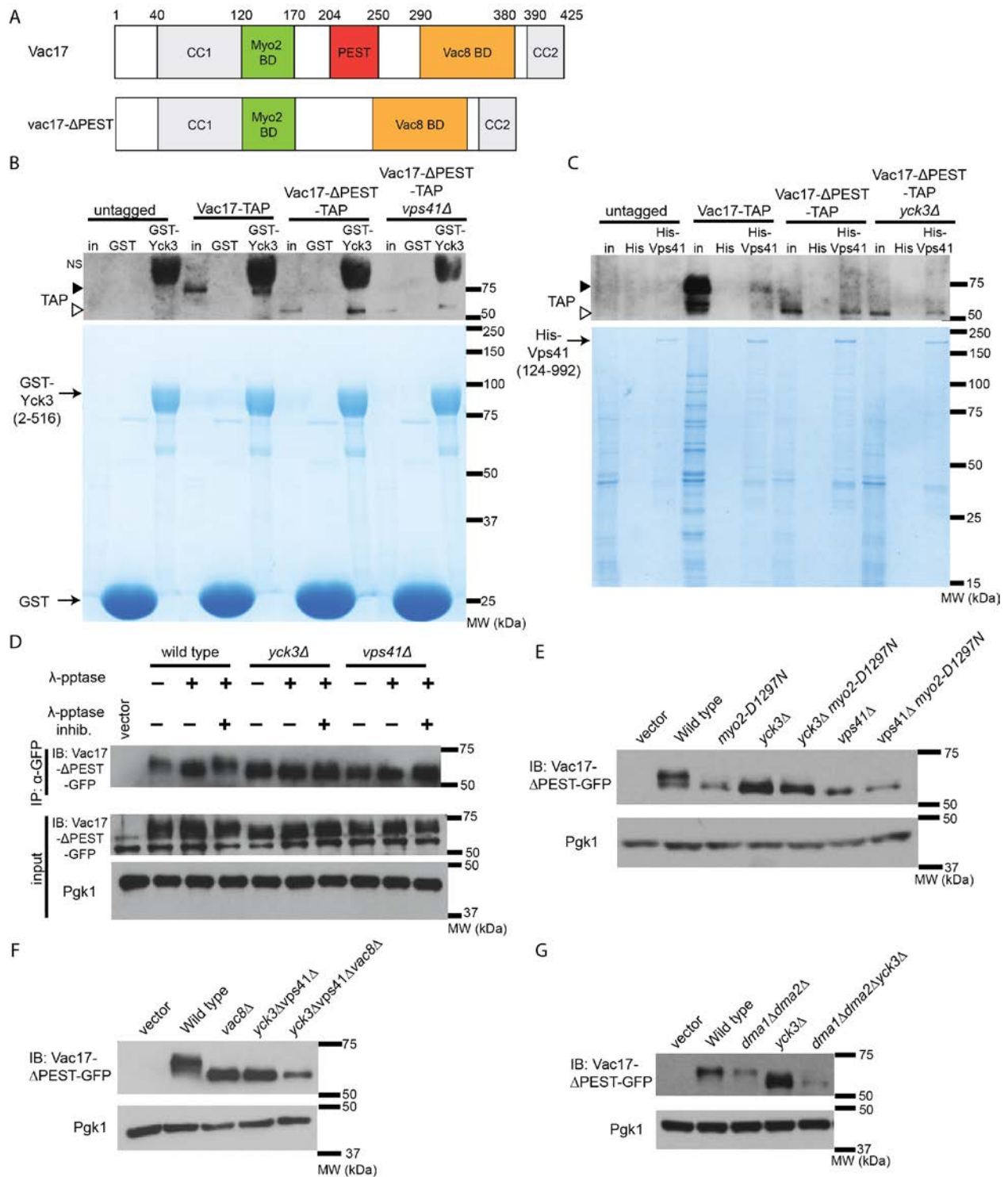


Figure 3.11. Yck3 and Vps41 are required for the phosphorylation of Vac17.

A) Schematic of Vac17 and Vac17- Δ PEST. CC = predicted coiled coil. BD = binding domain.
 B) Purified recombinant GST-Yck3 (2-516) but not GST alone binds Vac17-TAP and Vac17- Δ PEST-TAP from Vac17-TAP, Vac17- Δ PEST-TAP, and *vps41* Δ Vac17- Δ PEST-TAP lysates, respectively.

6.25% input (in). Molecular mass is shown in kilodaltons. Representative of n=3. NS = non-specific band. Black arrowhead = Vac17-TAP. White arrowhead = Vac17- Δ PEST-TAP

C) Purified recombinant HIS-MBP-ctVps41 (124-992) but not HIS alone binds Vac17- Δ PEST-TAP from Vac17-TAP, Vac17- Δ PEST-TAP, and *yck3 Δ* Vac17- Δ PEST-TAP lysates. 6.25% input (in). Molecular mass is shown in kilodaltons. Representative of n=3. Black arrowhead = VAC17-TAP. White arrowhead = VAC17- Δ PEST-TAP

D) Yck3 and Vps41 are required for the phosphorylation of Vac17- Δ PEST-GFP. Wild type, *yck3 Δ* , and *vps41 Δ* mutant cells were transformed with pRS415-Vac17- Δ PEST-GFP. λ -phosphatase treatment causes an increase in the electrophoretic mobility of Vac17-GFP in wild type, but not *yck3 Δ* or *vps41 Δ* mutant cells. Addition of phosphatase inhibitors restores the upper band in wild type cells. Representative of n=3.

E) Yck3 and Vps41 -dependent phosphorylation of Vac17 requires binding to Myo2. *vac17 Δ myo2 Δ* , *vac17 Δ myo2 Δ yck3 Δ* , and *vac17 Δ myo2 Δ vps41 Δ* mutant cells were co-transformed with pRS416-Vac17- Δ PEST-GFP and either pRS413-Myo2 or pRS413-myo2-D1297N. The gel mobility of Vac17- Δ PEST-GFP was analyzed via western blot. Pgk1 was used as a loading control. Molecular mass is shown in kilodaltons. Representative of n=3.

F) Yck3 and Vps41 -dependent phosphorylation requires Vac8. Wild type, *vac8 Δ* , and *vac8 Δ yck3 Δ vps41 Δ* mutant cells were transformed with pRS416-Vac17- Δ PEST-GFP. The gel mobility of Vac17- Δ PEST-GFP was analyzed via western blot. Pgk1 was used as a loading control. Molecular mass is shown in kilodaltons. Representative of n=3.

G) Yck3-dependent phosphorylation of Vac17 does not require Dma1/Dma2. Wild type, *dma1 Δ dma2 Δ* , *yck3 Δ* , and *dma1 Δ dma2 Δ yck3 Δ* mutant cells were transformed with pRS416-Vac17- Δ PEST-GFP and analyzed via western blot. Pgk1 was used as a loading control. Molecular mass is shown in kilodaltons. Representative of n=3.

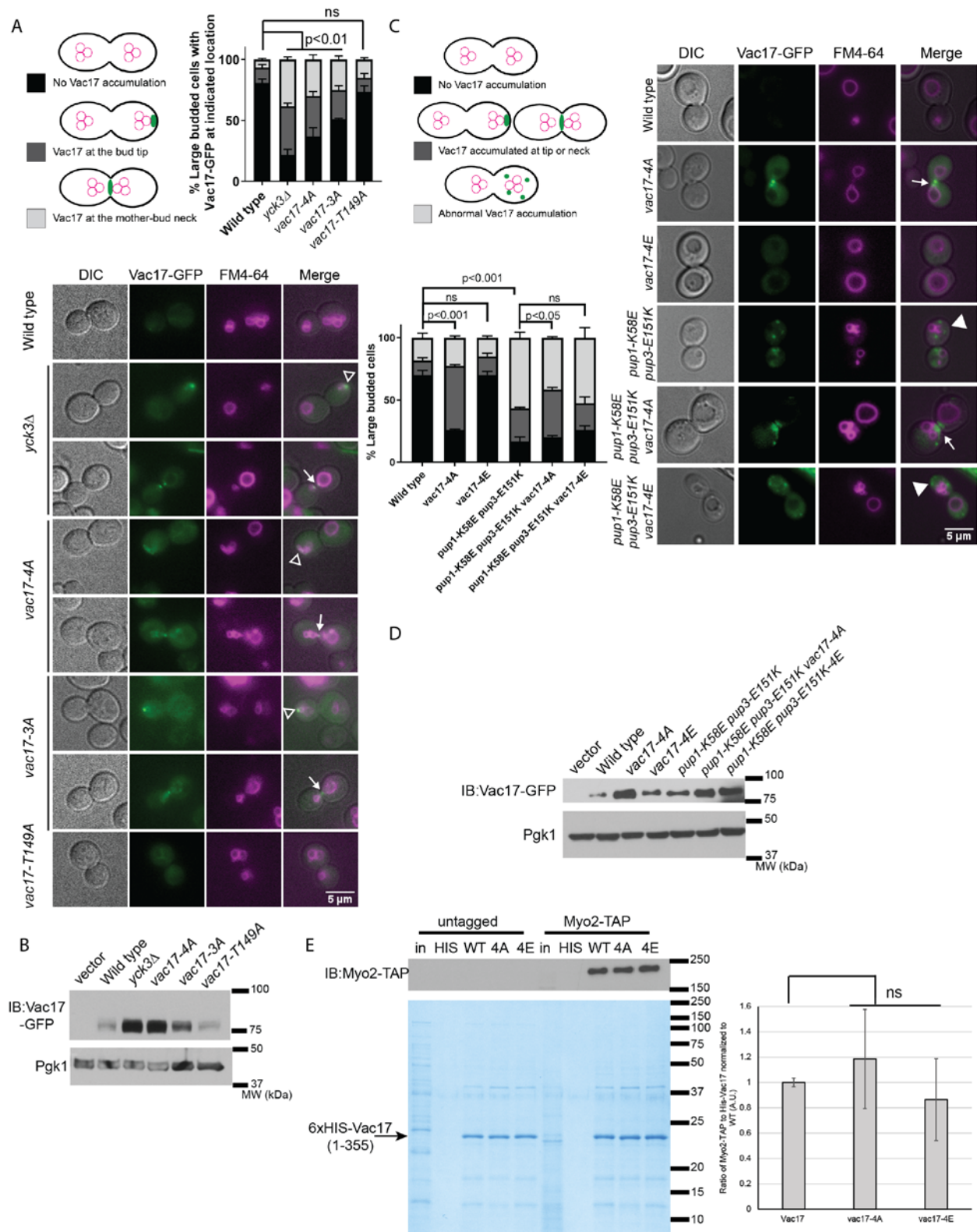


Figure 3.12. Yck3 and Vps41 regulate the phosphorylation of Vac17 in its Myo2 binding domain

A) Similar to deletion of Yck3, the *vac17-4A* mutant results in mislocalization of the vacuole (FM4-64) and accumulation of Vac17-GFP at the bud tip (open arrowheads) or mother-bud neck (closed arrows). *vac17Δ* or *yck3Δvac17Δ* mutant cells were transformed with pRS416-Vac17-GFP or the Vac17 mutant indicated. After FM4-64 labeling, cells were chased at 24°C for 3 hr before imaging. DIC, differential interference contrast. Quantification of 40 large-budded cells per n, n=3. Error bars indicate SEM. Two-way ANOVA and Dunnett's post-hoc test. Scale bar = 5 μM.

B) The non-phosphorylatable alanine mutant, *vac17-4A*, results in elevated levels of Vac17, similar to a *yck3Δ* mutant. *vac17Δ* or *yck3Δvac17Δ* mutant cells were transformed with pRS416-Vac17-GFP or the Vac17 mutant indicated and analyzed via western blot. Pgk1 was used as a loading control. Molecular mass is shown in kilodaltons. Representative of n=3.

C) Vac17-4A-GFP accumulates at the bud tip (open arrowheads) or mother-bud neck (closed arrows) in wild type and the *pup1-K58E pup3-E151K* mutant. This is in contrast to the *pup1-K58E pup3-E151K* mutant alone, which results in Vac17 puncta (closed arrowheads). The *vac17-4E* mutant had similar phenotypes to wild type Vac17. Wild type or *pup1-K58E pup3-E151K* mutant cells were transformed with pRS416-Vac17-GFP or the indicated Vac17 mutant. After FM4-64 labeling, cells were chased at 24°C for 3 hr before imaging. DIC, differential interference contrast. Quantification of 40 large-budded cells per n, n=3. Error bars indicate SEM. Two-way ANOVA and Dunnett's post-hoc test. Scale bar = 5 μM.

D) The *vac17-4A* and *pup1-K58E pup3-E151K* mutants elevate Vac17 levels above wild type. Wild type or *pup1-K58E pup3-E151K* mutant cells were transformed with pRS416-Vac17-GFP or the indicated mutant and analyzed via western blot. Pgk1 was used as a loading control. Molecular mass is shown in kilodaltons. Representative of n=3.

E) Mutation of the four phosphorylation sites in Vac17 at the Vac17-Myo2 interface does not alter binding to Myo2. Purified recombinant HIS-Vac17(1-355), either wild type, the *-4A*, or *-4E* mutants, but not HIS alone binds Myo2-TAP from yeast lysates. 6.25% input (in). Molecular mass is shown in kilodaltons. Representative of n=3.

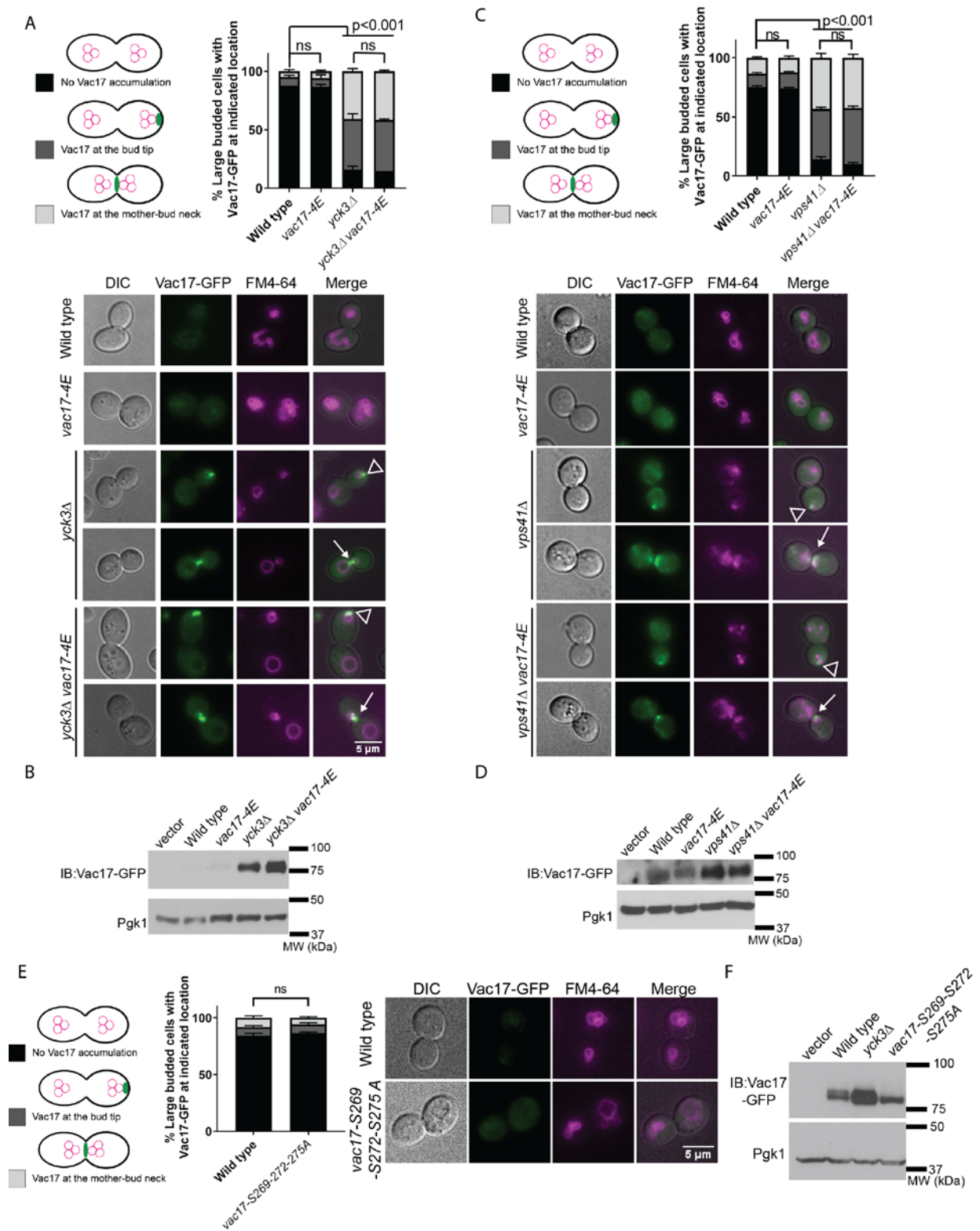


Figure 3.13. Yck3 and Vps41 regulate the phosphorylation of Vac17 in its Myo2 and Vac8 binding regions.

A) The phosphomimetic mutant, *vac17-4E*, does not have a defect in vacuole transport and does not suppress a *yck3Δ* mutant. *vac17Δ* or *yck3Δvac17Δ* mutant cells were transformed with pRS416-Vac17-GFP or pRS416-*vac17-4E*-GFP. After FM4-64 labeling, cells were chased at 24°C for 3 h before imaging. DIC, differential interference contrast. Quantification of 40 large-budded cells per n, n=3. Error bars indicate SEM. Two-way ANOVA and Dunnett's post-hoc test. Scale bar = 5 μM.

B) The phosphomimetic mutant, *vac17-4E*, does not have a defect in Vac17 degradation and does not suppress a *yck3Δ* mutant. *vac17Δ* or *yck3Δvac17Δ* mutant cells were transformed with pRS416-Vac17-GFP or pRS416-*vac17-4E*-GFP and analyzed via western blot. Pgk1 was used as a loading control. Molecular mass is shown in kilodaltons. Representative of n=3.

C) The phosphomimetic mutant, *vac17-4E*, does not have a defect in vacuole transport and does not suppress a *vps41Δ* mutant. *vac17Δ* or *vps41Δvac17Δ* mutant cells were transformed with pRS416-Vac17-GFP or pRS416-*vac17-4E*-GFP. After FM4-64 labeling, cells were chased at 24°C for 3 h before imaging. DIC, differential interference contrast. Quantification of 40 large-budded cells per n, n=3. Error bars indicate SEM. Two-way ANOVA and Dunnett's post-hoc test. Scale bar = 5 μM.

D) The phosphomimetic mutant, *vac17-4E*, does not have a defect in Vac17 degradation and does not suppress a *vps41Δ* mutant. *vac17Δ* or *vps41Δvac17Δ* mutant cells were transformed with pRS416-Vac17-GFP or pRS416-*vac17-4E*-GFP and analyzed via western blot. Pgk1 was used as a loading control. Molecular mass is shown in kilodaltons. Representative of n=3.

E) Similar to wild type, the *vac17-S269-272-275A* mutant allowed for proper vacuole delivery. *vac17Δ* mutant cells were transformed with pRS416-Vac17-GFP or the corresponding mutant. After FM4-64 labeling, cells were chased at 24°C for 3 h before imaging. DIC, differential interference contrast. Quantification of 40 large-budded cells per n, n=3. Error bars indicate SEM. Two-way ANOVA and Dunnett's post-hoc test. Scale bar = 5 μM.

F) Compared to the *yck3Δ* mutant, the *vac17-S269-272-275A* mutant does not elevate Vac17 levels, similar to wild type. *vac17Δ* or *yck3Δ* mutant cells were transformed with pRS416-Vac17-GFP or the *vac17-S269-272-275A* mutant and analyzed via western blot. Pgk1 was used as a loading control. Molecular mass is shown in kilodaltons. Representative of n=3.

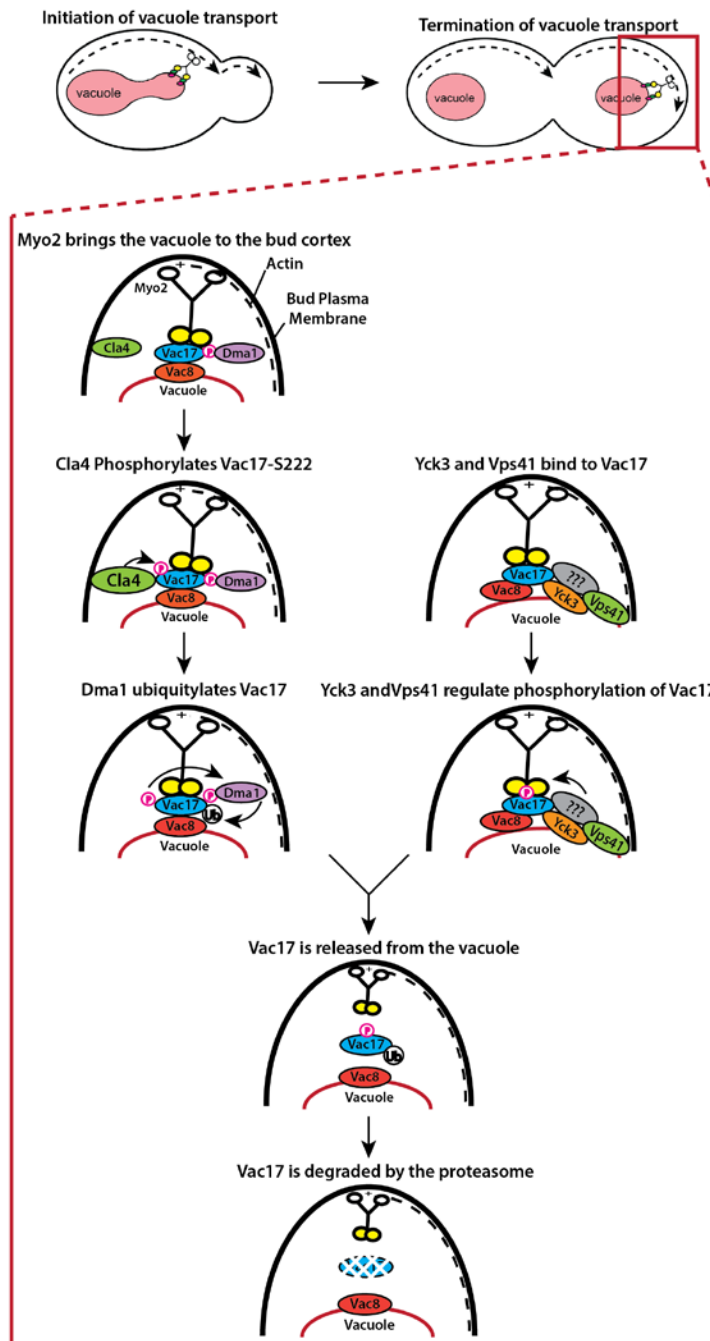


Figure 3.14. Ubiquitylation and Yck3 and Vps41 - dependent phosphorylation are required to release Vac17 from the vacuole.

Previous studies found that Cla4 phosphorylates Vac17-S222. This phosphorylation event triggers the Dma1-dependent ubiquitylation of Vac17. In an independent and non-redundant parallel pathway, Yck3 and Vps41 are responsible for the phosphorylation of Vac17 in the Myo2 binding domain. It is likely that additional unknown regulators are required in this pathway as well. The integration of these two signals lead to the dissociation of the Myo2-Vac17-Vac8 complex and allow for Vac17 to be degraded by the proteasome after cargo release.

CHAPTER IV

FUTURE DIRECTIONS

These studies have uncovered how Myo2 releases the vacuole at the right time and place. Previous studies revealed that the adaptor, Vac17, is ubiquitylated and degraded, and that the degradation of Vac17 is required for Myo2 to unload the vacuole. Our studies have identified a spatial cue that regulates this ubiquitylation step. Cla4, a p21-activated kinase, phosphorylates Vac17 when the vacuole reaches the bud cortex. This phosphorylation event is required for Dma1 to ubiquitylate Vac17 (Yau et al., 2017). It is also one of the few, if not only study, that identifies a spatial signal that triggers cargo release from a motor.

My studies also revealed that a second pathway is required for the release of the vacuole from Myo2. This pathway occurs independently of ubiquitylation. Yck3 and Vps41 are required for the phosphorylation of Vac17 in its Myo2 binding region. This phosphorylation event dissociates ubiquitylated Vac17 from the Myo2-Vac17-Vac8 complex, and thus unloads the vacuole from Myo2. In many cases, ubiquitylation is the final step before degradation by the proteasome. This is one of the few cases where ubiquitylation is not sufficient for degradation. Such cases usually involve an AAA-ATPase to pry apart protein complexes, but we have not yet identified a AAA-ATPase required for the termination of vacuole transport.

It is likely that the mechanisms that regulate vacuole transport apply to other organelles in yeast, as well as to cargoes in mammalian cells. Thus, it is of high importance to advance our understanding of yeast vacuole transport.

Dbf4 may regulate Dma1 to terminate vacuole transport

Our published studies show that Cla4 directly phosphorylates Vac17 at Ser222 and that phosphorylation of this site is essential for the termination of vacuole transport (Yau et al., 2017). Interestingly, phosphorylation of Vac17-S222 is not required for Dma1 recruitment because Dma1-3xGFP is recruited to the vacuole in the *vac17-S222A* mutant (Yau et al., 2014; Yau et al., 2017). However, phosphorylation of Vac17-S222 is required for Dma1 function, as the *vac17-S222A* mutant is not ubiquitylated and vacuole transport is not terminated (Yau et al., 2017). These data indicate that recruitment of Dma1 to the vacuole is necessary but not sufficient for the ubiquitylation and degradation of Vac17. It would be of great interest to determine how Cla4-dependent phosphorylation of Vac17 leads to the ubiquitylation of Vac17 by Dma1.

Cla4-dependent phosphorylation of Vac17-S222 may either (1) recruit a binding partner to facilitate Dma1 activity or (2) change the conformation of Vac17 to allow ubiquitylation. Based on our unpublished studies, the former is more likely. Vac17-F225, another residue in the PEST sequence, is also important for termination of vacuole transport and the *vac17-F225S* mutant shows a similar phenotype to *vac17-S222A* (**Fig 4.1**). Moreover, Vac17-S222 is still phosphorylated in the *vac17-F225S* mutant (data not shown). Together, these data suggest that pS₂₂₂xxF₂₂₅ recruits a binding partner that promotes Dma1 activity.

Notably, pSxxF is a known BRCT domain binding motif (Williams et al., 2004) and my preliminary data suggests that a BRCT domain protein, Dbf4 (Masai and Arai, 2000), plays a role in the termination of vacuole transport. Dbf4 is the activating subunit of Cdc7, which together form an essential kinase that has a known role in the initiation of DNA replication (Chapman and Johnston, 1989; Jackson et al., 1993). Notably, the *dbf4-DAmP* (Decreased Abundance by mRNA Perturbation (Breslow et al., 2008)) has a minor defect in the termination of vacuole transport (**Fig 4.2**). Note that DAmP alleles, used to test essential genes, lower the transcript level and are thus hypomorphs, which may not show robust phenotypes. Dbf4-Cdc7 is predominately found in the nucleus (Cheng et al., 1999; Lepke et al., 1999), thus it is surprising that it would have a role at the vacuole. However, it is possible that a small portion of Dbf4-Cdc7 moves to the vacuole. There is precedence for the regulation of the vacuole by nuclear proteins. Cdk1, which is predominately in the nucleus, directly phosphorylates Vac17 (Peng and Weisman, 2008). Thus, it is possible that a subset of Dbf4 binds to Vac17 after Vac17-S222 is phosphorylated.

While the Dbf4 may bind Vac17, the substrate may be a different member of the complex. Dbf4-Cdc7 is known to phosphorylate serines adjacent to acidic residues (Cho et al., 2006). Interestingly, both Dma1 and the redundant E3 ligase, Dma2, have ES repeats in their C-termini (Saccharomyces Genome Database). Dma1 has three potential phosphorylated serines, Dma1-S382, -S384, and -S386. Mutation of all three serines to alanines (*dma1-3SA*) results in defects in the termination of vacuole transport: Vac17-GFP accumulates with *dma1-3SA-tdTomato* at the bud tip and mother-bud neck and Vac17 levels are elevated in the *dma1-3SA* mutant (**Fig 4.3**). Moreover, levels of the *dma1-3SA-GFP* mutant are elevated compared to wild

type Dma1-GFP (**Fig 4.3**). Since Dma1 auto-ubiquitylates to regulate its levels (Loring et al., 2008; Yau et al., 2014), this further indicates a defect in its enzymatic activity. I hypothesize that Vac17-pS222 recruits Dbf4-Cdc7, which phosphorylates Dma1 and results in activation of Dma1 and the ubiquitylation of Vac17. An alternative hypothesis is that Dbf4-Cdc7 acts on Vac17 or other members of the complex, or other sites on Dma1, and it is possible that a different kinase regulates Dma1 at its C terminus.

Determine if Dbf4 interacts with Vac17-pS222

The first step would be to determine if and when Dbf4 interacts with Vac17. An *in vivo* assay, such as a BiFC (Hu et al., 2002) assay, could be utilized. Dbf4 would be tagged with the N terminus of Venus, while Vac17 would be tagged with the C terminus of Venus. If Dbf4 and Vac17 interact, fluorescence of the assembled Venus will be detected. BiFC between Vac8 and Vac17 could serve as a positive control for the assay. I expect that Dbf4 binds to Vac17 after Cla4 phosphorylates Vac17 at either the bud cortex or on the vacuole and that the *vac17-S222A* mutant ablates the interaction. As orthogonal approaches, *in vitro* binding and yeast two hybrid assays (Fields and Song, 1989) would corroborate if Vac17 directly binds to Dbf4. Vac8 (Tang et al., 2006) and Cdc7 (Ramer et al., 2013) will serve as positive controls known to directly interact with Vac17 and Dbf4, respectively. The *vac17-S222A* mutant and a Dbf4 mutant lacking the BRCT domain will serve as negative controls that will not interact with wild type Dbf4 and Vac17, respectively. These studies would reveal whether Dbf4 interacts with Vac17-pS222 in the bud.

Determine if Dbf4-Cdc7 activity is required for ubiquitylation of Vac17

If Vac17-pS222 recruits Dbf4, then it is possible that Dbf4-Cdc7 directly targets Dma1. I would test if Dbf4-Cdc7 directly phosphorylates Dma1 using an *in vitro* kinase assay (Jiang et al., 1999; Tsuji et al., 2006). A kinase dead Dbf4-Cdc7 (Gerard et al., 2006) and the *dma1-3SA* mutant would serve as negative controls. I expect that wild type, but not kinase dead, Dbf4-Cdc7 will phosphorylate Dma1, but not the *dma1-3SA* mutant, *in vitro*. A caveat is that previous studies used mammalian Dbf4-Cdc7 and it may be that an *in vitro* assay cannot be developed for the yeast proteins. As an orthogonal approach, I would determine if *in vivo* phosphorylation of Dma1 is ablated in loss-of-function Dbf4-Cdc7 temperature sensitive mutants (Jackson et al., 1993). Phosphorylation status will be assessed by gel shifts in molecular weight on a low percentage SDS-PAGE gel. I predict less phosphorylation in the non-phosphorylatable *dma1-3SA* mutant protein and in wild type Dma1 in the Dbf4-Cdc7 mutants at the restrictive temperature. These studies will determine whether Dma1 is directly phosphorylated by Dbf4-Cdc7 at the ESESES motif.

To determine if phosphorylation of Dma1 regulates the ubiquitylation of Vac17, I would perform *in vivo* ubiquitylation assays to determine if Vac17 is ubiquitylated by the *dma1-3SA* mutant. Wild type Dma1 would serve as a positive control for ubiquitylation of Vac17. *vac17-S222A*, which cannot be ubiquitylated, would serve as a negative control. These data would test whether there is a functional relationship between phosphorylation of Dma1 and its ability to ubiquitylate Vac17. I would also test if other Dma1 targets, Swe1 (Raspelli et al., 2011) and Pcl1 (Hernandez-Ortega et al., 2013), are stabilized in the *dma1-3SA* mutant via western blot and/or cannot be ubiquitylated by the *dma1-3SA* mutant via *in vivo* ubiquitylation assays. One caveat is

that the *dma1-3SA* mutant may be due to a general loss of function from an effect on the protein, as opposed to ablating its regulation.

The *dma1-3SD-GFP* mutant does not have defects in vacuole transport, suggesting that it may function as a phosphomimetic allele (**Fig 4.3**). This genetic tool may be used to determine if Dbf4 is required for phosphorylation of Dma1, and if this event is required for Vac17 turnover. For example, the *dma1-3SD* mutant may suppress the *Dbf4-DAmP* allele if Dbf4 is indeed regulating Dma1 at these sites.

Future studies will determine whether phosphorylation of Dma1 facilitates its binding to an E2 ubiquitin-conjugating enzyme or activates Dma1 via another mechanism. These studies would reveal how Dma1 E3 ligase activity is spatially and temporally regulated.

Yeast Two Hybrid Screen for Vac17-pS222xxF225 Binding Partners

It is possible that Dbf4 is not the regulator recruited by Vac17-pS222xxF225. As an unbiased approach, I developed a yeast two hybrid screen to identify binding partners of Vac17-pS222xxF225. I found that the phosphomimetic *vac17-S222E* mutant did not have defects in vacuole transport and was still able to bind to Myo2 by yeast two hybrid (**Fig 4.4**). This suggests that *vac17-S222E* may function as a true phosphomimetic and interact with its binding partner.

Preliminary screen suggests candidate may bind vac17-S222E but not vac17-S222A

For the initial screen, a pGAD library (C3, a gift from Dr. Mara Duncan, University of Michigan) was transformed into cells containing a pGBD vector fused to the *vac17-S222E* (1-

355) phosphomimetic mutant (**Fig 4.5**). The pGAD fragments of interacting clones were then isolated and sequenced. The isolated pGAD fragments were tested via a yeast two-hybrid assay for interaction with *vac17-S222E* and *vac17-S222A* mutants (**Fig 4.5**). This verified the interaction with *vac17-S222E*. Moreover, some candidates bound to *vac17-S222E* but not *vac17-S222A* and were pursued further as candidates that interact with Vac17-pS222. Sequencing analysis identified the gene at *Upc2*. However, deletion of *Upc2* and/or its paralog *Ecm22* did not result in elevated levels of Vac17 or defects in the termination of vacuole transport (**Fig 4.6**). Thus, it is likely that *Upc2* was a false positive. Future studies should further analyze hits that interacted with both *vac17-S222E* and *vac17-S222A*, as it is possible that the screen was too stringent in identifying potential binding partners.

Since this screen is not saturated, it is worth repeating with libraries containing different reading frames. The fact that some candidates bound *vac17-S222E* and not *vac17-S222A* suggest that this screen would be able to identify a true binding partner of Vac17-pS222. Mutation of the candidate should result in a defect in the termination of vacuole transport. Orthogonal verification may be conducted with *vac17-F225S*, which would be predicted to block binding to the candidate. This would provide support for the hypothesis that pS222xF225 is indeed the binding motif.

Determine if yeast two- hybrid screen candidates have a role in vacuole transport

After identification of potential candidates, further verification and analysis would determine if these candidates are true regulators of vacuole transport. First, isolated candidates should be verified by yeast two-hybrid assays for interaction with *vac17-S222E* and

vac17-S222A. Potential binding partners would interact with *vac17-S222E* but not *vac17-S222A*. Next, loss of function mutants of candidates should be tested for defects in the termination of vacuole transport and should show phenotypes similar to *vac17-S222A*. *In vitro* binding assays and/or *in vivo* pulldown experiments would determine if the candidate is able to bind to Vac17 but not *vac17-S222A* or *vac17-F225S*. If *in vivo* binding experiments cannot be performed, co-localization experiments may provide evidence that the candidate interacts with Vac17 in the cell. If a candidate appears to have a role in vacuole transport, even without interacting with Vac17, it would be worthwhile to determine if the gene is required for the ubiquitylation of Vac17. If the candidate is not required for ubiquitylation, it may be involved in the Yck3 and Vps41 -dependent pathway and should be tested in this context.

I predict that Vac17-pS222 recruits a kinase or kinase complex that phosphorylates, or otherwise activates, Dma1. This screen would reveal novel binding partners of Vac17-pS222 that will be further tested for roles in terminating vacuole transport.

Yck3 and Vps41 regulate peroxisome transport

Deletion of Dma1 results in the mis-localization of the vacuole to the mother-bud neck. Interestingly, peroxisomes also accumulate at the mother-bud neck in this mutant (Yau et al., 2014). Thus, we tested if Yck3 and Vps41 also regulate peroxisome transport. Peroxisomes were labeled by integration of PTS1-GFP. Deletion of Yck3 and/or Vps41 results in accumulation of peroxisomes at the mother bud neck (**Fig 4.7**). This suggests that Yck3 and Vps41 regulate the transport of multiple cargoes, including the vacuole and peroxisomes, in yeast.

Peroxisomes were shown to be transport via their tethering to other organelles (Guimaraes et al., 2015; Salogiannis et al., 2016), which suggested that this phenotype may be due to indirect effects from defects in vacuole transport. However, this phenotype is not due to a defect in the termination of vacuole transport, as the *vac17-ΔPEST* mutant is not defective in peroxisome transport (**Fig 4.7**). Thus, Yck3 and Vps41 may directly regulate peroxisome transport.

It would be interesting to determine how Yck3 and Vps41 regulate peroxisome transport. This mechanism could be through direct regulation of Inp2, the peroxisome adaptor. Although Yck3 and Vps41 have known roles on the vacuole, it is possible that a subset can localize to peroxisomes, either directly or through an organelle contact site. Similar to our studies on Vac17, it would be interesting to see if Inp2 is a direct target of Yck3 and Vps41. Alternatively, the defect in vacuole transport could be causing an indirect effect on peroxisome transport that is not apparent in the *vac17-ΔPEST* mutant. The *vac17-S127-S128-S131-T149A* mutant that is not phosphorylated in a Yck3 and Vps41 -dependent manner should be tested for defects in peroxisome transport. These studies would provide greater mechanistic insight into how yeast organelles are detached from Myo2, as well as show that these mechanisms are used by multiple organelles. That some organelles are regulated by the same mechanisms would suggest that these events are coordinated in space and time.

Vps41 and Yck3 may regulate the interaction between Myo2 and Vac17

Our studies revealed that Yck3 and Vps41 regulate the phosphorylation of Vac17. SILAC experiments revealed that the phosphorylation of Vac17-ΔPEST is altered in the *vps41Δ* and

yck3Δ mutants (**Table 3, Table 4**, respectively). Interestingly, Vps41 seems to be required for the phosphorylation of four Vac17 residues in its Myo2 binding region: S127, S128, S131, T149 (**Fig 3.12, 3.13**). However, Yck3 has a moderate effect on only one of the four sites identified, S131 (**Table 4**). Thus, it is likely that Vps41 recruits or regulates another kinase(s) that phosphorylates Vac17 in the Myo2 binding region. Alanine mutations in other potential phosphosites did not result in elevated Vac17 levels (**Figure 3.12, 3.13, Table 5**).

Yck3 may phosphorylate Vac17 after it is primed by another kinase. Alternatively, Yck3 may function as a priming kinase for another regulating kinase. For example, CK1 primes substrates for phosphorylation by GSK3 (Cesaro and Pinna, 2015; Xu et al., 2010). Interestingly, ILK and GSK3 regulate melanosome trafficking and transfer of melanin to keratinocytes (Crawford et al., 2020). Thus, Mck1 (Andoh et al., 2000), Ygk3 (Griffioen et al., 2003), Rim11 (Bowdish et al., 1994), and Mrk1 (Byrne and Wolfe, 2005), the four yeast homologs of GSK3, are candidate kinases for Vac17. First, a loss of function GSK3 mutant should be tested for a defect in the termination of vacuole transport. If GSK3 appears to have a role in vacuole transport, further studies should determine if it is responsible for the phosphorylation of Vac17 in a Vps41-dependent manner. One caveat is that construction of this quadruple mutant may be difficult.

Another possibility is that Yck3 may phosphorylate the Myo2 cargo binding domain. In one experiment, the phosphorylation of Myo2-S1131, -T1132, and -S1135 was slightly lowered in the *yck3Δ* mutant (**Table 4**). Note that our structure of Myo2 (1132-1572) includes residues beginning at 1152 (Pashkova et al., 2006), so it is unclear if Myo2-S1131, -T1132, and -S1135 are surface residues. If these residues reside on the surface, the non-phosphorylatable alanine

mutants should be tested for defects in the termination of vacuole transport. If no phenotype is observed, these mutations in Myo2 should be combined with the Vac17 phosphorylation mutants. Beyond testing these additional phosphorylation sites, it would be of great interest to determine how this event regulates the interaction between Vac17 and Myo2. This may be studied by in vitro binding assays, in vivo pulldowns, structural studies, or other methods. These studies would reveal if Yck3 has a role in regulating the interaction between Vac17 and Myo2.

Vps41 and Yck3 may regulate the interaction between Vac17 and Vac8

Our studies suggest that Vps41 and Yck3 regulate the phosphorylation of Vac17 in the Myo2 binding region. This phosphorylation event may lead to the dissociation of Vac17 from the Myo2-Vac17-Vac8 complex. It is tempting to speculate that additional steps promote the dissociation of Vac17 from Vac8. SILAC experiments suggest that Vps41 and Yck3 regulate the phosphorylation of Vac17 in and near the Vac8 binding region: S269, S272, S275, S337, S338, S359 (**Table 3, Table 4**). However, mutation of these residues to the non-phosphorylatable alanine mutants did not have defects in the termination of vacuole transport (**Fig 3.13, Table 5**). Moreover, Yck3 and Vps41 may regulate the phosphorylation of Vac8-S16 (**Table 3, Table 4**). The *vac8-S16A* mutant alone or combined with *vac17-S269-S272-S275-S337-S338-S359A* does not have defects in vacuole transport (**Fig 3.13**).

It is possible that currently unidentified events may be crucial to the dissociation of Vac17 and Vac8. SILAC experiments could be repeated with alpha factor arrest and release to test the phosphorylation of Vac17 during key points in the cell cycle, such as before (0min), during (50min), and after (100min) the vacuole is actively transported. Future investigation may

also want to include tests of full length Vac17, as the *vac17-ΔPEST* mutant may be missing key regulatory residues and binding partners. This may be especially pertinent to regulation by Yck3, as the casein kinase I isoforms, Yck1 and Yck2, have been shown to regulate a PEST sequence in another protein (Marchal et al., 2000).

Identification of the Vac17 ubiquitylation site

The Vac17 ubiquitylation site is currently unknown. We had previously assumed that it was within the PEST sequence, since our studies focused on the PEST sequence's role in Vac17 degradation. With our new studies on Yck3 and Vps41, we have new genetic tools to study a stabilized Vac17 that is ubiquitylated and not degraded.

Ubi4/ubiquitin (Ozkaynak et al., 1987) had increased interaction with Vac17 in *vps41Δ* (**Table 6**), but was not affected or perhaps even less interaction in *yck3Δ* (**Table 7**). This is opposite of our results from in vivo ubiquitylation assays, where ubiquitylation of Vac17 was increased in *yck3Δ* and about the same as wild type in *vps41Δ* (**Fig 3.6**). However, it is likely that Vac17 is more ubiquitylated in *yck3Δ* and/or *vps41Δ* since Vac17 is likely trapped in the complex in both mutants and has time to be hyper-ubiquitylated. It would be interested to test if increasing ubiquitylation of Vac17 can bypass *yck3Δ* and/or *vps41Δ* mutations. This can be done using inducible ubiquitylation of Vac17, such as auxin inducible degradation (AID) (Nishimura et al., 2009).

SILAC suggested that Vac17 is ubiquitlated within the PEST sequence at K277 (**Table 4**). It would be of interest to verify that this is the site of ubiquitylation. Further studies may determine whether this is mono-ubiquitin or branched ubiquitin and if branched, what are the

linkages, as these different types of ubiquitylation may indicate different modes of regulation and signaling.

Identification of Vac17 binding partners

Our initial SILAC experiments with the Jason MacGurn lab (Vanderbilt University), were designed to identify phosphorylated residues in Vac17, but also revealed phosphopeptides that were presumably from other interacting proteins (**Table 6, Table 7**). Vac17- Δ PEST appeared to interact less with Vac8, especially in *yck3 Δ* , and less with Myo2, especially in *vps41 Δ* . This aligns with our findings that Yck3 may regulate Vac17 dissociation with Vac8, and Vps41 may regulate Vac17 dissociation with Myo2. However, we would expect the deletion mutants to show increased binding with Vac8 or Myo2, while we observe the opposite. Further analysis may determine why this discrepancy occurs. One possibility is that it is an artifact of the experiment, which focused on detecting phosphorylated peptides.

One experiment showed Vac17 had increased interaction with Atg18 in a *yck3 Δ* mutant. Atg18 has roles in autophagy and the cytoplasm-to-vacuole targeting (CVT) pathway (Barth et al., 2001). It was previously shown that Atg18 and Vac17 interact *in vivo* and by yeast two-hybrid, but the *atg18 Δ* mutant did not have defects in vacuole transport (Efe et al., 2007). The functional significance of the interaction between Vac17 and Atg18 is currently unknown, but may indicate a role for Vac17 in vesicle trafficking that begins at the vacuole (Efe et al., 2007).

Since our experiments focused on identifying phosphorylation sites, it would be worth performing experiments dedicated to identifying interactors of Vac17. These experiments should utilize full length Vac17. If full length Vac17 levels are not sufficient to perform these

experiments, we should consider point mutants that elevate Vac17 levels, but still allow most interactions. For example, the *vac17-S222A* mutant would allow interaction with Dma1 and other regulators, but not what binds to Vac17-pS222.

It is likely that regulators related to the dissociation of the Myo2-Vac17-Vac8 complex will be identified. These regulators may work directly with the proteasome or somehow extract proteins from membrane complexes. If these experiments do not identify a new regulator, a more targeted screen should investigate AAA ATPases. One candidate is Msp1, a AAA ATPase on mitochondria that works with the proteasome (Nakai et al., 1993; Okreglak and Walter, 2014). Identification of new Vac17 binding partners will reveal details about how Vac17 is regulated.

Identification of novel genes required for vacuole transport

It is likely that additional regulators are required for vacuole inheritance. This includes a binding partner that interacts with Vac17-pS222xxF225, as well as additional kinases that act in the Yck3 and Vps41-dependent pathway. Moreover, little is known about how the Myo2-Vac17-Vac8 complex is formed aside from regulation by Cdk1, and phosphorylation by Cdk1 is likely not the only mode of regulation for the formation of the complex.

To identify genes with roles in vacuole transport, we performed a Synthetic Genetic Array (SGA) screen (Cohen and Schuldiner, 2011). A query strain expressing endogenous Vac17-Envy (a GFP variant (Slubowski et al., 2015)) was mated against the knockout (Guri Giaever, 2002) and DAMP (Breslow et al., 2008) yeast collections. Automated microscopy collected images of the mutants, which were then analyzed by eye for mutants with elevated Vac17.

From the initial screen, we identified 181 candidate genes (**Table 8**). As expected, several genes involved with the proteasome were identified. Additionally, Dbf4 and Vps41, which were shown to have defects in the termination of vacuole transport, were also identified. Thus, our screen likely identified genes required for vacuole transport. However, the screen was not very sensitive, as it was hard to detect Vac17-Envy, and a different screen may be a more suitable future approach.

To verify potential hits, we assessed candidates by microscopy. Candidates were transformed with a plasmid expressing Vac17-GFP and the vacuoles were stained with FM4-64. Top candidates were imaged and defects in either initiation or termination of vacuole transport were quantified compared to a *dma1Δ* control (**Fig 4.9**). Most candidates had defects in the initiation or termination of vacuole transport, while others had novel phenotypes that have not been previously reported. However, it is likely that these phenotypes were indirect effects or artifacts of the mutation and we suspect that many candidates are false positives.

One interesting example, the *pda1Δ* mutant, showed puncta of Vac17 that were not on the vacuole or with Myo2 (**Fig 4.9**). These puncta are reminiscent of the puncta observed in loss of function proteasome mutants (**Fig 3.7, Fig 3.8**). Pda1 is a pyruvate dehydrogenase (Steensma et al., 1990) found near ERMES and peroxisomes (Cohen et al., 2014). While it is unclear how Pda1 may function in Vac17 degradation, it may hint at a link between vacuole transport and other organelles. It would be interesting to determine if Pda1 functions in the ubiquitylation of Vac17, or acts in the Yck3 and Vps41 dependent pathway.

Further studies may closely examine other candidates. It is possible that subtle phenotypes may become more apparent if related deletions, such as paralogs or partially

redundant genes, are combined. Some genes currently have unknown functions and are not named, suggesting that novel players may have exclusive roles in vacuole transport. After verification of the phenotypes, it would be important to determine if these players directly regulate Vac17 or if the phenotypes are due to off target effects. Even if the candidates indirectly regulate vacuole transport, it may provide greater insight into how vacuole transport is coordinated with cellular processes.

A more rigorous approach would be to redesign an unbiased screen for regulators of vacuole transport. This screen should focus on increasing sensitivity, such as by tagging Vac17 with a brighter fluorophore. The screen should also be aware of new phenotypes that have only been described in recent years and may have been overlooked in past screening parameters.

Open Questions without preliminary data

Coordination between the initiation and termination of vacuole transport

There is likely interplay between the initiation and termination of vacuole transport. It is tempting to speculate that there are players that regulate both processes and/or signals that play into feedback loops. Some vacuole inheritance mutants are able to inherit vacuoles a minority of the time or are able to inherit small vacuoles. It would be interesting to determine if these inheritance mutants also have defects in the termination of vacuole transport. It is possible that some inheritance mutants will have defects in termination, while others do not. Further studies could determine why these differences exist.

Coordination between function of the vacuole and vacuole transport

Just as there is likely coordination between the initiation and termination of vacuole transport, there may be coordination between vacuole transport and the functional status of the vacuole itself. It would be interesting to test if affecting different functions of the vacuole (fission, fusion, degradation, trafficking) by genetics, stress, or drugs, also affect vacuole transport. For example, loss of function CORVET mutants have defects in the initiation of vacuole transport (Banta et al., 1990). In some cells, the mother vacuole appears to be one large vacuole during budding, but then several smaller vacuoles after cell division (Fusheng Tang, 2003). This phenotype has not yet been properly tested, or quantified, but may indicate a correlation between vacuole fusion/fission dynamics and vacuole transport. Alternatively, it may indicate a correlation between endosome-vacuole fusion and other vacuole processes.

Coordination of the termination of vacuole transport and the cell cycle

The presence and maturity of the vacuole is required for budding (Jin and Weisman, 2015). It is also possible that the termination of vacuole transport is coordinated with the cell cycle. Mutants that are defective in the termination of vacuole transport may have larger buds than wild type. This observation should be quantified. If significant, future studies may uncover how vacuole transport is coordinated with the cell cycle and bud size.

One interesting possibility is that phosphatases may regulate Vac17 in coordination with the cell cycle. The phosphorylation of Vac17 is tightly regulated by space and time and facilitates interaction with its binding partners. Thus, it is possible that the dephosphorylation of certain Vac17 residues also have a role in the regulation of vacuole transport. Cdc14 may

have a role in vacuole transport, as the DAmP allele may have had a minor defect in the termination of vacuole transport (data not shown).

Alternative pathways for Vac17 degradation

Some termination mutants appear to accumulate Vac17-GFP in the vacuole. This phenotype should be quantified. This observation suggests that there is an alternative pathway for degradation when Vac17 cannot be ubiquitylated. This pathway may be a previously established degradation pathway, or a new pathway that has not been described. One possibility is the ESCRT pathway, which can transport vacuole membrane proteins into the vacuole for degradation (Li et al., 2015a; Li et al., 2015b; Oku et al., 2017).

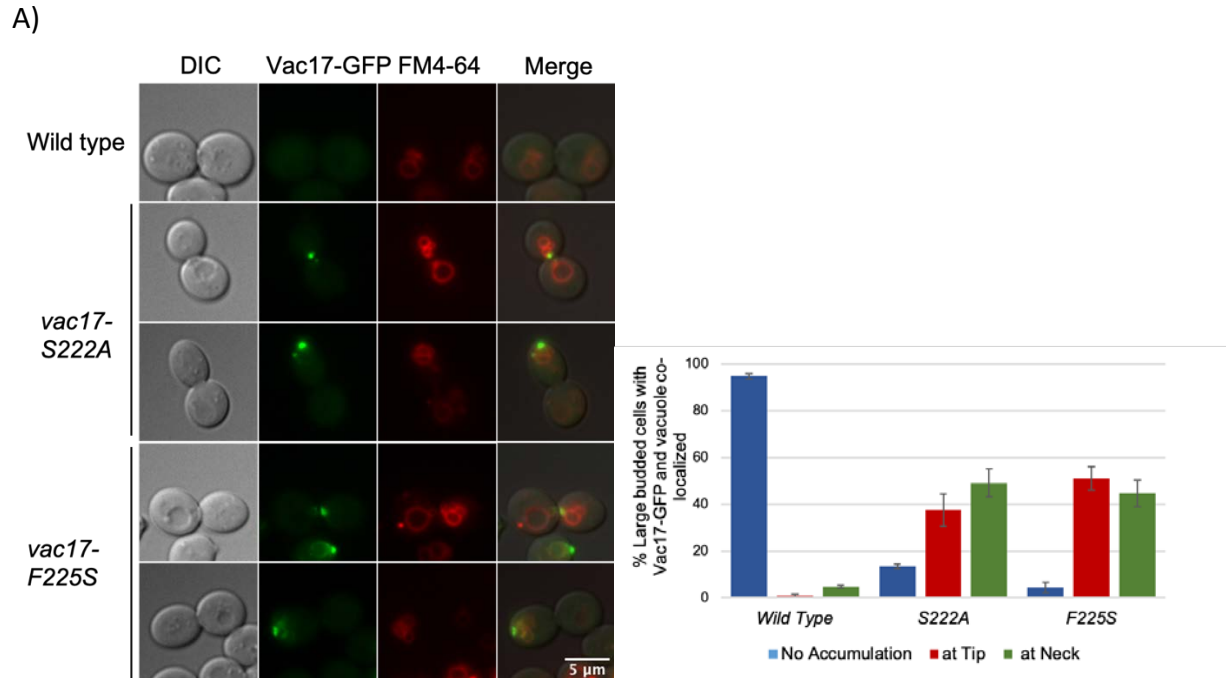


Figure 4.1. Vac17-F225 is required for the termination of vacuole transport. A) *vac17-F225S-GFP* mutant has a defect in the termination of vacuole transport similar to the *vac17-S222A-GFP* mutant, where Vac17 and the vacuole are accumulated at the bud tip or mother-bud neck. n=3, 40 cells per n. p<0.05 students t test. B) *vac17-F225S-GFP* mutant results in accumulation of Vac17, similar to the *vac17-S222A-GFP* mutant. Representative of n=3.

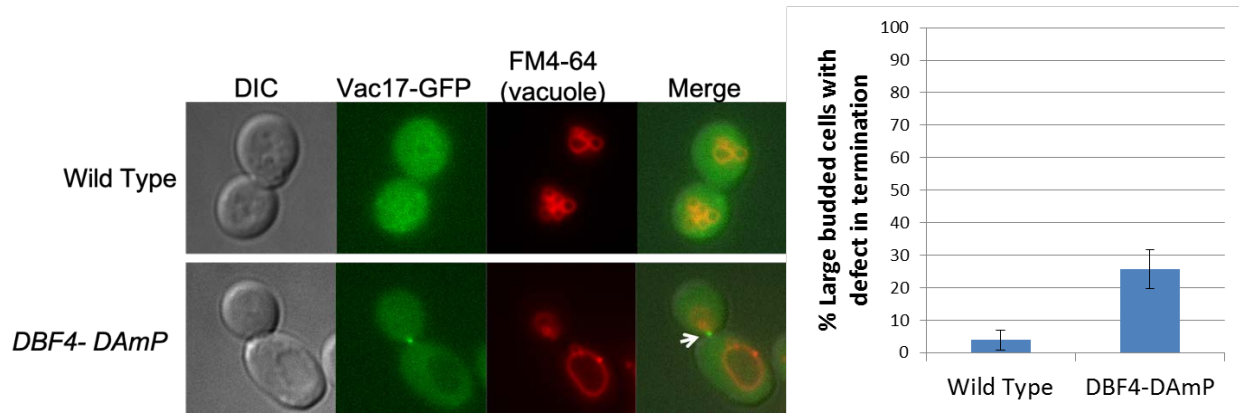


Figure 4.2. Dbf4 may have a role in vacuole transport. The *dbf4-DAMP* mutant has a minor defect in the termination of vacuole transport. $n=3$, >13 cells per strain per experiment p -value = 0.06. students t test.

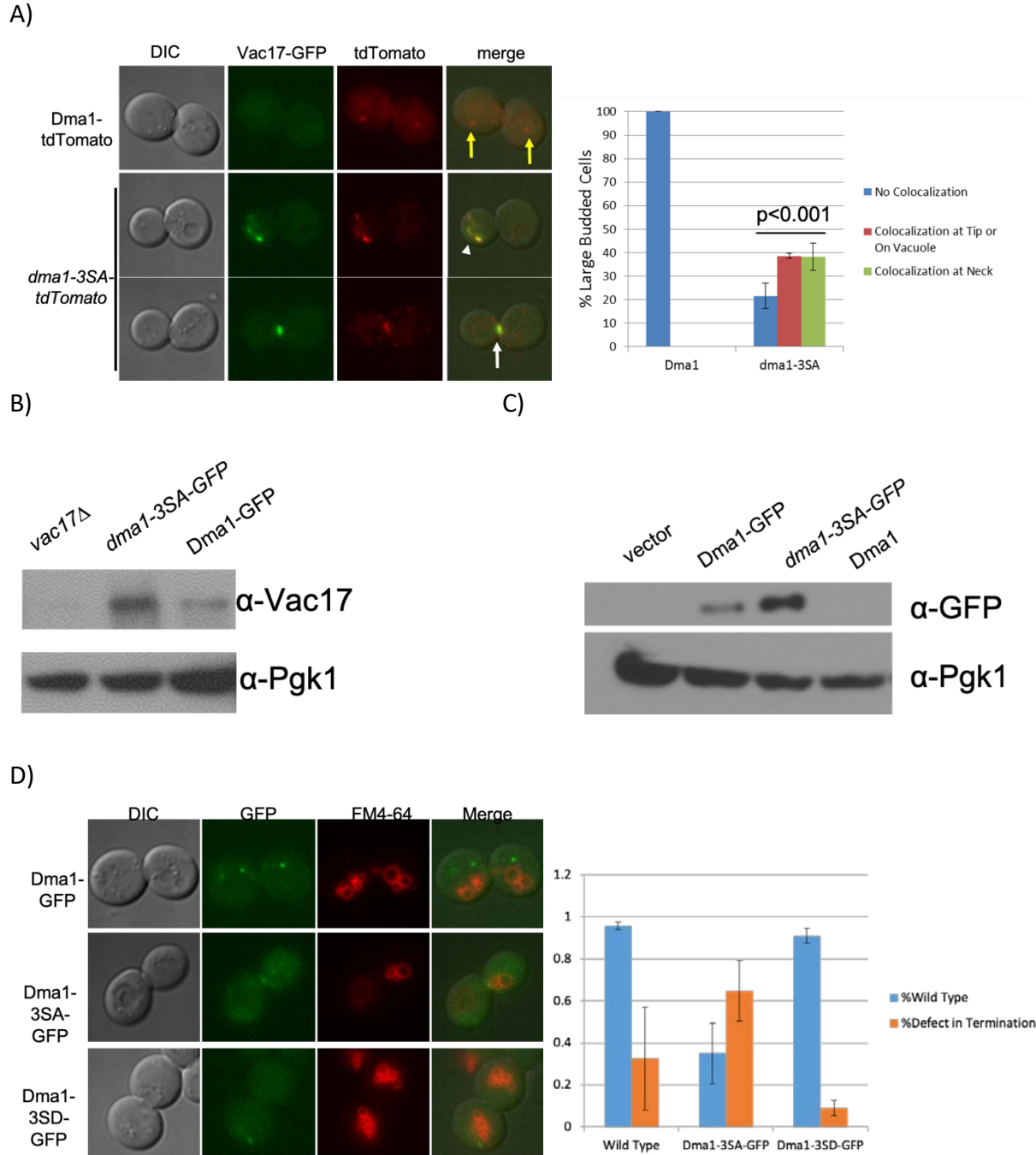
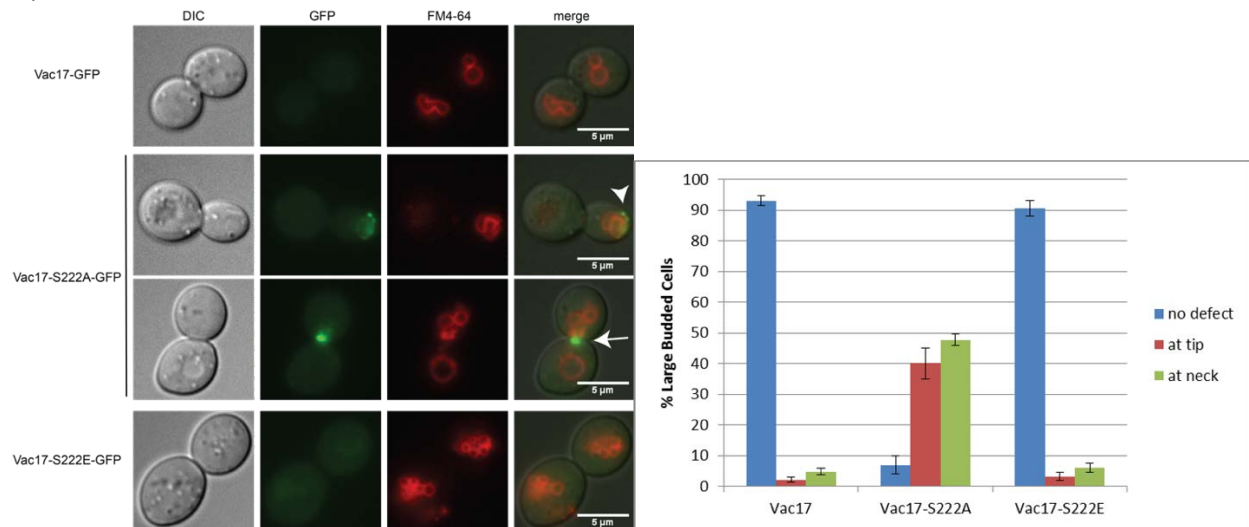


Figure 4.3. Dma1 may be regulated by phosphorylation. A) The *dma1-3SA-tdTomato* mutant results in a defect in the termination of vacuole transport, where Vac17-GFP is accumulated and co-localized at the bud tip and mother-bud neck. $n=3$, >17 cells per strain per experiment. Student's t test. B) The *dma1-3SA-GFP* mutant results in elevated levels of endogenous Vac17. Representative $n=3$. C) The *dma1-3SA-GFP* mutant results in elevated levels of Dma1. Representative $n=3$. D) The *dma1-3SD-GFP* mutant does not have a defect in the termination of vacuole transport. $n=3$, >20 cells per strain per experiment.

A)



B)

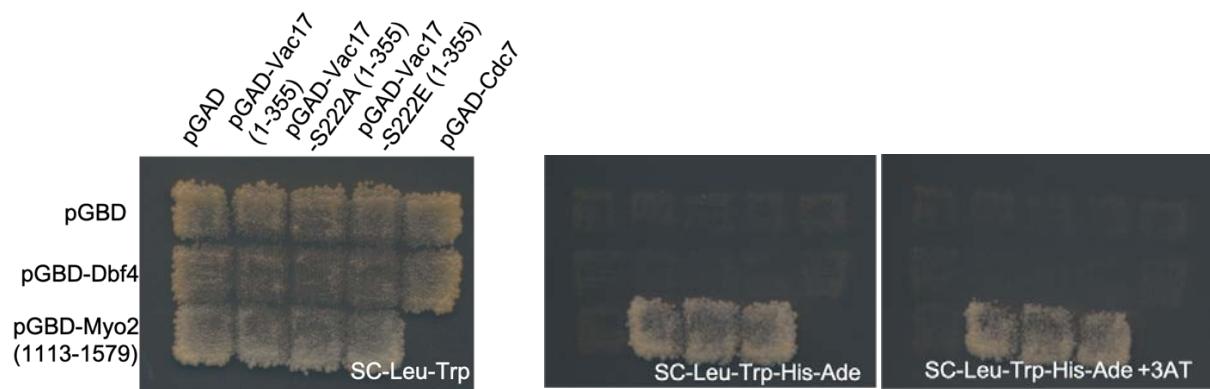
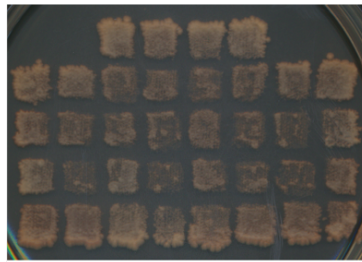


Figure 4.4. Vac17-S222E may function as a phosphomimetic allele. A) Vac17-S222E-GFP does not have defects in the termination of vacuole transport. $n=3$, 40 cells per n . $p<0.05$, students t test. B) Vac17-S222E and Vac17-S222A are able to bind to Myo2. Since Dbf4 did not bind to the positive control, Cdc7, it is unclear if Dbf4 may bind to Vac17.

A)



SC-Leu-Ura



SC-His-Leu-Ura+3AT

Day 14

		*13-2 SE	13-2 SA	*6-5 SE	6-5 SA		
*26-2 SE	26-2 SA	1-1 SE	1-1 SA	13-4 SE	13-4 SA	*17-1 SE	17-1 SA
2-1 SE	2-1 SA	2-4 SE	2-4 SA	2-5 SE	2-5 SA	*2-6 SE	2-6 SA
*2-7 SE	2-7 SA	*2-8 SE	2-8 SA	*4-3 SE	4-3 SA	7-4 SE	7-4 SA
7-5 SE	7-5 SA	*8-3 SE	8-3 SA	9-3 SE	9-3 SA	11-2 SE	11-2 SA

- * "LRG1" plasmids
- * "COS7" plasmids

B)

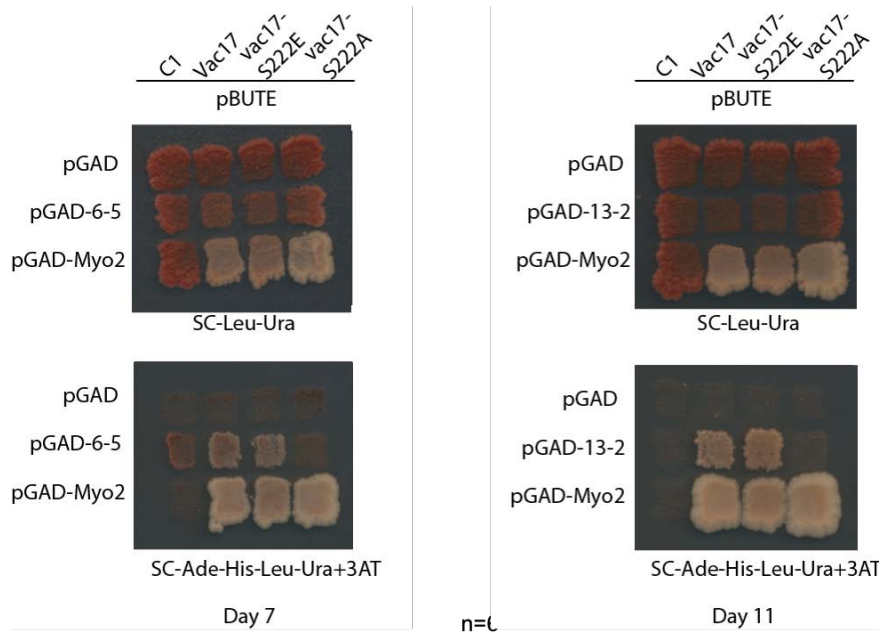


Figure 4.5. Yeast Two Hybrid screen reveals potential Vac17-pS222 interactors. A) The yeast two hybrid screen identified several clones that were able to interact with Vac17-S222E but not Vac17-S222A. Day 14. B) Verification of two clones, 6-5 and 13-2. Representative n=6, day 7 and day 11 as indicated.

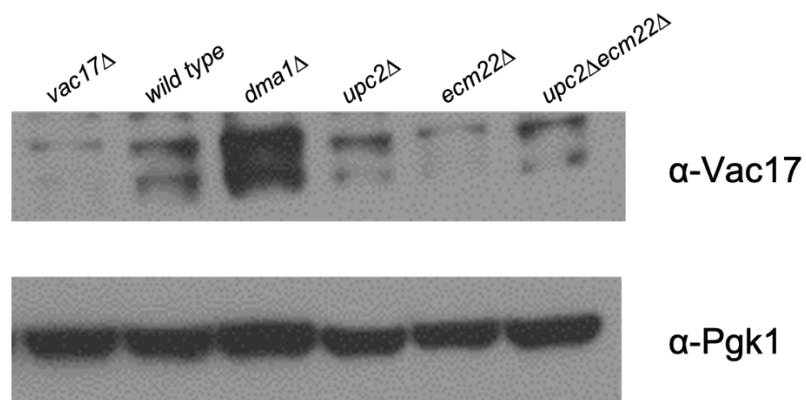


Figure 4.6. Upc2 and paralog Ecm22 are not required for Vac17 degradation. Representative n=3.

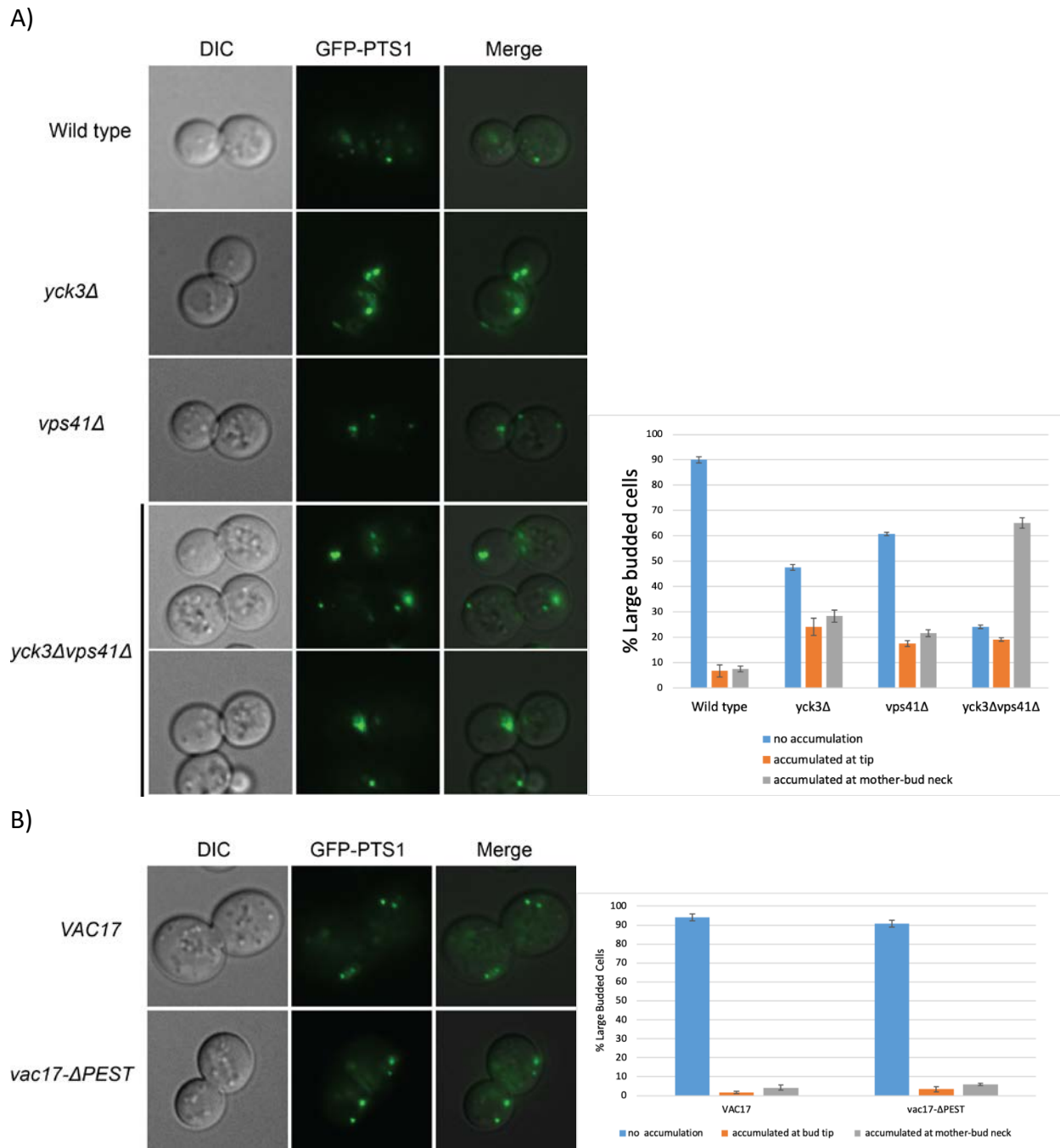
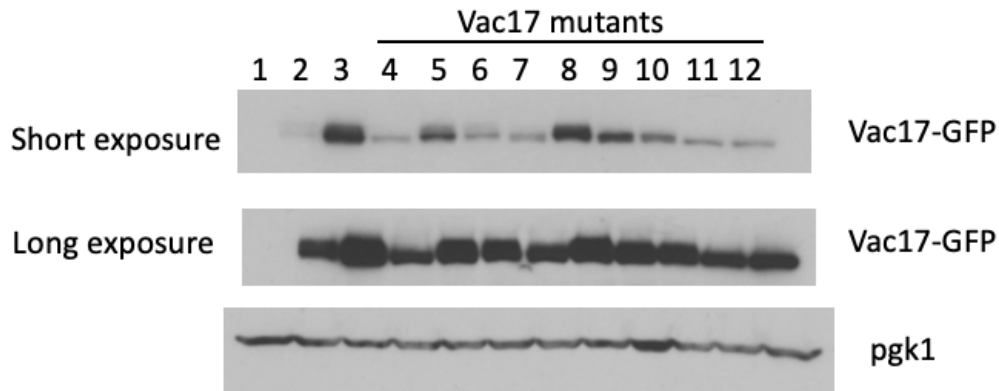


Figure 4.7. Yck3 and Vps41 regulate peroxisome transport. A) Deletion of Yck3 and/or Vps41 results in accumulation of peroxisomes at the bud tip and mother-bud neck. $n=3$, 40 cells per n . $p<0.05$, students t test. B) Peroxisome transport is not defective in the *vac17-ΔPEST* mutant. $n=3$, 40 cells per n . $p>0.3$, students t test.

A)



- | | |
|-------------------------------------|---|
| 1. Vector | 10. Myo2 sites (S127A, S128A, S131A, T149A, S170A, T172A, S174A) |
| 2. Wild type | 11. S269A, S272A, S275A, S127A, S128A, S131A, T149A, S170A, T172A, S174A (clone #1) |
| 3. Yck3-delta | 12. S269A, S272A, S275A, S127A, S128A, S131A, T149A, S170A, T172A, S174A (clone #2) |
| 4. Vac8 sites (S269A, S272A, S275A) | |
| 5. S127A, S128A, S131A | |
| 6. T149A | |
| 7. S170A, T172A, S174A | |
| 8. S127A, S128A, S131A, T149A | |
| 9. T149A, S170A, T172A, S174A | |

B)

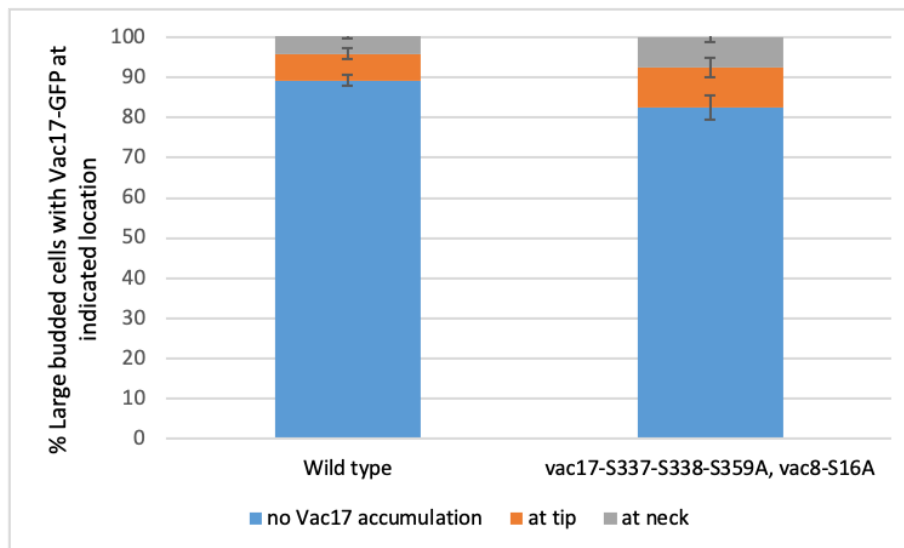
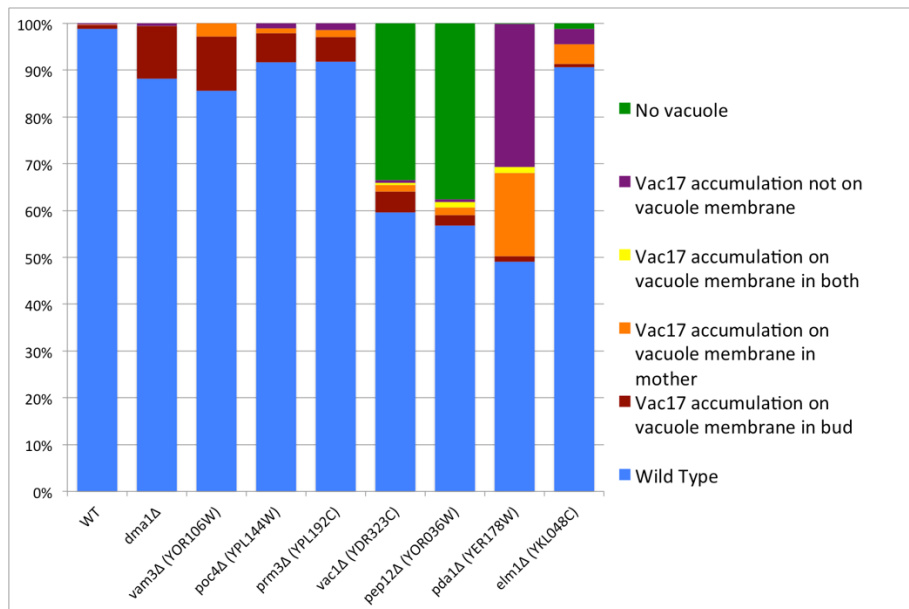


Figure 4.8. Yck3 and Vps41 may regulate phosphorylation of Vac17 and Vac17 binding partners.

A) *vac17Δ* mutant cells were transformed with pRS416-Vac17-GFP (wild type or indicated mutant) and analyzed by western blot. Pgk1 served as a loading control.

B) *vac17Δvac8Δ* mutant cells were co-transformed with pRS416-Vac17-GFP (wild type or S337A-S338A-S359A) and pRS415-Vac8-mCherry (wild type or S16A). Cultures were grown to log phase and imaged. Quantification of n=3, 40 cells per n. p>0.05, students t test.

A)



B)

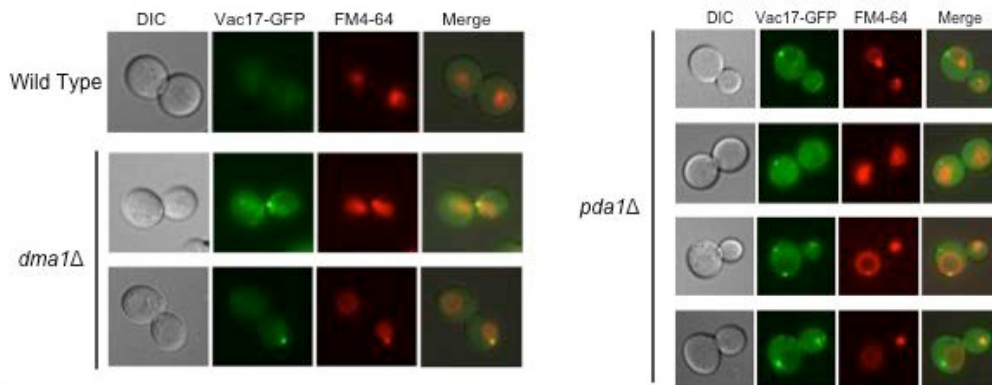


Figure 4.9. Identification of potential regulators of vacuole transport. A) Analysis of verified candidates. n=1, 40 cells per n. B) Pda1 has an abnormal phenotype where Vac17-GFP accumulates in puncta that are not always on the vacuole or with Myo2. Representative images of 40 cells.

CHAPTER VI

METHODS

Yeast strains, plasmids, and media

Yeast cultures were grown in yeast extract peptone dextrose (YEPD) containing 1% yeast extract, 2% peptone and 2% dextrose or synthetic complete (SC) media lacking the indicated amino acid(s) at 24°C unless specified. Yeast strains and plasmids listed in Tables 1 and 2, respectively.

Western Blot analysis

2-10 OD's of cells were lysed in ice-cold 1 mL 0.2 M NaOH/ 0.2% β -mercaptoethanol and incubated on ice for 10 min. 100 μ L trichloroacetic acid (TCA) was added to the lysates and incubated on ice for 5 min. Precipitated proteins were harvested via centrifugation at 13,000 rpm for 5 min. Pellets were resuspended in 100 μ L 2X SDS sample buffer (0.12M Tris-HCl (pH 6.8), 19% Glycerol, 0.15 mM Bromophenol Blue, 3.8% SDS, 0.05% β -mercaptoethanol). 20 μ L of 1 M Tris base (pH 11) was then added and the samples were heated at 75°C for 10 min. Protein samples were loaded on 9% SDS PAGE gels made with Acrylamide/bis (30% 37.5:1; Bio-Rad) and run at 70-100V. Proteins were transferred onto nitrocellulose membrane at 35V for 19 hours. Membranes were blocked in milk before incubated in primary antibodies indicated. Membranes were washed 3x10min in TBST, incubated in secondary antibodies, washed again,

and developed with ECL or ECL prime. For immunoblot analyses, mouse anti-GFP (1:1,000; Roche), rabbit anti-TAP (1:1,000; Thermo Scientific), mouse anti-Pgk1 (1:10,000; Invitrogen), sheep anti-Vac17 (1:1,000; custom made, Twenty First Century Biochemicals), rabbit anti-phosphoThr240 (1:2,500; custom made, 21st Century Biochemicals) and rabbit anti-phosphoSer222 (1:2,500; custom made, 21st Century Biochemicals) antibodies were used (see Antibody Preparation).

Immunoprecipitation experiments

Cells were lysed and proteins were precipitated as described above. Precipitated proteins were washed with acetone, dried, and resuspended in 200 μ L urea buffer (6 M urea, 1% SDS, 50 mM Tris-HCl pH 7.5), and heated at 75°C for 10 min. 1.8 ml TWIP buffer (50 mM Tris-HCl pH 7.5, 150 mM NaCl, 0.5% Tween-20, 0.1 mM EDTA) containing 1 mM Na₃VO₄ and 1X protease inhibitor cocktail (Sigma) was added to the resuspended protein and centrifuged. 4 μ g of mouse anti-GFP antibodies (Roche) were added to the supernatant and incubated with agitation at 4°C, overnight. Immune complexes were harvested via the addition of protein G beads, which were subsequently collected via centrifugation and washed with TWIP buffer. Bound proteins were analyzed via immunoblot.

In vivo ubiquitylation experiments

To detect ubiquitylated Vac17, pVT102U-Vac17-GFP was transformed into *vac17 Δ* , *dma1 Δ dma2 Δ vac17 Δ* , *yck3 Δ vac17 Δ* or *vps41 Δ vac17 Δ* mutant strains. pVT102U-Vac17 was transformed into *vac17 Δ* as a no-GFP control. A plasmid encoding Myc-Ub driven by a CUP1

promoter was co-transformed into the same strains. Myc-Ub expression was induced with 100 μ M CuCl₂. GFP fusion proteins were immunoprecipitated as described above and analyzed via immunoblot using rabbit anti-GFP (Abcam), and rabbit anti-myc antibodies (1:2,000; Cell Signaling).

Microscopy

To visualize vacuoles, cells were labeled with either (1) 12 μ g FM4-64 in 250 μ L media for 1 hour, then washed twice and grown in 5 ml fresh media for one doubling time (2-3 hours), or (2) 100 μ M CMAC (ThermoFisher) for 30 minutes, then washed twice in fresh media. Live cell images were obtained on a DeltaVision Restoration system (Applied Precision) using an inverted epifluorescence microscope (IX-71; Olympus) with a charge-coupled device camera (Cool-SNAP HQ; Photometrics) and processed in Photoshop and FIJI.

Time Lapse Microscopy

Glass-bottom chambers (Lab-Tek II; Thermo Fischer Scientific) were treated overnight at 4°C with concanavalin A dissolved at 1 mg/ml in 50 mM HEPES, pH 7.5, 20 mM calcium acetate, and 1 mM manganese sulfate, then washed with water and air dried for 30 minutes. Cells adsorbed to concanavalin A-treated chambers for 2 minutes. Unbound cells were removed by aspiration and 250 μ L of fresh media was added. Time lapse microscopy was performed at 2 minute intervals using a Nikon Ti-U inverted microscope with a 100x 1.4NA oil immersion objective, Lumencore light engine, Andor iXon DV897 camera, and GFP/mCherry dual-band filter set from Chroma.

Alpha Factor Cell Synchronization

100 ml of cells (OD = 0.2-0.4) were incubated in 2.5 μ M alpha-factor (Zymo Research) for 2-3 hours until 80% of cells were arrested in G1. Cells were washed in fresh media twice to remove alpha-factor. 1ml aliquots were collected every 10 minutes for live cell imaging, images taken within 5 minutes of collection.

GST Protein Purification

GST and GST-Yck3 were expressed in Rosetta (DE3) pLySS cells via induction with 0.1 mM IPTG at 30°C for 5 hours. Cells were resuspended in lysis buffer (50mM Tris pH 7.5, 150mM NaCl, 5mM EDTA, 1 mM Pefabloc [Sigma-Aldrich], and cOmplete EDTA-free protease inhibitor cocktail [Roche]) and lysed via sonication. Lysates were clarified via centrifugation at 20,000 g for 30 min at 4°C and incubated with glutathione beads at 4°C with agitation for 30min. The mixture was applied to a column and the beads were washed with wash buffer (50mM Tris pH 7.5, 150mM NaCl, 5mM EDTA) until no protein was detected in the flow through. The beads were resuspended in elution buffer (50mM Tris pH 7.5, 150mM NaCl, 5mM EDTA, 10mM glutathione) and incubated at 4°C with agitation for 30min. The elution was collected and dialyzed overnight at 4°C in storage buffer (20 mM HEPES-NaOH pH 7.4, 250 mM NaCl, 10% Glycerol, 2 mM DTT). The protein was concentrated and stored at -80°C.

GST Tag Binding Assay

GST and GST-Yck3 were expressed in Rosetta (DE3) pLySS cells (Novagen) via induction with 0.1 mM IPTG at 30°C for 5 hours. Cells were resuspended in GST lysis buffer (50mM Tris pH 7.5, 150mM NaCl, 5mM EDTA, 1 mM Pefabloc [Sigma-Aldrich], and cOmplete EDTA-free protease inhibitor cocktail [Roche]) and lysed via sonication. Lysates were clarified via centrifugation at 20,000 g for 30 min at 4°C and incubated with glutathione beads at 4°C with agitation. Immobilized proteins were washed once with GST lysis buffer. Yeast cells grown in yeast extract peptone dextrose at 24°C were resuspended in yeast lysis buffer (125mM NaCl, 50mM NaPO₄ pH 7.4, 10% glycerol, 2mM MgCl₂, 0.5% octylglucosidase, 1mM DTT, 1× protease inhibitor cocktail (Sigma-Aldrich), and cOmplete EDTA-free protease inhibitor cocktail (Roche)) and lysed with glass beads. GST- and GST-Yck3 bound beads were incubated with clarified yeast cell extracts for 1 hr at 4°C with agitation. Beads were then washed twice with yeast wash buffer (50mM HEPES-KOH pH 7.4, 150mM KCl, 1mM EDTA, 10% glycerol). Bound proteins were analyzed via SDS-PAGE, Gelcode blue staining, and immunoblotting. For input (6.25%), 20 µL lysate was resuspended in 20 µL sample buffer, and 5 µL was loaded into the gel.

HIS Tag Binding Assay

His and His-Vps41 were expressed in C43 (DE3) cells (Lucigen) via induction with 0.5mM IPTG at 30°C for 3 hours. Cells were resuspended in Vps41 lysis buffer (10mM HEPES pH 7.4, 350mM NaCl, 2mM MgCl₂, 5% glycerol, 50mM imidazole, 100µM PMSF, 5mM β-mercaptoethanol) and lysed via sonication. Lysates were clarified via centrifugation at 20,000 g for 30 min at 4°C and incubated with Ni-NTA beads at 4°C with agitation for 1 hour. Immobilized proteins were washed twice with Vps41 lysis buffer. Yeast cells grown in yeast extract peptone dextrose at

24°C were resuspended in yeast lysis buffer (125mM NaCl, 50mM NaPO₄ pH 7.4, 10% glycerol, 2mM MgCl₂, 0.5% octylglucosidase, 1mM DTT, 1× protease inhibitor cocktail (Sigma-Aldrich), and cOMplete EDTA-free protease inhibitor cocktail (Roche)) and lysed with glass beads. His- and His-Vps41 bound beads were incubated with clarified yeast cell extracts for 1 hr at 4°C with agitation. Beads were then washed twice with yeast wash buffer (50mM HEPES-KOH pH 7.4, 150mM KCl, 1mM EDTA, 10% glycerol). Bound proteins were analyzed via SDS-PAGE, Gelcode blue staining, and immunoblotting. For input (6.25%), 20 µL lysate was resuspended in 20 µL sample buffer, and 5 µL was loaded into the gel.

Lambda Phosphatase Treatment

Log phase cells (20 OD600 units) were suspended in 1 mL ice cold 0.2M NaOH, 0.2% β-mercaptoethanol (v/v), and incubated on ice for 10 min. 100µL trichloroacetic acid (TCA) was added and incubated on ice 10 min. Protein pellets were washed three times with acetone and air dried. The pellets were resuspended in 200 µL urea breaking buffer (6M Urea, 1% SDS, 50mM Tris-HCl pH 7.5) and heated at 75°C. 1800 µL of TWIP (50mM Tris-HCl pH 7.5, 150mM NaCl, 0.5% Tween-20, 1× protease inhibitor cocktail (Sigma-Aldrich), NaVO₄, 1mM PMSF) was added and the lysate was spun 5000rpm 5min. 4µg/µL of mouse-anti-GFP was added to the supernatant and incubated 1 hr at 4°C with agitation. Protein G beads were added and incubated 1 hr at 4°C with agitation. Beads were washed in TWIP and resuspended in 50 µL master mix (40uL water + 5uL 1 × λ-phosphatase buffer + 1× protease inhibitor cocktail (Sigma-Aldrich) + 5uL 10 mM MnCl₂). Either water, λ-phosphatase (400 U; New England Biolabs, Inc.), or λ-phosphatase plus phosphatase inhibitors (100 mM NaF, 10 mM Na₃VO₄, 50 mM EDTA, 20

mM β -glycerophosphate, and 20 mM sodium pyrophosphate) were added to the reaction.

Phosphatase reactions were incubated 1 hr at 30°C with agitation. Reactions were stopped with addition of 2x sample buffer (0.12M Tris-HCl (pH 6.8), 19% Glycerol, 0.15 mM Bromophenol Blue, 3.8% SDS, 0.05% β -mercaptoethanol). The resultant samples were subjected to immunoblot analysis.

SILAC

LWY18795, LWY18802, and LWY18813 were co-transformed with pVT102u-Vac17- Δ PEST-6xHis-TEV-3xFLAG and pRS413-Myo2-D1297N. Note that the pRS413-Myo2-D1297N mutant was included to improve viability of the yeast, which may be negatively affected by over expression of Vac17 mutants that occupy Myo2 and prevent Myo2 from performing essential functions. SILAC-based mass spectrometry for quantitation and mapping of Vac17 phosphosites was performed as previously described (Albuquerque et al., 2008; Lee et al., 2019) with slight modification. Briefly, equal amount of light (wildtype) and heavy ($\Delta yck3$ or $\Delta vps41$, as indicated) cells expressing exogenous Vac17- Δ PEST-FLAG were harvested from mid-log phase and disrupted by bead beating using ice-cold lysis buffer (50 mM Tris-HCl, pH 7.5, 150 mM NaCl, 5 mM EDTA, 0.2% NP-40, 10 mM iodoacetamide, 1X EDTA-free protease inhibitor cocktail (Roche), 1mM phenylmethylsulfonyl fluoride, 20 μ M MG132, 1X PhosStop (Roche), 10 mM NaF, 20 mM BGP, and 2 mM Na_3VO_4). Lysate was clarified by centrifugation at 21,000 x *g* for 10 min at 4°C and supernatant was transferred into a new tube and diluted with threefold volume of ice-cold TBS (50 mM Tris-HCl, pH7.5, 150 mM NaCl). Vac17- Δ PEST-FLAG in 12-ml diluted lysate was enriched by incubation with 50 μ L of EZview anti-FLAG M2 resin slurry (Sigma) for 2 hr at 4°C with rotation.

The resin was washed three times with cold TBS and incubated with 90µl elution buffer (100 mM Tris-HCl, pH 8.0, 1% SDS) at 98°C for 5 min. Collected eluate was reduced with 10mM DTT, alkylated with 20mM iodoacetamide, and precipitated with 300 µl PPT solution (50% acetone, 49.9% ethanol, and 0.1% acetic acid). Light and heavy protein pellets were dissolved with Urea-Tris solution (8 M urea, 50 mM Tris-HCl, pH 8.0). Heavy and light samples were combined, diluted fourfold with water, and digested with 1µg MS-grade trypsin (Gold, Promega) by overnight incubation at 37°C. Phosphopeptides were enriched by immobilized metal affinity chromatography (IMAC) using Fe(III)-nitrilotriacetic acid resin as previously described (MacGurn et al., 2011), redissolved in 0.1% trifluoroacetic acid, and loaded onto a Q-Exactive mass spectrometer (Thermo Scientific). Resolved spectra were searched using MaxQuant (ver. 1.6.5.0) and chromatograms were visualized using Skyline (ver. 19.1.0.193, MacCoss Lab).

Yeast Two Hybrid

Co-transform pGAD (LEU) and pGBD (URA) plasmids of interest into yeast and plate on SC-LEU-URA. When grown, patch single colonies onto SC-LEU-URA plates. After growth, replica plate using velvets onto SC-LEU-URA-HIS and SC-LEU-URA-HIS-ADE+3AT plates. Monitor growth at 24C.

Plasmid Purification from Yeast

15 ODs of yeast was pelleted at 3000rpm for 3 minutes. Pellet was resuspended in 250uL of P1 buffer with RNase (QIAGEN miniprep kit) and transferred to a fresh microcentrifuge tube. Cells were lysed at 4C via glass bead lysis for 10 minutes in bead beater. A hole was poked in the

bottom of the centrifuge tube and placed over a fresh centrifuge tube. Supernatant was recovered at 500g for 3 minutes. 250uL of P2 was added and the tube was inverted to mix. Within 5 min, 350uL of N3 was added and the tube was inverted to mix. Sample was centrifuged at 13000rpm for 10min. Supernatant was transferred to a DNA spin column and centrifuged at 13000rpm for 1min. 750uL PE buffer was added and the sample was centrifuged at 13000rpm for 1min. A dry spin at 13000rpm for 1min was performed to remove excess buffer. Plasmid DNA was eluted into a fresh tube with 40uL of elution buffer.

Bacteria transformation

Frozen aliquots of competent bacteria cells were thawed on ice. 5-10uL of plasmid was added to 100uL of cells and incubated on ice for 30min. Cells were heat shocked at 42C for 1min and subsequently incubated on ice for 2 min. 250uL SOC media was added to the cells and tubes were incubated shaking at 37C for 30min. Cells were pelleted and plated on LB plates with appropriate antibiotics.

TABLES

Table 1. Yeast strains used in this study

Strain	Description	Citation
LWY3250	MAT α , ura3-52, leu2-3,-112, his3- Δ 200, trp1- Δ 901, lys2-801, suc2- Δ 9	This study
LWY5798	MAT α , ura3-52, leu2-3,-112, his3- Δ 200, trp1- Δ 901, lys2-801, suc2- Δ 9, vac17 Δ ::TRP1	Tang et al., Nature 2003
LYW2887	MAT α , ura3-52, leu2-3,-112, his3- Δ 200, trp1- Δ 901, lys2-801, suc2- Δ 9, vac8 Δ ::HIS3	Wang et al., JCB 1998
LWY5826	MAT α , ura3-52, leu2-3,-112, his3- Δ 200, trp1- Δ 901, lys2-801, suc2- Δ 9, vac17 Δ ::TRP1, vac8 Δ ::HIS3	This study
LWY11102	MAT α , ura3-52, leu2-3,-112, his3- Δ 200, trp1- Δ 901, lys2-801, suc2- Δ 9, dma1 Δ ::KAN	Yau et al., Dev Cell 2014
LWY11683	MAT α , ura3-52, leu2-3,-112, his3- Δ 200, trp1- Δ 901, lys2-801, suc2- Δ 9, dma1 Δ ::KAN dma2 Δ ::KAN	Yau et al., Dev Cell 2014
LWY11687	MAT α , ura3-52, leu2-3,-112, his3- Δ 200, trp1- Δ 901, lys2-801, suc2- Δ 9, dma1 Δ ::KAN dma2 Δ ::KAN vac17 Δ ::TRP1	Yau et al., Dev Cell 2014
LWY11640	MAT α , ura3-52, leu2-3,-112, his3- Δ 200, trp1- Δ 901, lys2-801, suc2- Δ 9, dma1 Δ ::KAN dma2 Δ ::KAN yck3 Δ ::KAN	Wong et al., Curr Biol 2020
LWY14777	MAT α , ura3-52, leu2-3,-112, his3- Δ 200, trp1- Δ 901, lys2-801, suc2- Δ 9, vps41 Δ ::KAN	Wong et al., Curr Biol 2020
LWY14780	MAT α , ura3-52, leu2-3,-112, his3- Δ 200, trp1- Δ 901, lys2-801, suc2- Δ 9, vps41 Δ ::KAN, vac17 Δ ::TRP1	Wong et al., Curr Biol 2020
LWY10924	MAT α , ura3-52, leu2-3,-112, his3- Δ 200, trp1- Δ 901, lys2-801, suc2- Δ 9, vps39 Δ ::KAN	Wong et al., Curr Biol 2020
LWY16184	MAT α , ura3-52, leu2-3,-112, his3- Δ 200, trp1- Δ 901, lys2-801, suc2- Δ 9, yck3 Δ ::KAN	Wong et al., Curr Biol 2020
LWY17494	MAT α , ura3-52, leu2-3,-112, his3- Δ 200, trp1- Δ 901, lys2-801, suc2- Δ 9, yck3 Δ ::KAN vac17 Δ ::TRP1	Wong et al., Curr Biol 2020

LWY18601	MAT α , ura3-52, leu2-3,-112, his3- Δ 200, trp1- Δ 901, lys2-801, suc2- Δ 9, yck3 Δ ::KAN vps41 Δ ::KAN	Wong et al., Curr Biol 2020
LWY18556	MATa pep4 Δ ::HIS3 prb1- Δ 1.6R lys2-208 trp1 Δ 101 vps41 Δ ::KANMX URA3::pRS406-NOP1pr-VPS41wt	Cabrera et al., Molec Biol Cell 2009
LWY18558	LWY18558: MATa pep4 Δ ::HIS3 prb1- Δ 1.6R lys2-208 trp1 Δ 101 vps41 Δ ::KANMX URA3::pRS406-NOP1pr-VPS41 (S367, 368, 371, 372 A)	Cabrera et al., Molec Biol Cell 2009
LWY18560	LWY18560: MATa pep4 Δ ::HIS3 prb1- Δ 1.6R lys2-208 trp1 Δ 101 vps41 Δ ::KANMX URA3::pRS406-NOP1pr-VPS41 (S367, 368, 371, 372 D)	Cabrera et al., Molec Biol Cell 2009
LWY10332	MAT α , ura3-52, leu2-3,-112, his3- Δ 200, trp1- Δ 901, lys2-801, suc2- Δ 9, Vac17-TAP::LEU2	Wong et al., Curr Biol 2020
LWY18670	MAT α , ura3-52, leu2-3,-112, his3- Δ 200, trp1- Δ 901, lys2-801, suc2- Δ 9, Vac17-deltaPEST-TAP::LEU2	Wong et al., Curr Biol 2020
LWY19035	MAT α , ura3-52, leu2-3,-112, his3- Δ 200, trp1- Δ 901, lys2-801, suc2- Δ 9, Vac17-deltaPEST-TAP::LEU2, vps41-delta::KAN	Wong et al., Curr Biol 2020
LWY19196	MAT α , ura3-52, leu2-3,-112, his3- Δ 200, trp1- Δ 901, lys2-801, suc2- Δ 9, Vac17-deltaPEST-TAP::LEU2, yck3-delta::KAN	Wong et al., Curr Biol 2020
LWT18737	MAT α , GAL+ his3- Δ 200 leu2-3,2-112 lys2-801 suc2- Δ 9 trp1- Δ 9 ura3-52	Banta et al., Molec Cell Bio 1990
LWT18738	MAT α , vps33-4 GAL+ his3- Δ 200 leu2-3,2-112 lys2-801 suc2- Δ 9 trp1- Δ 9 ura3-52	Banta et al., Molec Cell Bio 1990
LWY18763	MAT α , vps11-delta::HIS3, pRS416-vps11-3, GAL+ his3- Δ 200 leu2-3,2-112 lys2-801 suc2- Δ 9 trp1- Δ 9 ura3-52	Peterson and Emr, Traffic 2001
LWY18764	MAT α , vps16-ts, GAL+ his3- Δ 200 leu2-3,2-112 lys2-801 suc2- Δ 9 trp1- Δ 9 ura3-52	Peterson and Emr, Traffic 2001
LWY18765	MAT α , vps18-ts, GAL+ his3- Δ 200 leu2-3,2-112 lys2-801 suc2- Δ 9 trp1- Δ 9 ura3-52	Peterson and Emr, Traffic 2001
LWY7235	MAT α , his3-11 leu2-3, 112 ura3-delta5 pre1-1::can	Chen and Hochstrasser, 1996 Cell
LWY7236	MAT α , his3-delta200 leu2-3, 112 ura3-52 lys2-801 trp1-1 doa3-delta1::HIS3[YEpDOA3LS][YCPubDOA3deltaLS]	Arendt and Hochstrasser, 1997 PNAS
LWY7237	MAT α , his3-delta200 leu2-3, 112 ura3-52 lys2-801 trp1-1 doa3-delta1::HIS3[YEpDOA3LS][YCPubDOA3deltaLS-T76A]	Arendt and Hochstrasser, 1997 PNAS

LWY7238	MAT α , his3-delta200 leu2-3, 112 ura3-52 lys2-801 trp1-1 pup1::leu2::HIS3 pup3-delta2::HIS3[Ycplac22PUP1][Yeplac181PUP3]	Arendt and Hochstrasser, 1997 PNAS
LWY7239	MAT α , his3-delta200 leu2-3, 112 ura3-52 lys2-801 trp1-1 pup1::leu2::HIS3 pup3-delta2::HIS3[Ycplac22pup1-K58E][Yeplac181pup3-E151K]	Arendt and Hochstrasser, 1997 PNAS
LWY18807	MAT α , his3-delta200 leu2-3, 112 ura3-52 lys2-801 trp1-1 pup1::leu2::HIS3 pup3-delta2::HIS3[Ycplac22PUP1][Yeplac181PUP3] yck3::KAN	Wong et al., Curr Biol 2020
LWY18808	MAT α , his3-delta200 leu2-3, 112 ura3-52 lys2-801 trp1-1 pup1::leu2::HIS3 pup3-delta2::HIS3[Ycplac22pup1-K58E][Yeplac181pup3-E151K] yck3::KAN	Wong et al., Curr Biol 2020
LWY18810	MAT α , his3-delta200 leu2-3, 112 ura3-52 lys2-801 trp1-1 pup1::leu2::HIS3 pup3-delta2::HIS3[Ycplac22PUP1][Yeplac181PUP3] vps41::KAN	Wong et al., Curr Biol 2020
LWY18811	MAT α , his3-delta200 leu2-3, 112 ura3-52 lys2-801 trp1-1 pup1::leu2::HIS3 pup3-delta2::HIS3[Ycplac22pup1-K58E][Yeplac181pup3-E151K] vps41::KAN	Wong et al., Curr Biol 2020
LWY12381	MAT α , can1-100, leu2-3,-112, his3-11,-15, trp1-1, ura3-1, ade2-1 cdc48-3 ts	Verma et al., Molec Cell 2011
LWY12382	MAT α , can1-100, leu2-3,-112, his3-11,-15, trp1-1, ura3-1, ade2-1	Verma et al., Molec Cell 2011
LWY6470	MAT α , his3 Δ 1, leu2 Δ 0, lys2 Δ 0, ura3 Δ 0	This study
LWY15465	MAT α , his3 Δ 1, leu2 Δ 0, lys2 Δ 0, ura3 Δ 0, vps4- Δ ::KAN	Horizon Discovery
LWY14289	MAT α , his3 Δ 1, leu2 Δ 0, lys2 Δ 0, ura3 Δ 0, dma1- Δ ::KAN	Horizon Discovery
LWY18911	MAT α , his3 Δ 1, leu2 Δ 0, lys2 Δ 0, ura3 Δ 0, apl5- Δ ::KAN	Horizon Discovery
LWY18912	MAT α , his3 Δ 1, leu2 Δ 0, lys2 Δ 0, ura3 Δ 0, aps3- Δ ::KAN	Horizon Discovery
LWY18913	MAT α , his3 Δ 1, leu2 Δ 0, lys2 Δ 0, ura3 Δ 0, apl6- Δ ::KAN	Horizon Discovery
LWY18665	MAT α , his3 Δ 1, leu2 Δ 0, lys2 Δ 0, ura3 Δ 0, vps3- Δ ::KAN	Horizon Discovery
LWY18666	MAT α , his3 Δ 1, leu2 Δ 0, lys2 Δ 0, ura3 Δ 0, vps8- Δ ::KAN	Horizon Discovery

LWY19052	MAT α , his3 Δ 1, leu2 Δ 0, lys2 Δ 0, ura3 Δ 0, apm3- Δ ::KAN	Horizon Discovery
LWY19425	MAT α , his3 Δ 1, leu2 Δ 0, lys2 Δ 0, ura3 Δ 0, sec18-DAmP::KAN	Breslow et al., Nature Methods 2008
LWY19072	MAT α , leu2-3,112 ura3-52 his3- Δ 200 trp1- Δ 901 suc2- Δ 9 lys2-801, arg4::KAN, pVT102u-Vac17-deltaPEST-FLAG, pRS413-Myo2-D1297N	Wong et al., Curr Biol 2020
LWY19073	MAT α , leu2-3,112 ura3-52 his3- Δ 200 trp1- Δ 901 suc2- Δ 9 lys2-801, arg4 Δ ::KAN, vps41 Δ ::KanMX, pVT102u-Vac17-deltaPEST-FLAG, pRS413-Myo2-D1297N, vps41-KO	Wong et al., Curr Biol 2020
LWY19074	MAT α , leu2-3,112 ura3-52 his3- Δ 200 trp1- Δ 901 suc2- Δ 9 lys2-801, arg4 Δ ::KAN, yck3 Δ ::KanMX, pVT102u-Vac17-deltaPEST-FLAG, pRS413-Myo2-D1297N, yck3-KO	Wong et al., Curr Biol 2020
LWY7664	MAT α , ura3-52, leu2-3,-112, his3- Δ 200, trp1- Δ 901, lys2-801, suc2- Δ 9, vac17 Δ ::TRP1, MYO2-GFP::HIS3	Peng et al. Dev Cell 2008
LWY8195	MAT α , ura3-52, leu2-3,-112, his3- Δ 200, trp1- Δ 901, lys2-801, suc2- Δ 9, pep4- Δ 1137, vac17 Δ ::TRP1, myo2 Δ ::TRP1 [YcP50-MYO2]	Yau and Wong et al. JCB 2017
LWY11109	MAT α , ura3-52, leu2-3,-112, his3- Δ 200, trp1- Δ 901, lys2-801, suc2- Δ 9, dma1 Δ ::kanMX	Yau and Wong et al. JCB 2017
LWY7422	MAT α , ura3-52, leu2-3,-112, his3- Δ 200, trp1- Δ 901, lys2-801, suc2- Δ 9, cla4 Δ ::kanMX	Yau and Wong et al. JCB 2017
LWY7429	MAT α , ura3-52, leu2-3,-112, his3- Δ 200, trp1- Δ 901, lys2-801, suc2- Δ 9, ste20 Δ ::kanMX	Yau and Wong et al. JCB 2017
LWY11860	MAT α , ura3-52, leu2-3,-112, his3- Δ 200, trp1- Δ 901, lys2-801, suc2- Δ 9, ste20 Δ ::kanMX, cla4 Δ ::LEU2, Ycp-TRP1-cla4-75	Yau and Wong et al. JCB 2017
LWY14298	MAT α , ura3-52, leu2-3,-112, his3- Δ 200, trp1- Δ 901, lys2-801, suc2- Δ 9, cla4 Δ ::kanMX, vac17 Δ ::TRP1	Yau and Wong et al. JCB 2017
LWY14919	MAT α , ura3-52, leu2-3,-112, his3- Δ 200, trp1- Δ 901, lys2-801, suc2- Δ 9, vac17 Δ ::TRP1, Dma1-3xGFP::HIS3	Yau and Wong et al. JCB 2017
LWY14430	MAT α , ura3-52, leu2-3,-112, his3- Δ 200, trp1- Δ 901, lys2-801, suc2- Δ 9, cla4 Δ ::kanMX, vac17-3xGFP::TRP1	Yau and Wong et al. JCB 2017
LWY11389	MAT α , ura3-52, leu2-3,-112, his3- Δ 200, trp1- Δ 901, lys2-801, suc2- Δ 9, dma1 Δ ::kanMX, dma2 Δ ::kanMX, VAC17-TAP::LEU2	Yau and Wong et al. JCB 2017

LWY15778	MAT α , ura3-52, leu2-3,-112, his3- Δ 200, trp1- Δ 901, lys2-801, suc2- Δ 9, Cla4-3xGFP::HIS3, Vph1-mCherry::KAN	Yau and Wong et al. JCB 2017
LWY17427	MAT α , ura3-52, leu2-3,-112, his3- Δ 200, trp1- Δ 901, lys2-801, suc2- Δ 9, lte1 Δ ::kanMX	Yau and Wong et al. JCB 2017
LWY18484	MAT α , ura3-52, leu2-3,-112, his3- Δ 200, trp1- Δ 901, lys2-801, suc2- Δ 9, Ste20-GFP::HIS3	Yau and Wong et al. JCB 2017
LWY18493	MAT α , ura3-52, leu2-3,-112, his3- Δ 200, trp1- Δ 901, lys2-801, suc2- Δ 9, Ste20-GFP::HIS3, cla4 Δ ::kanMX	Yau and Wong et al. JCB 2017
LWY15569	MAT α , his3 Δ 1, leu2 Δ 0, lys2 Δ 0, ura3 Δ 0, dbf4-DAMP::KANMX	Horizon Discovery
LWY18286	MAT α , his3 Δ 1, leu2 Δ 0, lys2 Δ 0, ura3 Δ 0, upc2 Δ ::KANMX	Horizon Discovery
LWY18396	MAT α , his3 Δ 1, leu2 Δ 0, lys2 Δ 0, ura3 Δ 0, Upc2-GFP::HIS3MX6	ThermoFisher Scientific
LWY18747	MAT α , ura3-52, leu2-3,-112, his3- Δ 200, trp1- Δ 901, lys2-801, suc2- Δ 9, promHIS3-GFPS65T-PTS1::URA3	This study
LWY18748	MAT α , ura3-52, leu2-3,-112, his3- Δ 200, trp1- Δ 901, lys2-801, suc2- Δ 9, promHIS3-GFPS65T-PTS1::URA3, yck3 Δ ::KANMX	This study
LWY18749	MAT α , ura3-52, leu2-3,-112, his3- Δ 200, trp1- Δ 901, lys2-801, suc2- Δ 9, promHIS3-GFPS65T-PTS1::URA3, vps41 Δ ::KANMX	This study
LWY18750	MAT α , ura3-52, leu2-3,-112, his3- Δ 200, trp1- Δ 901, lys2-801, suc2- Δ 9, promHIS3-GFPS65T-PTS1::URA3, yck3 Δ ::KANMX, vps41 Δ ::KANMX	This study
LWY18819	MAT α , ura3-52, leu2-3,-112, his3- Δ 200, trp1- Δ 901, lys2-801, suc2- Δ 9, promHIS3-GFPS65T-PTS1::URA3, vac17 Δ ::TRP1	This study
LWY5055	PJ69: MAT α , trp1-901 leu2-3,112 ura3-52 his 3-200 gal4delta gal80delta GAL2-ADE2 LYS2::GAL1-HIS3 met2::GAL7-lacZ	

Table 2. Plasmids used in this study

Plasmid	Description	Citation
pRS415-Vac17-GFP	AMP, LEU	Tang et al., Nature 2003
pRS416-Vac17-GFP	AMP, URA	Tang et al., Nature 2003
pRS415-Vac17- Δ PEST	AMP, URA	Tang et al., Nature 2003
pRS416-Vac17- Δ PEST	AMP, URA	Tang et al., Nature 2003
pRS416-Vac17- Δ PEST-GFP	AMP, URA	Tang et al., Nature 2003
pRS416-Dma1-GFP	AMP, URA	Yau et al., Dev Cell 2014
pRS413-Cla4-GFP	AMP, HIS	Yau and Wong et al., JCB 2017
pRS413-Myo2-Venus	AMP, HIS	Yau and Wong et al., JCB 2017
pRS416-Myo2-Venus	AMP, URA	Wong et al., Curr Biol 2020
pRS413-Myo2-D1297N	AMP, HIS	Pashkova et al., EMBO J 2005
pRS413-mCherry-Myo2	AMP, HIS	Jin et al., Dev Cell 2011
pRS406-VPS41pr-Vps41-WT	AMP, URA	Cabrera et al., MBOC 2009
pRS406-VPS41pr-Vps41-4A	AMP, URA	Cabrera et al., MBOC 2009
pRS406-VPS41pr-Vps41-4D	AMP, URA	Cabrera et al., MBOC 2009
CUP1-Myc-Ubiquitin	AMP, LEU	Yau et al., Dev Cell 2014
pvt102u-Vac17-GFP	AMP, URA	Yau et al., Dev Cell 2014
pvt102u-Vac17	AMP, URA	Yau et al., Dev Cell 2014
pVT102u-Vac17- Δ PEST-6xHis-TEV-3xFLAG	AMP, URA	Wong et al., Curr Biol 2020
pGEX-Yck3 (2-516)	AMP	Wong et al., Curr Biol 2020
pSAP0162 (pQLinkHM-Vps41 (124-992))	AMP	Wong et al., Curr Biol 2020
pRS416-VAC17	CEN, URA3	Catlett et al., PNAS 1998
pRS416-vac17-S222A-GFP	CEN, URA3	Yau et al., Dev Cell 2014
pRS416-vac17-T240A-GFP	CEN, URA3	Yau et al., Dev Cell 2014
pRS415-VAC17	CEN, LEU2	Yau et al., Dev Cell 2014
pRS415-vac17-S222A	CEN, LEU2	Yau et al., Dev Cell 2014
pRS415-vac17-T240A	CEN, LEU2	Yau et al., Dev Cell 2014
pRS415-VAC17-GFP	CEN, LEU2	Yau et al., Dev Cell 2014
pRS415-vac17-S222A-GFP	CEN, LEU2	Yau et al., Dev Cell 2014
pRS415-vac17-T240A-GFP	CEN, LEU2	Yau et al., Dev Cell 2014
pRS413-CLA4	CEN, HIS3	Yau and Wong et al., JCB 2017
pRS413-CLA4-tdTomato	CEN, HIS3	Yau and Wong et al., JCB 2017
pGEX4T- Cla4	Amp	Versel et al., JCB 2004
pGEX4T-cla4-K594A	Amp	Versel et al., JCB 2004
pET-Vac17(97-260)	Kan	Yau and Wong et al., JCB 2017
pRS415-Vac17-F225S-GFP	Amp, LEU2	Richard Yau, unpublished
pRS415-Vac17-S222E-GFP	Amp, LEU2	Sara Wong, unpublished
pGBD- Vac17-S222E (1-355)	Amp, URA3	Sara Wong, unpublished

pGBD- Vac17-S222A (1-355)	Amp, URA3	Sara Wong, unpublished
pGBD- Vac17 (1-355)	Amp, URA3	Ishikawa et al., JCB 2003
pGAD-Upc2	Amp, LEU2	Nadia Azad, unpublished
pRS416-Dma1-3SA-tdTomato	Amp, URA3	Sara Wong, unpublished
pRS416-Dma1-3SD-tdTomato	Amp, URA3	Sara Wong, unpublished
pRS416-Dma1-tdTomato	Amp, URA3	Yau et al., Dev Cell 2014
pRS416-Vac17-S269-S272-S275A-GFP	Amp, URA3	Wong et al., Curr Biol 2020
pRS416-Vac17-S127-S128-S131-T149A-GFP	Amp, URA3	Wong et al., Curr Biol 2020
pRS416-Vac17-S127-S128-S131- GFP	Amp, URA3	Wong et al., Curr Biol 2020
pRS416-Vac17-T149A-GFP	Amp, URA3	Wong et al., Curr Biol 2020
pRS416-Vac17-S337-S338-S359A-GFP	Amp, URA3	Sara Wong, unpublished
pRS415-Vac8-mCherry	Amp, LEU2	Sara Wong, unpublished
pRS415-Vac8-S16A-mCherry	Amp, LEU2	Sara Wong, unpublished
pRS413-Vac8-mCherry	Amp, HIS3	Noah Steinfeld, unpublished
pEW161 (promHIS3-GFPS65T-PTS1::URA3)	Amp, URA3	Hoepfner et. al. 2001

Table 3. Quantitative analysis of Vac17 phosphorylation in *vps41Δ* mutant cells

Vac17-FLAG was affinity purified from wildtype (light) and *vps41Δ* (heavy) cell lysates, and SILAC-MS was used to quantify relative abundance of phosphorylated peptides between the two samples. Individual H:L ratios in this table have been normalized to the average H:L ratio for unmodified Vac17 peptides in each respective experiment.

Position	H:L ratio (experiment 1)	H:L ratio (experiment 2)
Vac17-S34	0.68912	
Vac17-S35	0.68912	
Vac17-S68	0.738111	
Vac17-S127	0.575253	0.520017
Vac17-S128	0.592645	0.616237
Vac17-S131	0.388322	0.558716
Vac17-T149	0.472177	0.281926
Vac17-S170	0.675639	
Vac17-T172	0.724191	0.360831
Vac17-S174	0.690914	0.414631
Vac17-S178	0.679003	0.541881
Vac17-S194		0.791404
Vac17-S269	0.832837	0.589798
Vac17-S272	0.200448	0.180742
Vac17-S275	0.141797	0.133062
Vac17-S337		0.39957
Vac17-S359	0.396888	0.681269
Vac8-S16	0.128755874	

Table 4. Quantitative analysis of Vac17 phosphorylation in *yck3Δ* mutant cells

Vac17-FLAG was affinity purified from wildtype (light) and *yck3Δ* (heavy) cell lysates, and SILAC-MS was used to quantify relative abundance of phosphorylated peptides between the two samples. One experiment detected a change in the ubiquitylation of Vac17-K277. Individual H:L ratios in this table have been normalized to the average H:L ratio for unmodified Vac17 peptides in each respective experiment.

Position	H:L ratio (experiment 1)	H:L ratio (experiment 2)
Vac17-S44	1.47432	
Vac17-S127	1.280887	0.825995
Vac17-S128	1.053939	0.997896
Vac17-S131	0.824886	0.59168
Vac17-T149	1.105163	1.420743
Vac17-S170	0.902029	
Vac17-T172	0.931135	
Vac17-S174	0.748762	1.606786
Vac17-S178	0.962073	1.83307
Vac17-Y267		0.378862
Vac17-S269	0.902164	0.872216
Vac17-S272	0.898501	0.68222
Vac17-S275	0.459455	0.452034
Vac17-S337		0.989742
Vac17-S338		1.014203
Vac17-S359	1.332655	1.092934
Vac17-K277 (Ub)		0.9239
Vac8-S16		0.37341
Myo2-S1131		0.644607
Myo2-T1132		0.884532
Myo2-S1135		0.755098

Table 5. Alanine mutants tested for defects in the termination.

pRS416-Vac17-GFP or pRS415-Vac8-mCherry was mutated by site directed mutagenesis PCR, and then transformed into LWY5798 or LWY5826. Mutants were assayed by western blot and/or microscopy. Mutants with a defect in vacuole transport are bold.

Vac17		
	127, 128, 131	
	149	
	127, 128, 131, 149	
	170, 172, 174	
	149, 170, 172, 174	
	127, 128, 131, 149, 170, 172, 174	
	269, 272, 275	
	269, 272, 275, 127, 128, 131, 149, 170, 172, 174	
	337, 338, 359	
	269, 272, 275, 337, 338, 359	
Vac8	16	
	11, 16	
Vac17 + Vac8	Vac17	Vac8
	269, 272, 275	16
	269, 272, 275, 337, 338, 359	16
	267, 269, 272, 275	11, 16

Table 6. Quantitative analysis of Vac17 interactions in vps41Δ mutant cells

Vac17-FLAG was affinity purified from wildtype (light) and *vps41Δ* (heavy) cell lysates, and SILAC-MS was used to quantify relative abundance of interacting peptides between the two samples. Note that experiment 1 interaction analysis was performed on the IMAC sample and experiment 2 was performed on the input sample.

Summary	Experiment 1		Experiment 2	
	raw H:L	normalized (to Vac17) H:L	raw H:L	normalized (to Vac17) H:L
Vac17	1.1149	1	0.64591	1
Vac8	0.92788	0.832254	0.71194	1.102228
Myo2	0.71222	0.63882	0.17463	0.270363
Ubi4	3.7754	3.386313	1.1775	1.823009

Table 7. Quantitative analysis of Vac17 interactions in *yck3Δ* mutant cells

Vac17-FLAG was affinity purified from wildtype (light) and *yck3Δ* (heavy) cell lysates, and SILAC-MS was used to quantify relative abundance of interacting peptides between the two samples.

Note that experiment 1 interaction analysis was performed on the IMAC sample and experiment 2 was performed on the input sample.

Summary	Experiment 1		Experiment 2	
	raw H:L	normalized (to Vac17) H:L	raw H:L	normalized (to Vac17) H:L
Vac17	1.4739	1	1.0973	1
Vac8	0.74668	0.506602	0.91816	0.836745
Myo2	1.232	0.835878	0.94442	0.860676
Ubi4	1.2287	0.833639	1.0657	0.971202
Atg18			1.3847	1.261916

Table 8. Potential regulators of vacuole transport. Results from the SGA screen.

Systematic Name	Standard Name	Function/Localization
YLL040C	vps13	cell organization
YAL067C	seo1	organelle membrane
YLR121C	yps3	organelle membrane
YMR141C	unknown	unknown
YML086C	alo1	enzyme
YMR144W	fdo1	nucleus
YAL053W	flc2	organelle membrane
YAL045C	unknown	unknown
YAL040C	cln3	cell cycle
YLR011W	lot6	enzyme
YML084W	unknown	unknown
YMR145C	nde1	mitochondria
YAL021C	ccr4	nucleus
YML057W	cmp2	enzyme
YML056C	imd4	enzyme
YMR166C	mme1	mitochondria
YMR169C	ald3	enzyme
YMR174C	pai3	enzyme
YLR047C	fre3	enzyme
YAL005C	ssa1	nucleus
YLR059C	rex2	mitochondria
YAR028W	unknown	unknown
YMR195W	icy1	unknown
YML008C	erg6	ergosterol synthesis
YAR030C	unknown	unknown
YAR035W	yat1	mitochondria
YAR037W	unknown	unknown
YAR040C	unknown	unknown
YLL001W	dnm1	mitochondria
YML006C	gis4	unknown
YMR219W	esc1	nucleus
YMR221C	fmp42	unknown
YMR232W	fus2	cell organization
YMR031C	eis1	cell trafficking
YNL270C	alp1	organelle membrane
YNL266W	unknown	unknown
YNL264C	pdr17	lipid regulation
YOL024W	unknown	unknown
YOL028C	yap7	nucleus

YOR295W	uag30	nucleus
YOL042W	ngl1	nucleus
YOR007C	sgt2	stress response
YOR008C	slg1	stress response
YOR320C	gnt1	enzyme
YOR036W	pep12	cell trafficking
YOR052C	tmc1	stress response
YOR376W	unknown	unknown
YPL259C	apm1	cell trafficking
YPL232W	sso1	cell trafficking
YDR080W	vps41	cell trafficking
YPL194W	ddc1	nucleus
YDR090C	unknown	unknown
YDR097C	msh6	nucleus
YDR415C	unknown	unknown
YPL157W	tgs1	nucleus
YPL144W	poc4	proteasome
YPL136W	unknown	unknown
YDR144C	mkc7	enzyme
YPL111W	car1	enzyme
YPL105C	syh1	unknown
YGR153W	unknown	unknown
YHR200W	rpn10	proteasome
YGR181W	tim13	mitochondria
YCL008C	stp22	cell trafficking
YHR075C	ppe1	enzyme
YHR077C	nmd2	nucleus
YER048C	caj1	nucleus
YGR202C	pct1	lipid regulation
YCL026C	unknown	unknown
YCL040W	glk1	enzyme
YCL044C	mgr1	mitochondria
YHL044W	unknown	unknown
YCR004C	ycp4	unknown
YLR170C	aps1	cell trafficking
YKL075C	unknown	unknown
YKL106W	aat1	mitochondria
YKL109W	hap4	nucleus
YOR211C	mgm1	mitochondria
YGR107W	unknown	unknown
YKL142W	mrp8	unknown

YOR106W	vam3	cell trafficking
YOR252W	tma16	unknown
YKL048C	elm1	cell cycle
YKL055C	oar1	mitochondria
YKL062W	msn4	nucleus
YOR135C	irc4	unknown
YJL204C	rcy1	cell trafficking
YGL237C	hap2	nucleus
YLR239C	lip2	mitochondria
YJL148W	rpa34	nucleus
YLR257W	unknown	unknown
YPL089C	rlm1	nucleus
YPL055C	lge1	unknown
YBL007C	sla1	cell organization
YPL048W	cam1	nucleus
YBL021C	hap3	nucleus
YDR363W-A	sem1	proteasome
YPL002C	snf8	cell trafficking
YPR122W	axl1	cell organization
YNL205C	unknown	unknown
YNL179C	unknown	unknown
YIL070C	mam33	mitochondria
YMR063W	rim9	unknown
YFR021W	atg18	cell trafficking
YGR263C	say1	organelle membrane
YMR316C-A	unknown	unknown
YOL109W	zeo1	cell organization
YJR035W	rad26	nucleus
YLR438W	car2	stress response
YLR449W	fpr2	nucleus
YDR043C	nrg1	nucleus
YJR060W	cbf1	nucleus
YJR061W	mnn14	unknown
YBR296C	pho89	enzyme
YAL058C-A	unknown	unknown
YCL074W	unknown	unknown
YCR077C	pat1	nucleus
YGL219C	mdm34	organelle membrane
YIL132C	csm2	nucleus
YIL153W	rrd1	cell cycle
YNR001C	cit1	mitochondria

YIR001C	sgn1	nucleus
YMR048W	csm3	nucleus
YMR160W	unknown	unknown
YDR497C	itr1	lipid regulation
YBR082C	ubc4	ubiquitin
YNL142W	mep2	enzyme
YER178W	pda1	enzyme
YML073C	rpl6a	ribosome
YPL050C	mnn9	enzyme
YDR512C	emi1	unknown
YML111W	bul2	ubiquitin
YAL037C-A	unknown	unknown
YBL008W-A	unknown	unknown
YBL101W-C	unknown	unknown
YBR196C-B	unknown	unknown
YBR221W-A	unknown	unknown
YCL057C-A	mic10	mitochondria
YBR072C-A	unknown	unknown
YBR221W-A	unknown	unknown
YGL006W-A	unknown	unknown
YMR013W-A	unknown	unknown
YGR146C-A	unknown	unknown
YOL077W-A	atp19	mitochondria
YJL136W-A	unknown	unknown
YBR109C	cmd1	cell organization
YBR121C	grs1	mitochondria
YBR143C	sup45	nucleus
YDR052C	dbf4	nucleus
YFL038C	ypt1	cell trafficking
YGR083C	gcd2	nucleus
YGR280C	Pxr1	nucleus
YCR057C	pwp2	ribosome
YIR012W	sqt1	ribosome
YDR238C	sec26	cell trafficking
YDL015C	tsc13	organelle membrane
YBL004W	upt20	ribosome
YDL097C	rpn6	proteasome
YDR331W	gpi8	enzyme
YDR362C	tfc6	nucleus
YIL171W	unknown	unknown
YKL144C	rpc25	nucleus

YER012W	pre1	proteasome
YGR186W	tfg1	nucleus
YHR042W	ncp1	ergosterol synthesis
YGL011C	scl1	proteasome
YGL022W	stt3	enzyme
YJR057W	cdc8	nucleus
YLR141W	rrn5	nucleus
YLR166C	sec10	cell trafficking
YMR314W	pre5	proteasome
YNL038W	gpi15	enzyme
YPR103W	pre2	proteasome
YOR261C	rpn8	proteasome
YOL038W	pre6	proteasome
YPL128C	tbf1	nucleus
YMR220W	erg8	ergosterol synthesis
YOR060C	unknown	unknown

REFERENCES

1. Albuquerque, C., Smolka, M., Payne, S., Bafna, V., Eng, J., and Zhou, H. (2008). A multidimensional chromatography technology for in-depth phosphoproteome analysis. *Mol Cell Proteomics* 7, 1389-1396.
2. Ali, M.Y., Lu, H., Bookwalter, C.S., Warshaw, D.M., and Trybus, K.M. (2008). Myosin V and Kinesin act as tethers to enhance each others' processivity. *Proceedings of the National Academy of Sciences of the United States of America* 105, 4691-4696.
3. Andoh, T., Hirata, Y., and Kikuchi, A. (2000). Yeast glycogen synthase kinase 3 is involved in protein degradation in cooperation with Bul1, Bul2, and Rsp5. *Mol Cell Biol* 20, 6712-6720.
4. Angers, C.G., and Merz, A.J. (2009). HOPS interacts with Apl5 at the vacuole membrane and is required for consumption of AP-3 transport vesicles. *Molecular biology of the cell* 20, 4563-4574.
5. Arai, S., Noda, Y., Kainuma, S., Wada, I., and Yoda, K. (2008). Ypt11 functions in bud-directed transport of the Golgi by linking Myo2 to the coatomer subunit Ret2. *Curr Biol* 18, 987-991.
6. Arendt, C.S., and Hochstrasser, M. (1997). Identification of the yeast 20S proteasome catalytic centers and subunit interactions required for active-site formation. *Proceedings of the National Academy of Sciences of the United States of America* 94, 7156-7161.
7. Asensio, C.S., Sirkis, D.W., Maas, J.W., Jr., Egami, K., To, T.L., Brodsky, F.M., Shu, X., Cheng, Y., and Edwards, R.H. (2013). Self-assembly of VPS41 promotes sorting required for biogenesis of the regulated secretory pathway. *Developmental cell* 27, 425-437.
8. Babour, A., Bicknell, A.A., Tourtellotte, J., and Niwa, M. (2010). A surveillance pathway monitors the fitness of the endoplasmic reticulum to control its inheritance. *Cell* 142, 256-269.
9. Banta, L.M., Vida, T.A., Herman, P.K., and Emr, S.D. (1990). Characterization of yeast Vps33p, a protein required for vacuolar protein sorting and vacuole biogenesis. *Mol Cell Biol* 10, 4638-4649.
10. Barral, D.C., and Seabra, M.C. (2004). The melanosome as a model to study organelle motility in mammals. *Pigment Cell Res* 17, 111-118.
11. Barth, H., Meiling-Wesse, K., Epple, U.D., and Thumm, M. (2001). Autophagy and the cytoplasm to vacuole targeting pathway both require Aut10p. *FEBS Lett* 508, 23-28.
12. Bartholomew, C.R., and Hardy, C.F. (2009). p21-activated kinases Cla4 and Ste20 regulate vacuole inheritance in *Saccharomyces cerevisiae*. *Eukaryotic cell* 8, 560-572.
13. Bockler, S., Chelius, X., Hock, N., Klecker, T., Wolter, M., Weiss, M., Braun, R.J., and Westermann, B. (2017). Fusion, fission, and transport control asymmetric inheritance of mitochondria and protein aggregates. *J Cell Biol* 216, 2481-2498.
14. Bodnar, N., and Rapoport, T. (2017). Toward an understanding of the Cdc48/p97 ATPase. *F1000Res* 6, 1318.
15. Boldogh, I., Vojtov, N., Karmon, S., and Pon, L.A. (1998). Interaction between mitochondria and the actin cytoskeleton in budding yeast requires two integral mitochondrial outer membrane proteins, Mmm1p and Mdm10p. *J Cell Biol* 141, 1371-1381.

16. Boldogh, I.R., Nowakowski, D.W., Yang, H.C., Chung, H., Karmon, S., Royes, P., and Pon, L.A. (2003). A protein complex containing Mdm10p, Mdm12p, and Mmm1p links mitochondrial membranes and DNA to the cytoskeleton-based segregation machinery. *Molecular biology of the cell* *14*, 4618-4627.
17. Boldogh, I.R., Yang, H.C., Nowakowski, W.D., Karmon, S.L., Hays, L.G., Yates, J.R., 3rd, and Pon, L.A. (2001). Arp2/3 complex and actin dynamics are required for actin-based mitochondrial motility in yeast. *Proceedings of the National Academy of Sciences of the United States of America* *98*, 3162-3167.
18. Bowdish, K.S., Yuan, H.E., and Mitchell, A.P. (1994). Analysis of RIM11, a yeast protein kinase that phosphorylates the meiotic activator IME1. *Mol Cell Biol* *14*, 7909-7919.
19. Boyce, K.J., and Andrianopoulos, A. (2011). Ste20-related kinases: effectors of signaling and morphogenesis in fungi. *Trends Microbiol* *19*, 400-410.
20. Breslow, D.K., Cameron, D.M., Collins, S.R., Schuldiner, M., Stewart-Ornstein, J., Newman, H.W., Braun, S., Madhani, H.D., Krogan, N.J., and Weissman, J.S. (2008). A comprehensive strategy enabling high-resolution functional analysis of the yeast genome. *Nature methods* *5*, 711-718.
21. Bretscher, A. (2003). Polarized growth and organelle segregation in yeast: the tracks, motors, and receptors. *The Journal of cell biology* *160*, 811-816.
22. Brockerhoff, S.E., Stevens, R.C., and Davis, T.N. (1994). The unconventional myosin, Myo2p, is a calmodulin target at sites of cell growth in *Saccharomyces cerevisiae*. *The Journal of cell biology* *124*, 315-323.
23. Brozzi, F., Diraison, F., Lajus, S., Rajatileka, S., Philips, T., Regazzi, R., Fukuda, M., Verkade, P., Molnar, E., and Varadi, A. (2012). Molecular mechanism of myosin Va recruitment to dense core secretory granules. *Traffic* *13*, 54-69.
24. Buvelot Frei, S., Rahl, P.B., Nussbaum, M., Briggs, B.J., Calero, M., Janeczko, S., Regan, A.D., Chen, C.Z., Barral, Y., Whittaker, G.R., *et al.* (2006). Bioinformatic and comparative localization of Rab proteins reveals functional insights into the uncharacterized GTPases Ypt10p and Ypt11p. *Mol Cell Biol* *26*, 7299-7317.
25. Byrne, K.P., and Wolfe, K.H. (2005). The Yeast Gene Order Browser: combining curated homology and syntenic context reveals gene fate in polyploid species. *Genome Res* *15*, 1456-1461.
26. Cabrera, M., Langemeyer, L., Mari, M., Rethmeier, R., Orban, I., Perz, A., Brocker, C., Griffith, J., Klose, D., Steinhoff, H.J., *et al.* (2010). Phosphorylation of a membrane curvature-sensing motif switches function of the HOPS subunit Vps41 in membrane tethering. *The Journal of cell biology* *191*, 845-859.
27. Cabrera, M., Ostrowicz, C.W., Mari, M., LaGrassa, T.J., Reggiori, F., and Ungermann, C. (2009). Vps41 phosphorylation and the Rab Ypt7 control the targeting of the HOPS complex to endosome-vacuole fusion sites. *Molecular biology of the cell* *20*, 1937-1948.
28. Çağdaş, D., Özgür, T.T., Asal, G.T., Tezcan, İ., Metin, A., Lambert, N., de Saint Basile, G., and Sanal, Ö. (2012). Griscelli syndrome types 1 and 3: analysis of four new cases and long-term evaluation of previously diagnosed patients. *European Journal of Pediatrics* *171*, 1527-1531.
29. Cao, Q.J., Zhang, N., Zhou, R., Yao, L.L., and Li, X.D. (2019). The cargo adaptor proteins RILPL2 and melanophilin co-regulate myosin-5a motor activity. *J Biol Chem* *294*, 11333-11341.
30. Carton-Garcia, F., Overeem, A.W., Nieto, R., Bazzocco, S., Dopeso, H., Macaya, I., Bilic, J., Landolfi, S., Hernandez-Losa, J., Schwartz, S., Jr., *et al.* (2015). Myo5b knockout mice as a model of microvillus inclusion disease. *Sci Rep* *5*, 12312.
31. Cesaro, L., and Pinna, L.A. (2015). The generation of phosphoserine stretches in phosphoproteins: mechanism and significance. *Mol Biosyst* *11*, 2666-2679.

32. Chang, W., Zaarour, R.F., Reck-Peterson, S., Rinn, J., Singer, R.H., Snyder, M., Novick, P., and Mooseker, M.S. (2008). Myo2p, a class V myosin in budding yeast, associates with a large ribonucleic acid-protein complex that contains mRNAs and subunits of the RNA-processing body. *RNA* *14*, 491-502.
33. Chapman, J.W., and Johnston, L.H. (1989). The yeast gene, DBF4, essential for entry into S phase is cell cycle regulated. *Exp Cell Res* *180*, 419-428.
34. Chen, P., and Hochstrasser, M. (1996). Autocatalytic subunit processing couples active site formation in the 20S proteasome to completion of assembly. *Cell* *86*, 961-972.
35. Chen, Y., Tian, L., Zhang, F., Liu, C., Lu, T., Ruan, Y., Wang, L., Yan, H., Yan, J., Liu, Q., *et al.* (2013). Myosin Vb gene is associated with schizophrenia in Chinese Han population. *Psychiatry Research* *207*, 13-18.
36. Cheng, L., Collyer, T., and Hardy, C.F. (1999). Cell cycle regulation of DNA replication initiator factor Dbf4p. *Mol Cell Biol* *19*, 4270-4278.
37. Chernyakov, I., Santiago-Tirado, F., and Bretscher, A. (2013). Active segregation of yeast mitochondria by Myo2 is essential and mediated by Mmr1 and Ypt11. *Curr Biol* *23*, 1818-1824.
38. Chesarone-Cataldo, M., Guerin, C., Yu, J.H., Wedlich-Soldner, R., Blanchoin, L., and Goode, B.L. (2011). The myosin passenger protein Smy1 controls actin cable structure and dynamics by acting as a formin damper. *Dev Cell* *21*, 217-230.
39. Cho, W.H., Lee, Y.J., Kong, S.I., Hurwitz, J., and Lee, J.K. (2006). CDC7 kinase phosphorylates serine residues adjacent to acidic amino acids in the minichromosome maintenance 2 protein. *Proceedings of the National Academy of Sciences of the United States of America* *103*, 11521-11526.
40. Cohen, Y., Klug, Y.A., Dimitrov, L., Erez, Z., Chuartzman, S.G., Elinger, D., Yofe, I., Soliman, K., Gartner, J., Thoms, S., *et al.* (2014). Peroxisomes are juxtaposed to strategic sites on mitochondria. *Mol Biosyst* *10*, 1742-1748.
41. Cohen, Y., and Schuldiner, M. (2011). Advanced methods for high-throughput microscopy screening of genetically modified yeast libraries. *Methods in molecular biology* *781*, 127-159.
42. Crawford, M., Liu, N., Mahdipour, E., Barr, K., Heit, B., and Dagnino, L. (2020). Integrin-linked kinase regulates melanosome trafficking and melanin transfer in melanocytes. *Mol Biol Cell* *31*, 768-781.
43. Cross, J.A., and Dodding, M.P. (2019). Motor-cargo adaptors at the organelle-cytoskeleton interface. *Current opinion in cell biology* *59*, 16-23.
44. Cvrckova, F., De Virgilio, C., Manser, E., Pringle, J.R., and Nasmyth, K. (1995). Ste20-like protein kinases are required for normal localization of cell growth and for cytokinesis in budding yeast. *Genes & Development* *9*, 1817-1830.
45. Darsow, T., Katzmann, D.J., Cowles, C.R., and Emr, S.D. (2001). Vps41p function in the alkaline phosphatase pathway requires homo-oligomerization and interaction with AP-3 through two distinct domains. *Molecular biology of the cell* *12*, 37-51.
46. Dolce, L.G., Ohbayashi, N., Silva, D., Ferrari, A.J.R., Pirolla, R.A.S., Schwarzer, A., Zanphorlin, L.M., Cabral, L., Fioramonte, M., Ramos, C.H.I., *et al.* (2020). Unveiling the interaction between the molecular motor Myosin Vc and the small GTPase Rab3A. *J Proteomics* *212*, 103549.
47. Dong, W., Chen, X., Chen, P., Yue, D., Zhu, L., and Fan, Q. (2012). Inactivation of MYO5B promotes invasion and motility in gastric cancer cells. *Digestive diseases and sciences* *57*, 1247-1252.
48. Donovan, K.W., and Bretscher, A. (2012). Myosin-V is activated by binding secretory cargo and released in coordination with Rab/exocyst function. *Dev Cell* *23*, 769-781.
49. Donovan, K.W., and Bretscher, A. (2015). Head-to-tail regulation is critical for the in vivo function of myosin V. *The Journal of cell biology* *209*, 359-365.

50. Dunn, B.D., Sakamoto, T., Hong, M.S., Sellers, J.R., and Takizawa, P.A. (2007). Myo4p is a monomeric myosin with motility uniquely adapted to transport mRNA. *The Journal of cell biology* *178*, 1193-1206.
51. Efe, J.A., Botelho, R.J., and Emr, S.D. (2007). Atg18 regulates organelle morphology and Fab1 kinase activity independent of its membrane recruitment by phosphatidylinositol 3,5-bisphosphate. *Mol Biol Cell* *18*, 4232-4244.
52. Elodie Pastural, F.J.B., Remi Dufourcq-Lagelouse, Stephanie Certain, Ozden Sanal, Nada Jabado, Reinhard Seger, Claude Griscelli, Alain Fischer, Genevieve de Saint Basile (1997). Griscelli disease maps to chromosome 15q21 and is associated with mutations in the Myosin-Va gene. *Nature genetics* *16*, 289-292.
53. Eskin, J.A., Rankova, A., Johnston, A.B., Alioto, S.L., and Goode, B.L. (2016). Common formin-regulating sequences in Smy1 and Bud14 are required for the control of actin cable assembly in vivo. *Mol Biol Cell* *27*, 828-837.
54. Estrada, P., Kim, J., Coleman, J., Walker, L., Dunn, B., Takizawa, P., Novick, P., and Ferro-Novick, S. (2003). Myo4p and She3p are required for cortical ER inheritance in *Saccharomyces cerevisiae*. *The Journal of cell biology* *163*, 1255-1266.
55. Eves, P.T., Jin, Y., Brunner, M., and Weisman, L.S. (2012). Overlap of cargo binding sites on myosin V coordinates the inheritance of diverse cargoes. *The Journal of cell biology* *198*, 69-85.
56. Fagarasanu, A., Fagarasanu, M., Eitzen, G.A., Aitchison, J.D., and Rachubinski, R.A. (2006). The peroxisomal membrane protein Inp2p is the peroxisome-specific receptor for the myosin V motor Myo2p of *Saccharomyces cerevisiae*. *Developmental cell* *10*, 587-600.
57. Fagarasanu, A., Mast, F.D., Knoblach, B., Jin, Y., Brunner, M.J., Logan, M.R., Glover, J.N., Eitzen, G.A., Aitchison, J.D., Weisman, L.S., *et al.* (2009). Myosin-driven peroxisome partitioning in *S. cerevisiae*. *The Journal of cell biology* *186*, 541-554.
58. Fagarasanu, M., Fagarasanu, A., Tam, Y.Y., Aitchison, J.D., and Rachubinski, R.A. (2005). Inp1p is a peroxisomal membrane protein required for peroxisome inheritance in *Saccharomyces cerevisiae*. *J Cell Biol* *169*, 765-775.
59. Fields, S., and Song, O. (1989). A novel genetic system to detect protein-protein interactions. *Nature* *340*, 245-246.
60. Flotow, H., Graves, P.R., Wang, A.Q., Fiol, C.J., Roeske, R.W., and Roach, P.J. (1990). Phosphate groups as substrate determinants for casein kinase I action. *The Journal of biological chemistry* *265*, 14264-14269.
61. Fransson, A., Ruusala, A., and Aspenstrom, P. (2003). Atypical Rho GTPases have roles in mitochondrial homeostasis and apoptosis. *J Biol Chem* *278*, 6495-6502.
62. Fransson, S., Ruusala, A., and Aspenstrom, P. (2006). The atypical Rho GTPases Miro-1 and Miro-2 have essential roles in mitochondrial trafficking. *Biochem Biophys Res Commun* *344*, 500-510.
63. Frederick, R.L., Okamoto, K., and Shaw, J.M. (2008). Multiple pathways influence mitochondrial inheritance in budding yeast. *Genetics* *178*, 825-837.
64. Fukuda, M., and Itoh, T. (2004). Slac2-a/melanophilin contains multiple PEST-like sequences that are highly sensitive to proteolysis. *The Journal of biological chemistry* *279*, 22314-22321.
65. Fukuda, M., Kuroda, T.S., and Mikoshiba, K. (2002). Slac2-a/melanophilin, the missing link between Rab27 and myosin Va: implications of a tripartite protein complex for melanosome transport. *The Journal of biological chemistry* *277*, 12432-12436.
66. Fusheng Tang, E.J.K., Jennifer L. Novak, Johnathan J. Nau, Natalie L. Catlett, Lois S. Weisman (2003). Regulated degradation of a class V myosin receptor directs movement of the yeast vacuole. *Nature* *422*, 87-92.

67. Garcia-Rodriguez, L.J., Gay, A.C., and Pon, L.A. (2007). Puf3p, a Pumilio family RNA binding protein, localizes to mitochondria and regulates mitochondrial biogenesis and motility in budding yeast. *The Journal of cell biology* *176*, 197-207.
68. Gerard, A., Koundrioukoff, S., Ramillon, V., Sergere, J.C., Mailand, N., Quivy, J.P., and Almouzni, G. (2006). The replication kinase Cdc7-Dbf4 promotes the interaction of the p150 subunit of chromatin assembly factor 1 with proliferating cell nuclear antigen. *EMBO Rep* *7*, 817-823.
69. Govindan, B., Bowser, R., and Novick, P. (1995). The role of Myo2, a yeast class V myosin, in vesicular transport. *The Journal of cell biology* *128*, 1055-1068.
70. Griffioen, G., Swinnen, S., and Thevelein, J.M. (2003). Feedback inhibition on cell wall integrity signaling by Zds1 involves Gsk3 phosphorylation of a cAMP-dependent protein kinase regulatory subunit. *J Biol Chem* *278*, 23460-23471.
71. Guimaraes, S.C., Schuster, M., Bielska, E., Dagdas, G., Kilaru, S., Meadows, B.R., Schrader, M., and Steinberg, G. (2015). Peroxisomes, lipid droplets, and endoplasmic reticulum "hitchhike" on motile early endosomes. *The Journal of cell biology* *211*, 945-954.
72. Guri Giaeever, A.M.C., Li Ni, Carla Connelly, Linda Riles, Steeve Ve´ronneau, Sally Dow, Ankuta Lucau-Danila, Keith Anderson, Bruno Andre´, Adam P. Arkin, Anna Astromoff, Mohamed El Bakkoury, Rhonda Bangham, Rocio Benito, Sophie Brachat, Stefano Campanaro, Matt Curtiss, Karen Davis, Adam Deutschbauer, Karl-Dieter Entian, Patrick Flaherty, Francoise Foury, David J. Garfinkel, Mark Gerstein, Deanna Gotte, Ulrich Gu¨ Idener, Johannes H. Hegemann, Svenja Hempel, Zelek Herman, Daniel F. Jaramillo, Diane E. Kelly, Steven L. Kelly, Peter Ko¨ tter, Darlene LaBonte, David C. Lamb, Ning Lan, Hong Liang, Hong Liao, Lucy Liu, Chuanyun Luo, Marc Lussier, Rong Mao, Patrice Menard, Siew Loon Ooi, Jose L. Revuelta, Christopher J. Roberts, Matthias Rose, Petra Ross-Macdonald, Bart Scherens, Greg Schimmack, Brenda Shafer, Daniel D. Shoemaker, Sharon Sookhai-Mahadeo, Reginald K. Storms, Jeffrey N. Strathern, Giorgio Valle, Marleen Voet, Guido Volckaert, Ching-yun Wang, Teresa R. Ward, Julie Wilhelmy, Elizabeth A. Winzeler, Yonghong Yang, Grace Yen, Elaine Youngman, Kexin Yu, Howard Bussey, Jef D. Boeke, Michael Snyder, Peter Philippsen, Ronald W. Davis, and Mark Johnston (2002). Functional profiling of the *Saccharomyces cerevisiae* genome. *Nature* *418*, 387- 391.
73. Hammer, J.A., 3rd, and Sellers, J.R. (2012). Walking to work: roles for class V myosins as cargo transporters. *Nature reviews Molecular cell biology* *13*, 13-26.
74. Hammer, J.A., 3rd, and Wagner, W. (2013). Functions of class V myosins in neurons. *The Journal of biological chemistry* *288*, 28428-28434.
75. Hammond, J.W., Blasius, T.L., Soppina, V., Cai, D., and Verhey, K.J. (2010). Autoinhibition of the kinesin-2 motor KIF17 via dual intramolecular mechanisms. *The Journal of cell biology* *189*, 1013-1025.
76. Hancock, W.O. (2014). Bidirectional cargo transport: moving beyond tug of war. *Nature reviews Molecular cell biology* *15*, 615-628.
77. Heissler, S.M., and Sellers, J.R. (2016). Various Themes of Myosin Regulation. *J Mol Biol* *428*, 1927-1946.
78. Hernandez-Ortega, S., Bru, S., Ricco, N., Ramirez, S., Casals, N., Jimenez, J., Isasa, M., Crosas, B., and Clotet, J. (2013). Defective in mitotic arrest 1 (Dma1) ubiquitin ligase controls G1 cyclin degradation. *The Journal of biological chemistry* *288*, 4704-4714.
79. Hickey, C.M., Stroupe, C., and Wickner, W. (2009). The major role of the Rab Ypt7p in vacuole fusion is supporting HOPS membrane association. *The Journal of biological chemistry* *284*, 16118-16125.
80. Higuchi, R., Vevea, J.D., Swayne, T.C., Chojnowski, R., Hill, V., Boldogh, I.R., and Pon, L.A. (2013). Actin dynamics affect mitochondrial quality control and aging in budding yeast. *Curr Biol* *23*, 2417-2422.

81. Hill, S.M., Hao, X., Gronvall, J., Spikings-Nordby, S., Widlund, P.O., Amen, T., Jorhov, A., Josefson, R., Kaganovich, D., Liu, B., *et al.* (2016). Asymmetric Inheritance of Aggregated Proteins and Age Reset in Yeast Are Regulated by Vac17-Dependent Vacuolar Functions. *Cell reports* *16*, 826-838.
82. Hill, S.M., Hao, X., Liu, B., and Nystrom, T. (2014). Life-span extension by a metacaspase in the yeast *Saccharomyces cerevisiae*. *Science* *344*, 1389-1392.
83. Hodges, A.R., Krementsova, E.B., Bookwalter, C.S., Fagnant, P.M., Sladewski, T.E., and Trybus, K.M. (2012). Tropomyosin is essential for processive movement of a class V myosin from budding yeast. *Curr Biol* *22*, 1410-1416.
84. Hoepfner, D., van den Berg, M., Philippsen, P., Tabak, H.F., and Hettema, E.H. (2001). A role for Vps1p, actin, and the Myo2p motor in peroxisome abundance and inheritance in *Saccharomyces cerevisiae*. *The Journal of cell biology* *155*, 979-990.
85. Holly, S.P., and Blumer, K.J. (1999). PAK-family kinases regulate cell and actin polarization throughout the cell cycle of *Saccharomyces cerevisiae*. *The Journal of cell biology* *147*, 845-856.
86. Hu, C.D., Chinenov, Y., and Kerppola, T.K. (2002). Visualization of interactions among bZIP and Rel family proteins in living cells using bimolecular fluorescence complementation. *Mol Cell* *9*, 789-798.
87. Hughes, A.L., and Gottschling, D.E. (2012). An early age increase in vacuolar pH limits mitochondrial function and lifespan in yeast. *Nature* *492*, 261-265.
88. Hwang, E., Kusch, J., Barral, Y., and Huffaker, T.C. (2003). Spindle orientation in *Saccharomyces cerevisiae* depends on the transport of microtubule ends along polarized actin cables. *The Journal of cell biology* *161*, 483-488.
89. Inoshita, M., and Mima, J. (2017). Human Rab small GTPase- and class V myosin-mediated membrane tethering in a chemically defined reconstitution system. *The Journal of biological chemistry* *292*, 18500-18517.
90. Ishikawa, K., Catlett, N.L., Novak, J.L., Tang, F., Nau, J.J., and Weisman, L.S. (2003). Identification of an organelle-specific myosin V receptor. *The Journal of cell biology* *160*, 887-897.
91. Itoh, T., Toh, E.A., and Matsui, Y. (2004). Mmr1p is a mitochondrial factor for Myo2p-dependent inheritance of mitochondria in the budding yeast. *The EMBO journal* *23*, 2520-2530.
92. Itoh, T., Watabe, A., Toh, E.A., and Matsui, Y. (2002). Complex formation with Ypt11p, a rab-type small GTPase, is essential to facilitate the function of Myo2p, a class V myosin, in mitochondrial distribution in *Saccharomyces cerevisiae*. *Mol Cell Biol* *22*, 7744-7757.
93. Jackson, A.L., Pahl, P.M., Harrison, K., Rosamond, J., and Sclafani, R.A. (1993). Cell cycle regulation of the yeast Cdc7 protein kinase by association with the Dbf4 protein. *Mol Cell Biol* *13*, 2899-2908.
94. Jiang, W., McDonald, D., Hope, T.J., and Hunter, T. (1999). Mammalian Cdc7-Dbf4 protein kinase complex is essential for initiation of DNA replication. *The EMBO journal* *18*, 5703-5713.
95. Jin, Y., Sultana, A., Gandhi, P., Franklin, E., Hamamoto, S., Khan, A.R., Munson, M., Schekman, R., and Weisman, L.S. (2011). Myosin V transports secretory vesicles via a Rab GTPase cascade and interaction with the exocyst complex. *Developmental cell* *21*, 1156-1170.
96. Jin, Y., Taylor Eves, P., Tang, F., and Weisman, L.S. (2009). PTC1 is required for vacuole inheritance and promotes the association of the myosin-V vacuole-specific receptor complex. *Molecular biology of the cell* *20*, 1312-1323.
97. Jin, Y., and Weisman, L.S. (2015). The vacuole/lysosome is required for cell-cycle progression. *Elife* *4*.
98. Johnson, D.E., Ostrowski, P., Jaumouille, V., and Grinstein, S. (2016). The position of lysosomes within the cell determines their luminal pH. *The Journal of cell biology* *212*, 677-692.

99. Johnston, G.C., Prendergast, J.A., and Singer, R.A. (1991). The *Saccharomyces cerevisiae* MYO2 gene encodes an essential myosin for vectorial transport of vesicles. *The Journal of cell biology* *113*, 539-551.
100. Jongsma, M.L., Berlin, I., and Neefjes, J. (2015). On the move: organelle dynamics during mitosis. *Trends Cell Biol* *25*, 112-124.
101. Kammerer, D., Stevermann, L., and Liakopoulos, D. (2010). Ubiquitylation regulates interactions of astral microtubules with the cleavage apparatus. *Curr Biol* *20*, 1233-1243.
102. Kapitein, L.C., van Bergeijk, P., Lipka, J., Keijzer, N., Wulf, P.S., Katrukha, E.A., Akhmanova, A., and Hoogenraad, C.C. (2013). Myosin-V opposes microtubule-based cargo transport and drives directional motility on cortical actin. *Curr Biol* *23*, 828-834.
103. Karcher, R.L., Roland, J.T., Zappacosta, F., Huddleston, M.J., Annan, R.S., Carr, S.A., and Gelfand, V.I. (2001). Cell cycle regulation of myosin-V by calcium/calmodulin-dependent protein kinase II. *Science* *293*, 1317-1320.
104. Kelliher, M.T., Yue, Y., Ng, A., Kamiyama, D., Huang, B., Verhey, K.J., and Wildonger, J. (2018). Autoinhibition of kinesin-1 is essential to the dendrite-specific localization of Golgi outposts. *The Journal of cell biology* *217*, 2531-2547.
105. Kent L. Hill, N.L.C., and Lois S. Weisman (1996). Actin and Myosin Function in Directed Vacuole Movement during Cell Division in *Saccharomyces cerevisiae*. *The Journal of cell biology* *135*, 1535-1549.
106. Klecker, T., Scholz, D., Fortsch, J., and Westermann, B. (2013). The yeast cell cortical protein Num1 integrates mitochondrial dynamics into cellular architecture. *Journal of cell science* *126*, 2924-2930.
107. Klecker, T., and Westermann, B. (2020). Asymmetric inheritance of mitochondria in yeast. *Biol Chem*.
108. Knoblach, B., and Rachubinski, R.A. (2014). Transport and Retention Mechanisms Govern Lipid Droplet Inheritance in *Saccharomyces cerevisiae*. *Traffic*.
109. Knoblach, B., and Rachubinski, R.A. (2015). Sharing the cell's bounty - organelle inheritance in yeast. *Journal of cell science* *128*, 621-630.
110. Knoblach, B., and Rachubinski, R.A. (2016). How peroxisomes partition between cells. A story of yeast, mammals and filamentous fungi. *Current opinion in cell biology* *41*, 73-80.
111. Knoblach, B., Sun, X., Coquelle, N., Fagarasanu, A., Poirier, R.L., and Rachubinski, R.A. (2013). An ER-peroxisome tether exerts peroxisome population control in yeast. *The EMBO journal* *32*, 2439-2453.
112. Kornmann, B., Currie, E., Collins, S.R., Schuldiner, M., Nunnari, J., Weissman, J.S., and Walter, P. (2009). An ER-mitochondria tethering complex revealed by a synthetic biology screen. *Science* *325*, 477-481.
113. Kremmentsov, D.N., Kremmentsova, E.B., and Trybus, K.M. (2004). Myosin V: regulation by calcium, calmodulin, and the tail domain. *The Journal of cell biology* *164*, 877-886.
114. Kumar, A., Molli, P.R., Pakala, S.B., Bui Nguyen, T.M., Rayala, S.K., and Kumar, R. (2009). PAK thread from amoeba to mammals. *J Cell Biochem* *107*, 579-585.
115. Kvam, E., and Goldfarb, D.S. (2007). Nucleus-vacuole junctions and piecemeal microautophagy of the nucleus in *S. cerevisiae*. *Autophagy* *3*, 85-92.
116. Lackner, L.L., Ping, H., Graef, M., Murley, A., and Nunnari, J. (2013). Endoplasmic reticulum-associated mitochondria-cortex tether functions in the distribution and inheritance of mitochondria. *Proceedings of the National Academy of Sciences of the United States of America* *110*, E458-467.

117. LaGrassa, T.J., and Ungermann, C. (2005). The vacuolar kinase Yck3 maintains organelle fragmentation by regulating the HOPS tethering complex. *The Journal of cell biology* *168*, 401-414.
118. Larson, R.E. (1996). Myosin-V: a class of unconventional molecular motors. *Braz J Med Biol Res* *29*, 309-318.
119. Lawrence, G., Brown, C.C., Flood, B.A., Karunakaran, S., Cabrera, M., Nordmann, M., Ungermann, C., and Fratti, R.A. (2014). Dynamic association of the PI3P-interacting Mon1-Ccz1 GEF with vacuoles is controlled through its phosphorylation by the type 1 casein kinase Yck3. *Molecular biology of the cell* *25*, 1608-1619.
120. Lee, L., Tirnauer, J.S., Li, J., Schuyler, S.C., Liu, J.Y., and Pellman, D. (2000). Positioning of the mitotic spindle by a cortical-microtubule capture mechanism. *Science* *287*, 2260-2262.
121. Lee, S., Ho, H.C., Tumolo, J.M., Hsu, P.C., and MacGurn, J.A. (2019). Methionine triggers Ppz-mediated dephosphorylation of Art1 to promote cargo-specific endocytosis. *J Cell Biol*.
122. Lepke, M., Putter, V., Staib, C., Kneissl, M., Berger, C., Hoehn, K., Nanda, I., Schmid, M., and Grummt, F. (1999). Identification, characterization and chromosomal localization of the cognate human and murine DBF4 genes. *Mol Gen Genet* *262*, 220-229.
123. Lewandowska, A., Macfarlane, J., and Shaw, J.M. (2013). Mitochondrial association, protein phosphorylation, and degradation regulate the availability of the active Rab GTPase Ypt11 for mitochondrial inheritance. *Mol Biol Cell* *24*, 1185-1195.
124. Li, M., Koshi, T., and Emr, S.D. (2015a). Membrane-anchored ubiquitin ligase complex is required for the turnover of lysosomal membrane proteins. *J Cell Biol* *211*, 639-652.
125. Li, M., Rong, Y., Chuang, Y.S., Peng, D., and Emr, S.D. (2015b). Ubiquitin-dependent lysosomal membrane protein sorting and degradation. *Mol Cell* *57*, 467-478.
126. Li, X.D., Ikebe, R., and Ikebe, M. (2005). Activation of myosin Va function by melanophilin, a specific docking partner of myosin Va. *The Journal of biological chemistry* *280*, 17815-17822.
127. Li, X.D., Mabuchi, K., Ikebe, R., and Ikebe, M. (2004). Ca²⁺-induced activation of ATPase activity of myosin Va is accompanied with a large conformational change. *Biochem Biophys Res Commun* *315*, 538-545.
128. Liakopoulos, D., Kusch, J., Grava, S., Vogel, J., and Barral, Y. (2003). Asymmetric loading of Kar9 onto spindle poles and microtubules ensures proper spindle alignment. *Cell* *112*, 561-574.
129. Lillie, S.H., and Brown, S.S. (1994). Immunofluorescence localization of the unconventional myosin, Myo2p, and the putative kinesin-related protein, Smy1p, to the same regions of polarized growth in *Saccharomyces cerevisiae*. *The Journal of cell biology* *125*, 825-842.
130. Lipatova, Z., Tokarev, A.A., Jin, Y., Mulholland, J., Weisman, L.S., and Segev, N. (2008). Direct interaction between a myosin V motor and the Rab GTPases Ypt31/32 is required for polarized secretion. *Molecular biology of the cell* *19*, 4177-4187.
131. Lister, I., Roberts, R., Schmitz, S., Walker, M., Trinick, J., Veigel, C., Buss, F., and Kendrick-Jones, J. (2004). Myosin VI: a multifunctional motor. *Biochem Soc Trans* *32*, 685-688.
132. Liu, J., Taylor, D.W., Kremontsova, E.B., Trybus, K.M., and Taylor, K.A. (2006). Three-dimensional structure of the myosin V inhibited state by cryoelectron tomography. *Nature* *442*, 208-211.
133. Lobingier, B.T., Nickerson, D.P., Lo, S.Y., and Merz, A.J. (2014). SM proteins Sly1 and Vps33 co-assemble with Sec17 and SNARE complexes to oppose SNARE disassembly by Sec18. *Elife* *3*, e02272.

134. Long, R.M., Gu, W., Lorimer, E., Singer, R.H., and Chartrand, P. (2000). She2p is a novel RNA-binding protein that recruits the Myo4p-She3p complex to ASH1 mRNA. *The EMBO journal* *19*, 6592-6601.
135. Loring, G.L., Christensen, K.C., Gerber, S.A., and Brenner, C. (2008). Yeast Chfr homologs retard cell cycle at G1 and G2/M via Ubc4 and Ubc13/Mms2-dependent ubiquitination. *Cell Cycle* *7*, 96-105.
136. Lu, Q., Li, J., and Zhang, M. (2014). Cargo recognition and cargo-mediated regulation of unconventional myosins. *Acc Chem Res* *47*, 3061-3070.
137. Lu, W., Lakonishok, M., Liu, R., Billington, N., Rich, A., Glotzer, M., Sellers, J.R., and Gelfand, V.I. (2020). Competition between kinesin-1 and myosin-V defines *Drosophila* posterior determination. *Elife* *9*.
138. Lwin, K.M., Li, D., and Bretscher, A. (2016). Kinesin-related Smy1 enhances the Rab-dependent association of myosin-V with secretory cargo. *Mol Biol Cell* *27*, 2450-2462.
139. MacGurn, J.A., Hsu, P.C., Smolka, M.B., and Emr, S.D. (2011). TORC1 regulates endocytosis via Npr1-mediated phosphoinhibition of a ubiquitin ligase adaptor. *Cell* *147*, 1104-1117.
140. Marchal, C., Haguenaer-Tsapis, R., and Urban-Grimal, D. (2000). Casein kinase I-dependent phosphorylation within a PEST sequence and ubiquitination at nearby lysines signal endocytosis of yeast uracil permease. *The Journal of biological chemistry* *275*, 23608-23614.
141. Marin, O., Meggio, F., Sarno, S., Andretta, M., and Pinna, L.A. (1994). Phosphorylation of synthetic fragments of inhibitor-2 of protein phosphatase-1 by casein kinase-1 and -2. Evidence that phosphorylated residues are not strictly required for efficient targeting by casein kinase-1. *Eur J Biochem* *223*, 647-653.
142. Martin, H., Mendoza, A., Rodriguez-Pachon, J.M., Molina, M., and Nombela, C. (1997). Characterization of SKM1, a *Saccharomyces cerevisiae* gene encoding a novel Ste20/PAK-like protein kinase. *Mol Microbiol* *23*, 431-444.
143. Masai, H., and Arai, K. (2000). Dbf4 motifs: conserved motifs in activation subunits for Cdc7 kinases essential for S-phase. *Biochem Biophys Res Commun* *275*, 228-232.
144. Maschi, D., Gramlich, M.W., and Klyachko, V.A. (2018). Myosin V functions as a vesicle tether at the plasma membrane to control neurotransmitter release in central synapses. *Elife* *7*.
145. McConnell, S.J., Stewart, L.C., Talin, A., and Yaffe, M.P. (1990). Temperature-sensitive yeast mutants defective in mitochondrial inheritance. *J Cell Biol* *111*, 967-976.
146. McFaline-Figueroa, J.R., Vevea, J., Swayne, T.C., Zhou, C., Liu, C., Leung, G., Boldogh, I.R., and Pon, L.A. (2011). Mitochondrial quality control during inheritance is associated with lifespan and mother-daughter age asymmetry in budding yeast. *Aging Cell* *10*, 885-895.
147. Migliano, S.M., and Teis, D. (2018). ESCRT and Membrane Protein Ubiquitination. *Prog Mol Subcell Biol* *57*, 107-135.
148. Miller, R.K., Cheng, S.C., and Rose, M.D. (2000). Bim1p/Yeb1p mediates the Kar9p-dependent cortical attachment of cytoplasmic microtubules. *Molecular biology of the cell* *11*, 2949-2959.
149. Mok, J., Kim, P.M., Lam, H.Y., Piccirillo, S., Zhou, X., Jeschke, G.R., Sheridan, D.L., Parker, S.A., Desai, V., Jwa, M., *et al.* (2010). Deciphering protein kinase specificity through large-scale analysis of yeast phosphorylation site motifs. *Sci Signal* *3*, ra12.
150. Moore, A.S., Wong, Y.C., Simpson, C.L., and Holzbaur, E.L. (2016). Dynamic actin cycling through mitochondrial subpopulations locally regulates the fission-fusion balance within mitochondrial networks. *Nature communications* *7*, 12886.

151. Muller, T., Hess, M.W., Schiefermeier, N., Pfaller, K., Ebner, H.L., Heinz-Erian, P., Ponstingl, H., Partsch, J., Rollinghoff, B., Kohler, H., *et al.* (2008). MYO5B mutations cause microvillus inclusion disease and disrupt epithelial cell polarity. *Nature genetics* *40*, 1163-1165.
152. Munck, J.M., Motley, A.M., Nuttall, J.M., and Hettema, E.H. (2009). A dual function for Pex3p in peroxisome formation and inheritance. *J Cell Biol* *187*, 463-471.
153. Nakai, M., Endo, T., Hase, T., and Matsubara, H. (1993). Intramitochondrial protein sorting. Isolation and characterization of the yeast MSP1 gene which belongs to a novel family of putative ATPases. *J Biol Chem* *268*, 24262-24269.
154. Nakamura, N., Hirata, A., Ohsumi, Y., and Wada, Y. (1997). Vam2/Vps41p and Vam6/Vps39p are components of a protein complex on the vacuolar membranes and involved in the vacuolar assembly in the yeast *Saccharomyces cerevisiae*. *The Journal of biological chemistry* *272*, 11344-11349.
155. Natalie L. Catlett, a.L.S.W. (1998). The terminal tail region of a yeast myosin-V mediates its attachment to vacuole membranes and sites of polarized growth. *Proc Natl Acad Sci USA* *95*, 14799-14804.
156. Neuwald, A.F., Aravind, L., Spouge, J.L., and Koonin, E.V. (1999). AAA+: A class of chaperone-like ATPases associated with the assembly, operation, and disassembly of protein complexes. *Genome Res* *9*, 27-43.
157. Nishimura, K., Fukagawa, T., Takisawa, H., Kakimoto, T., and Kanemaki, M. (2009). An auxin-based degron system for the rapid depletion of proteins in nonplant cells. *Nature methods* *6*, 917-922.
158. Nystrom, T., and Liu, B. (2014). Protein quality control in time and space - links to cellular aging. *FEMS Yeast Res* *14*, 40-48.
159. Oberhofer, A., Spieler, P., Rosenfeld, Y., Stepp, W.L., Cleetus, A., Hume, A.N., Mueller-Planitz, F., and Okten, Z. (2017). Myosin Va's adaptor protein melanophilin enforces track selection on the microtubule and actin networks in vitro. *Proceedings of the National Academy of Sciences of the United States of America* *114*, E4714-E4723.
160. Oeljeklaus, S., Schummer, A., Mastalski, T., Platta, H.W., and Warscheid, B. (2016). Regulation of peroxisome dynamics by phosphorylation. *Biochim Biophys Acta* *1863*, 1027-1037.
161. Okreglak, V., and Walter, P. (2014). The conserved AAA-ATPase Msp1 confers organelle specificity to tail-anchored proteins. *Proceedings of the National Academy of Sciences of the United States of America* *111*, 8019-8024.
162. Oku, M., Maeda, Y., Kagohashi, Y., Kondo, T., Yamada, M., Fujimoto, T., and Sakai, Y. (2017). Evidence for ESCRT- and clathrin-dependent microautophagy. *J Cell Biol* *216*, 3263-3274.
163. Otzen, M., Rucktaschel, R., Thoms, S., Emmrich, K., Krikken, A.M., Erdmann, R., and van der Klei, I.J. (2012). Pex19p contributes to peroxisome inheritance in the association of peroxisomes to Myo2p. *Traffic* *13*, 947-959.
164. Oyarzun, J.E., Lagos, J., Vazquez, M.C., Valls, C., De la Fuente, C., Yuseff, M.I., Alvarez, A.R., and Zanlungo, S. (2019). Lysosome motility and distribution: Relevance in health and disease. *Biochim Biophys Acta Mol Basis Dis* *1865*, 1076-1087.
165. Ozkaynak, E., Finley, D., Solomon, M.J., and Varshavsky, A. (1987). The yeast ubiquitin genes: a family of natural gene fusions. *The EMBO journal* *6*, 1429-1439.
166. Park, J., Kim, H.I., Jeong, H., Lee, M., Jang, S.H., Yoon, S.Y., Kim, H., Park, Z.Y., Jun, Y., and Lee, C. (2019a). Quaternary structures of Vac8 differentially regulate the Cvt and PMN pathways. *Autophagy*, 1-16.
167. Park, J.I., Lee, J.E., Myung, C.H., Jo, C.S., Jang, H.S., and Hwang, J.S. (2019b). The absence of Rab27a accelerates the degradation of Melanophilin. *Exp Dermatol* *28*, 90-93.

168. Pashkova, N., Jin, Y., Ramaswamy, S., and Weisman, L.S. (2006). Structural basis for myosin V discrimination between distinct cargoes. *The EMBO journal* *25*, 693-700.
169. Peng, Y., and Weisman, L.S. (2008). The cyclin-dependent kinase Cdk1 directly regulates vacuole inheritance. *Developmental cell* *15*, 478-485.
170. Peplowska, K., Markgraf, D.F., Ostrowicz, C.W., Bange, G., and Ungermann, C. (2007). The CORVET tethering complex interacts with the yeast Rab5 homolog Vps21 and is involved in endo-lysosomal biogenesis. *Developmental cell* *12*, 739-750.
171. Pernice, W.M., Vevea, J.D., and Pon, L.A. (2016). A role for Mfb1p in region-specific anchorage of high-functioning mitochondria and lifespan in *Saccharomyces cerevisiae*. *Nature communications* *7*, 10595.
172. Peter, M., Neiman, A.M., Park, H.O., van Lohuizen, M., and Herskowitz, I. (1996). Functional analysis of the interaction between the small GTP binding protein Cdc42 and the Ste20 protein kinase in yeast. *The EMBO journal* *15*, 7046-7059.
173. Pols, M.S., van Meel, E., Oorschot, V., ten Brink, C., Fukuda, M., Swetha, M.G., Mayor, S., and Klumperman, J. (2013). hVps41 and VAMP7 function in direct TGN to late endosome transport of lysosomal membrane proteins. *Nature communications* *4*, 1361.
174. Provance, D.W., James, T.L., and Mercer, J.A. (2002). Melanophilin, the product of the leaden locus, is required for targeting of myosin-Va to melanosomes. *Traffic* *3*, 124-132.
175. Pruyne, D.W., Schott, D.H., and Bretscher, A. (1998). Tropomyosin-containing actin cables direct the Myo2p-dependent polarized delivery of secretory vesicles in budding yeast. *The Journal of cell biology* *143*, 1931-1945.
176. Pulgar, V., Marin, O., Meggio, F., Allende, C.C., Allende, J.E., and Pinna, L.A. (1999). Optimal sequences for non-phosphate-directed phosphorylation by protein kinase CK1 (casein kinase-1)--a re-evaluation. *Eur J Biochem* *260*, 520-526.
177. Pylypenko, O., Attanda, W., Gauquelin, C., Lahmani, M., Coulibaly, D., Baron, B., Hoos, S., Titus, M.A., England, P., and Houdusse, A.M. (2013). Structural basis of myosin V Rab GTPase-dependent cargo recognition. *Proceedings of the National Academy of Sciences of the United States of America* *110*, 20443-20448.
178. Qiu, R., Zhang, J., and Xiang, X. (2019). LIS1 regulates cargo-adaptor-mediated activation of dynein by overcoming its autoinhibition in vivo. *The Journal of cell biology* *218*, 3630-3646.
179. Radisky, D.C., Snyder, W.B., Emr, S.D., and Kaplan, J. (1997). Characterization of VPS41, a gene required for vacuolar trafficking and high-affinity iron transport in yeast. *Proceedings of the National Academy of Sciences of the United States of America* *94*, 5662-5666.
180. Rafelski, S.M., Viana, M.P., Zhang, Y., Chan, Y.H., Thorn, K.S., Yam, P., Fung, J.C., Li, H., Costa Lda, F., and Marshall, W.F. (2012). Mitochondrial network size scaling in budding yeast. *Science* *338*, 822-824.
181. Ramer, M.D., Suman, E.S., Richter, H., Stanger, K., Spranger, M., Bieberstein, N., and Duncker, B.P. (2013). Dbf4 and Cdc7 proteins promote DNA replication through interactions with distinct Mcm2-7 protein subunits. *The Journal of biological chemistry* *288*, 14926-14935.
182. Raspelli, E., Cassani, C., Lucchini, G., and Fraschini, R. (2011). Budding yeast Dma1 and Dma2 participate in regulation of Swe1 levels and localization. *Molecular biology of the cell* *22*, 2185-2197.
183. Rehling, P., Darsow, T., Katzmann, D.J., and Emr, S.D. (1999). Formation of AP-3 transport intermediates requires Vps41 function. *Nature cell biology* *1*, 346-353.
184. Rodriguez, O.C., and Cheney, R.E. (2002). Human myosin-Vc is a novel class V myosin expressed in epithelial cells. *Journal of cell science* *115*, 991-1004.

185. Roeder, A.D., Hermann, G.J., Keegan, B.R., Thatcher, S.A., and Shaw, J.M. (1998). Mitochondrial inheritance is delayed in *Saccharomyces cerevisiae* cells lacking the serine/threonine phosphatase PTC1. *Mol Biol Cell* *9*, 917-930.
186. Rogers, S.L., Karcher, R.L., Roland, J.T., Minin, A.A., Steffen, W., and Gelfand, V.I. (1999). Regulation of melanosome movement in the cell cycle by reversible association with myosin V. *The Journal of cell biology* *146*, 1265-1276.
187. Salogiannis, J., Egan, M.J., and Reck-Peterson, S.L. (2016). Peroxisomes move by hitchhiking on early endosomes using the novel linker protein PxdA. *The Journal of cell biology* *212*, 289-296.
188. Sato, O., Li, X.D., and Ikebe, M. (2007a). Myosin Va becomes a low duty ratio motor in the inhibited form. *The Journal of biological chemistry* *282*, 13228-13239.
189. Sato, T., Mushiake, S., Kato, Y., Sato, K., Sato, M., Takeda, N., Ozono, K., Miki, K., Kubo, Y., Tsuji, A., *et al.* (2007b). The Rab8 GTPase regulates apical protein localization in intestinal cells. *Nature* *448*, 366-369.
190. Schneeberger, K., Vogel, G.F., Teunissen, H., van Ommen, D.D., Begthel, H., El Bouazzaoui, L., van Vugt, A.H., Beekman, J.M., Klumperman, J., Muller, T., *et al.* (2015). An inducible mouse model for microvillus inclusion disease reveals a role for myosin Vb in apical and basolateral trafficking. *Proceedings of the National Academy of Sciences of the United States of America* *112*, 12408-12413.
191. Schott, D., Ho, J., Pruyne, D., and Bretscher, A. (1999). The COOH-terminal domain of Myo2p, a yeast myosin V, has a direct role in secretory vesicle targeting. *The Journal of cell biology* *147*, 791-808.
192. Sckolnick, M., Kremontsova, E.B., Warshaw, D.M., and Trybus, K.M. (2013). More than just a cargo adapter, melanophilin prolongs and slows processive runs of myosin Va. *The Journal of biological chemistry* *288*, 29313-29322.
193. Seals, D.F., Eitzen, G., Margolis, N., Wickner, W.T., and Price, A. (2000). A Ypt/Rab effector complex containing the Sec1 homolog Vps33p is required for homotypic vacuole fusion. *Proceedings of the National Academy of Sciences of the United States of America* *97*, 9402-9407.
194. Sheltzer, J.M., and Rose, M.D. (2009). The class V myosin Myo2p is required for Fus2p transport and actin polarization during the yeast mating response. *Molecular biology of the cell* *20*, 2909-2919.
195. Siddiqui, N., Zwetsloot, A.J., Bachmann, A., Roth, D., Hussain, H., Brandt, J., Kaverina, I., and Straube, A. (2019). PTPN21 and Hook3 relieve KIF1C autoinhibition and activate intracellular transport. *Nature communications* *10*, 2693.
196. Simon, V.R., Karmon, S.L., and Pon, L.A. (1997). Mitochondrial inheritance: cell cycle and actin cable dependence of polarized mitochondrial movements in *Saccharomyces cerevisiae*. *Cell Motil Cytoskeleton* *37*, 199-210.
197. Simon, V.R., Swayne, T.C., and Pon, L.A. (1995). Actin-dependent mitochondrial motility in mitotic yeast and cell-free systems: identification of a motor activity on the mitochondrial surface. *The Journal of cell biology* *130*, 345-354.
198. Singer-Kruger, B., and Jansen, R.P. (2014). Here, there, everywhere. mRNA localization in budding yeast. *RNA Biol* *11*, 1031-1039.
199. Slubowski, C.J., Funk, A.D., Roesner, J.M., Paulissen, S.M., and Huang, L.S. (2015). Plasmids for C-terminal tagging in *Saccharomyces cerevisiae* that contain improved GFP proteins, Envy and Ivy. *Yeast* *32*, 379-387.

200. Sobajima, T., Yoshimura, S., Iwano, T., Kunii, M., Watanabe, M., Atik, N., Mushiaka, S., Morii, E., Koyama, Y., Miyoshi, E., *et al.* (2014). Rab11a is required for apical protein localisation in the intestine. *Biol Open* 4, 86-94.
201. Song, H., Orr, A., Duan, M., Merz, A.J., and Wickner, W. (2017). Sec17/Sec18 act twice, enhancing membrane fusion and then disassembling cis-SNARE complexes. *Elife* 6.
202. Steel, G.J., Laude, A.J., Boojawan, A., Harvey, D.J., and Morgan, A. (1999). Biochemical analysis of the *Saccharomyces cerevisiae* SEC18 gene product: implications for the molecular mechanism of membrane fusion. *Biochemistry* 38, 7764-7772.
203. Steensma, H.Y., Holterman, L., Dekker, I., van Sluis, C.A., and Wenzel, T.J. (1990). Molecular cloning of the gene for the E1 alpha subunit of the pyruvate dehydrogenase complex from *Saccharomyces cerevisiae*. *Eur J Biochem* 191, 769-774.
204. Stefan, C.J., and Blumer, K.J. (1999). A syntaxin homolog encoded by VAM3 mediates down-regulation of a yeast G protein-coupled receptor. *The Journal of biological chemistry* 274, 1835-1841.
205. Stevens, R.C., and Davis, T.N. (1998). Mlc1p is a light chain for the unconventional myosin Myo2p in *Saccharomyces cerevisiae*. *The Journal of cell biology* 142, 711-722.
206. Stewart, A., and Deacon, J.W. (1995). Vital fluorochromes as tracers for fungal growth studies. *Biotech Histochem* 70, 57-65.
207. Strom, M., Hume, A.N., Tarafder, A.K., Barkagianni, E., and Seabra, M.C. (2002). A family of Rab27-binding proteins. Melanophilin links Rab27a and myosin Va function in melanosome transport. *The Journal of biological chemistry* 277, 25423-25430.
208. Sun, B., Chen, L., Cao, W., Roth, A.F., and Davis, N.G. (2004). The yeast casein kinase Yck3p is palmitoylated, then sorted to the vacuolar membrane with AP-3-dependent recognition of a YXXPhi adaptin sorting signal. *Molecular biology of the cell* 15, 1397-1406.
209. Swayne, T.C., Zhou, C., Boldogh, I.R., Charalel, J.K., McFaline-Figueroa, J.R., Thoms, S., Yang, C., Leung, G., McInnes, J., Erdmann, R., *et al.* (2011). Role for cER and Mmr1p in anchorage of mitochondria at sites of polarized surface growth in budding yeast. *Curr Biol* 21, 1994-1999.
210. Takagishi, Y., and Murata, Y. (2006). Myosin Va mutation in rats is an animal model for the human hereditary neurological disease, Griscelli syndrome type 1. *Annals of the New York Academy of Sciences* 1086, 66-80.
211. Takahashi, S., and Pryciak, P.M. (2007). Identification of novel membrane-binding domains in multiple yeast Cdc42 effectors. *Molecular biology of the cell* 18, 4945-4956.
212. Tang, F., Kauffman, E.J., Novak, J.L., Nau, J.J., Catlett, N.L., and Weisman, L.S. (2003). Regulated degradation of a class V myosin receptor directs movement of the yeast vacuole. *Nature* 422, 87-92.
213. Tang, F., Peng, Y., Nau, J.J., Kauffman, E.J., and Weisman, L.S. (2006). Vac8p, an armadillo repeat protein, coordinates vacuole inheritance with multiple vacuolar processes. *Traffic* 7, 1368-1377.
214. Tang, K., Li, Y., Yu, C., and Wei, Z. (2019). Structural mechanism for versatile cargo recognition by the yeast class V myosin Myo2. *The Journal of biological chemistry*.
215. Tatebayashi, K., Yamamoto, K., Tanaka, K., Tomida, T., Maruoka, T., Kasukawa, E., and Saito, H. (2006). Adaptor functions of Cdc42, Ste50, and Sho1 in the yeast osmoregulatory HOG MAPK pathway. *The EMBO journal* 25, 3033-3044.
216. Thirumurugan, K., Sakamoto, T., Hammer, J.A., 3rd, Sellers, J.R., and Knight, P.J. (2006). The cargo-binding domain regulates structure and activity of myosin 5. *Nature* 442, 212-215.
217. Thoeni, C.E., Vogel, G.F., Tancevski, I., Geley, S., Lechner, S., Pfaller, K., Hess, M.W., Müller, T., Janecke, A.R., Avitzur, Y., *et al.* (2014). Microvillus Inclusion Disease: Loss of Myosin Vb Disrupts Intracellular Traffic and Cell Polarity. *Traffic* 15, 22-42.

218. Torisawa, T., Ichikawa, M., Furuta, A., Saito, K., Oiwa, K., Kojima, H., Toyoshima, Y.Y., and Furuta, K. (2014). Autoinhibition and cooperative activation mechanisms of cytoplasmic dynein. *Nature cell biology* *16*, 1118-1124.
219. Trybus, K.M. (2008). Myosin V from head to tail. *Cellular and molecular life sciences : CMLS* *65*, 1378-1389.
220. Trybus, K.M., Gushchin, M.I., Lui, H., Hazelwood, L., Kremmentsova, E.B., Volkmann, N., and Hanein, D. (2007). Effect of calcium on calmodulin bound to the IQ motifs of myosin V. *The Journal of biological chemistry* *282*, 23316-23325.
221. Tsuji, T., Ficarro, S.B., and Jiang, W. (2006). Essential role of phosphorylation of MCM2 by Cdc7/Dbf4 in the initiation of DNA replication in mammalian cells. *Molecular biology of the cell* *17*, 4459-4472.
222. Ungermann, C., Price, A., and Wickner, W. (2000). A new role for a SNARE protein as a regulator of the Ypt7/Rab-dependent stage of docking. *Proceedings of the National Academy of Sciences of the United States of America* *97*, 8889-8891.
223. Vale, R.D. (2000). AAA proteins. Lords of the ring. *The Journal of cell biology* *150*, F13-19.
224. van der Beek, J., Jonker, C., van der Welle, R., Liv, N., and Klumperman, J. (2019). CORVET, CHEVI and HOPS - multisubunit tethers of the endo-lysosomal system in health and disease. *Journal of cell science* *132*.
225. van der Velde, K.J., Dhekne, H.S., Swertz, M.A., Sirigu, S., Ropars, V., Vinke, P.C., Rengaw, T., van den Akker, P.C., Rings, E.H.H.M., Houdusse, A., *et al.* (2013). An Overview and Online Registry of Microvillus Inclusion Disease Patients and their MYO5B Mutations. *Human Mutation* *34*, 1597-1605.
226. Van Gele, M., Dynoodt, P., and Lambert, J. (2009). Griscelli syndrome: a model system to study vesicular trafficking. *Pigment Cell Melanoma Res* *22*, 268-282.
227. Verhey, K.J., and Hammond, J.W. (2009). Traffic control: regulation of kinesin motors. *Nature reviews Molecular cell biology* *10*, 765-777.
228. Versele, M., and Thorner, J. (2004). Septin collar formation in budding yeast requires GTP binding and direct phosphorylation by the PAK, Cla4. *The Journal of cell biology* *164*, 701-715.
229. Vevea, J.D., Alessi Wolken, D.M., Swayne, T.C., White, A.B., and Pon, L.A. (2013). Ratiometric biosensors that measure mitochondrial redox state and ATP in living yeast cells. *J Vis Exp*, 50633.
230. Vogel, G.F., Klee, K.M., Janecke, A.R., Muller, T., Hess, M.W., and Huber, L.A. (2015). Cargo-selective apical exocytosis in epithelial cells is conducted by Myo5B, Slp4a, Vamp7, and Syntaxin 3. *The Journal of cell biology* *211*, 587-604.
231. Wada, Y., Ohsumi, Y., and Anraku, Y. (1992). Genes for directing vacuolar morphogenesis in *Saccharomyces cerevisiae*. I. Isolation and characterization of two classes of vam mutants. *The Journal of biological chemistry* *267*, 18665-18670.
232. Wagner, W., Brenowitz, S.D., and Hammer, J.A., 3rd (2011). Myosin-Va transports the endoplasmic reticulum into the dendritic spines of Purkinje neurons. *Nature cell biology* *13*, 40-48.
233. Wang, F., Thirumurugan, K., Stafford, W.F., Hammer, J.A., 3rd, Knight, P.J., and Sellers, J.R. (2004). Regulated conformation of myosin V. *The Journal of biological chemistry* *279*, 2333-2336.
234. Wang, Y.X., Kauffman, E.J., Duex, J.E., and Weisman, L.S. (2001). Fusion of docked membranes requires the armadillo repeat protein Vac8p. *The Journal of biological chemistry* *276*, 35133-35140.

235. Wang, Z., Edwards, J.G., Riley, N., Provance, D.W., Jr., Karcher, R., Li, X.D., Davison, I.G., Ikebe, M., Mercer, J.A., Kauer, J.A., *et al.* (2008). Myosin Vb mobilizes recycling endosomes and AMPA receptors for postsynaptic plasticity. *Cell* **135**, 535-548.
236. Wei, Z., Liu, X., Yu, C., and Zhang, M. (2013). Structural basis of cargo recognitions for class V myosins. *Proceedings of the National Academy of Sciences of the United States of America* **110**, 11314-11319.
237. Weisman, L.S. (2003). Yeast vacuole inheritance and dynamics. *Annu Rev Genet* **37**, 435-460.
238. Weisman, L.S. (2006). Organelles on the move: insights from yeast vacuole inheritance. *Nature Reviews Molecular Cell Biology* **7**, 251-251.
239. Welz, T., and Kerkhoff, E. (2019). Exploring the iceberg: Prospects of coordinated myosin V and actin assembly functions in transport processes. *Small GTPases* **10**, 111-121.
240. Westermann, B. (2014). Mitochondrial inheritance in yeast. *Biochim Biophys Acta* **1837**, 1039-1046.
241. Williams, R.S., Lee, M.S., Hau, D.D., and Glover, J.N. (2004). Structural basis of phosphopeptide recognition by the BRCT domain of BRCA1. *Nature structural & molecular biology* **11**, 519-525.
242. Wu, C., Lee, S.F., Furmaniak-Kazmierczak, E., Cote, G.P., Thomas, D.Y., and Leberer, E. (1996). Activation of Myosin-I by Members of the Ste20p Protein Kinase Family. *Journal of Biological Chemistry* **271**, 31787-31790.
243. Wu, X., Bowers, B., Rao, K., Wei, Q., and Hammer, J.A., 3rd (1998). Visualization of melanosome dynamics within wild-type and dilute melanocytes suggests a paradigm for myosin V function *In vivo*. *The Journal of cell biology* **143**, 1899-1918.
244. Wu, X., Wang, F., Rao, K., Sellers, J.R., and Hammer, J.A., 3rd (2002a). Rab27a is an essential component of melanosome receptor for myosin Va. *Mol Biol Cell* **13**, 1735-1749.
245. Wu, X.S., Rao, K., Zhang, H., Wang, F., Sellers, J.R., Matesic, L.E., Copeland, N.G., Jenkins, N.A., and Hammer, J.A., 3rd (2002b). Identification of an organelle receptor for myosin-Va. *Nature cell biology* **4**, 271-278.
246. Xu, Y., Lee, S.H., Kim, H.S., Kim, N.H., Piao, S., Park, S.H., Jung, Y.S., Yook, J.I., Park, B.J., and Ha, N.C. (2010). Role of CK1 in GSK3beta-mediated phosphorylation and degradation of snail. *Oncogene* **29**, 3124-3133.
247. Yau, R.G., Peng, Y., Valiathan, R.R., Birkeland, S.R., Wilson, T.E., and Weisman, L.S. (2014). Release from myosin V via regulated recruitment of an E3 ubiquitin ligase controls organelle localization. *Developmental cell* **28**, 520-533.
248. Yau, R.G., Wong, S., and Weisman, L.S. (2017). Spatial regulation of organelle release from myosin V transport by p21-activated kinases. *The Journal of cell biology* **216**, 1557-1566.
249. Yin, H., Pruyne, D., Huffaker, T.C., and Bretscher, A. (2000). Myosin V orientates the mitotic spindle in yeast. *Nature* **406**, 1013-1015.
250. Yin, X., Feng, X., Takei, Y., and Hirokawa, N. (2012). Regulation of NMDA receptor transport: a KIF17-cargo binding/releasing underlies synaptic plasticity and memory *in vivo*. *J Neurosci* **32**, 5486-5499.
251. Yong-Xu Wang, N.L.C., and Lois S. Weisman (1998). Vac8p, a Vacuolar Protein with Armadillo Repeats, Functions in both Vacuole Inheritance and Protein Targeting from the Cytoplasm to Vacuole. *The Journal of cell biology* **140**, 1063-1074.